HYPERELASTIC SWELLING OF SPHERES AND CYLINDERS AND ITS GENERALIZATION TO ELASTIC INTERNALLY BALANCED MATERIALS

By

Vahid Zamani

A DISSERTATION

Submitted to
Michigan State University
in partial fulfillment of the requirements
for the degree of

Mechanical Engineering – Doctor of Philosophy

2018

ABSTRACT

HYPERELASTIC SWELLING OF SPHERES AND CYLINDERS AND ITS GENERALIZATION TO ELASTIC INTERNALLY BALANCED MATERIALS

By

Vahid Zamani

Swelling as a notion of free volume change is typically due to some added mass procedures. We use modified constitutive laws that incorporate swelling into a continuum mechanics treatment. By incorporating local volume change (swelling) as a parametric constraint into the conventional theory of hyperelasticity it is possible to model a variety of swelling effects. We consider these effects in the study of certain boundary value problems for spherical and cylindrical finite deformations. In addition to the traditional hyperelastic model, we also employ a relatively new type of constitutive treatment, termed internal balance. The theory of internally balanced materials employs energy minimization to obtain an additional balance principle to treat more complex behaviors. This is useful when conventional elastic behavior is modified by substructural reconfiguration. Hence, we also formulate our problems in the context of the internally balanced material theory for the case of cylindrical deformation where the results are compared to that of the conventional hyperelastic model.

For thick spherical shells, the incompressible hyperelastic Mooney-Rivlin constitutive model allows for response to pressure-inflation that could either be globally stable (a monotonic pressure-radius graph) or could instead involve instability jumps of various kinds as pressurization proceeds. The latter occurs when the pressure-radius graph is not monotonic, allowing for a snap-through bifurcation that gives a sudden burst

of inflation. Internal swelling of the material that makes up the shell wall will generally change the response. Not only does it alter the quantitative pressure-inflation relation but it can also change the qualitative stability response, allowing burst phenomena for certain ranges of swelling and preventing burst phenomena for other ranges of swelling. These issues are examined both for the case of uniform swelling for the case of a spatially varying swelling field.

For cylindrical deformations, we examine the finite strain swelling of a soft solid plug within a rigid tube of circular cross section. The eventual channel wall contact as the swelling proceeds generates a confinement pressure that increases as the plug expands. We consider plug geometries that incorporate an internal channel as well as a simpler case of a solid plug. For the case of a plug with a channel, the wall contact now gives a deformation in which swelling combines axial lengthening with internal channel narrowing. Of particular interest is the closing behavior as the swelling proceeds and we treat the problem using asymptotic expansions. Finally, the same problem is examined in the context of the internal balance constitutive theory.

To my great parents, Seyfollah and Behjat,
who were my first teachers,
and to my wonderful wife Mahdieh
and my adorable sisters, and
dedicated to our little angel who is on her way coming to this world.

ACKNOWLEDGEMENTS

I would like to express my deepest respects to my graduate adviser Dr. Thomas Pence who patiently mentored me throughout the years, who showed me the paradigm of professional language and strength of simplicity. I always figure him in my mind as an exemplar of trust and honesty that reinvigorated my hope for a better face of the world. I also should highly appreciate my other committee members and MSU engineering faculties and staff who were indeed helpful in this part of my education.

My dear love Mahdieh educated me and planted the finest of hope in me. During the hardest of the years of my education her true love made me a better person for our lives. Without her love this achievement would not have come true.

My parents and my sisters, who are my true origin and I could not live a lovely life without them, whom I gave them pain by being far far away from my home country during the years, are of my best wishes for the rest of my life.

PREFACE

"What we observe is not nature in itself,

but nature exposed to our method of questioning."

W. Heisenberg

TABLE OF CONTENTS

LIST OF FIGURES

KEY TO ABBREVIATIONS

α: Mooney-Rivilin material parameter

$\hat{\alpha}$, α^*: internal balance material parameters

β: internal balance material parameter ratio

$\mathbf{F}$: deformation gradient tensor

ξ, ζ: thickness ratio parameter

$\hat{\xi}$, ξ^*: internal balance deformation variables

$\mathbf{I}$: identity tensor

λ_i: principal stretches

λ_{lat}: lateral elongation

λ_z: axial elongation

μ: elastic modulus

p: Lagrange multiplier

P_{lat}: lateral confinement pressure

q: internal balance Lagrange multiplier

R_i: inner radius

R_o: outer radius

R_c: confinement radius

ρ: internal balance variable

s: radial deformation ratio (r/R)

$\mathbf{T}$: Cauchy stress tensor

$\Phi^{(i)}$: strain energy densities

v: swelling amount

CHAPTER I

Introduction

Swelling can be viewed as a general phenomena that represents free volume change, typically due to mass addition resulting from some diffusive or transport mechanism. It is seen that many biological tissues and cells exhibit this type of volume and shape change as a result of biological growth, hydration and mass exchange. In many cases osmotic pressure is the causal agent that drives water and other mass transport across bio-membranes such as those surrounding red blood cells and inter-cellular vesicles and lipids *Graf et al.* (1995); *Vinod Kumar and Demeke* (2011); *Li et al.* (2013). For our purposes, swelling is regarded as a general process that encompasses free-volume change at the microscopic level. This would typically be due to mass addition but other fine scale processes of a mechanical or chemical nature can also be regarded as contributing to volume change. Polymers, elastomers and hydrogels naturally swell when exposed to liquid or when subject to high humidity *Treloar* (1975); *Stuart et al.* (2010); *Drozdov* (2013). Biological tissues and cells exhibit volume and shape change under similar processes of hydration and mass exchange *Van der Sman* (2015), but also more generally as a result of biological growth *Goriely et al.* (2010); *Sadik et al.* (2016).

The scientific literature on swelling is vast, and can be approached from a variety of perspectives: material science, physical chemistry, continuum mechanics, etc. We focus on continuum mechanics in which case the literature is still extensive (and

overlapping): mixture theory, biphasic theory, transport theory, poroelasticity, large strain at the outset, small strain on top of a base swollen state, etc, as described for example by a variety of related approaches (see e.g., *Bowen* (1980); *Wineman and Rajagopal* (1992); *Ateshian* (2007); *Hong et al.* (2008); *Markert et al.* (2008); *Duda et al.* (2010); *Chester and Anand* (2010); *Pence* (2012); *Drozdov et al.* (2013); *Selvadurai and Suvorov* (2016)). The treatment given in this thesis is of a generalized hyperelastic nature. By this we mean it specifically does not seek to model the microstructural mechanisms associated with the swelling process, although, as discussed for example in *Baek and Pence* (2011), with suitable modification it could be related to the broader frameworks mentioned above .

The mechanical consequences of these swelling-involved processes are significant. Swelling can lead to qualitative changes in the material's mechanical properties such as the deformability, stability of the overall structure (possibly triggering various bifurcation phenomena associated with localization, buckling and other forms of non-uniqueness), maximum stretch and rupture of membranes and also the capacitance of cells. These are mainly because of the fact that material properties and structure of the solid may be altered as a result of the mass exchanges, leading to associated reconfigurations in stresses and deformations and in some cases instabilities. Hence, the significant impacts on the mechanical properties of the materials require attentions in the study of the interaction between swelling and other mechanical effects. This has been a major issue in many recent studies. This includes the study of *Li et al.* (2013) where an impulsive-like forcing is employed to quantify the yield strain threshold of red blood cell's membranes before rupture. *Vinod Kumar and Demeke* (2011) uses spherically symmetric deformation with neo-Hookean model to analyze infected red blood cell's membrane stress-stretch behavior. *Nagel et al.* (2009) investigates the effects of cellular stiffening and changes in material properties on the damage

evolution in deep tissue pressure-induced injury. The effect of osmotic swelling on the conductance and capacitance of hepatocytes' membrane is studied in *Graf et al.* (1995). *Van der Sman* (2015) represents a hyperelastic neo-Hookean model for hydration of cellular tissue under pressurization of the internal cavity where an elastic shell undergoes inhomogeneous deformation. Other related studies include those of *Gibbons and Klug* (2008) and *Evans et al.* (2003).

The interaction of mechanical responses and absorption of a swelling agent arises in a variety of contexts that go beyond biology. In particular, it associates with many important phenomena in porous absorbent or polymeric solids, elastomers and hydrogels exposed to any surrounding liquid. Among those, hydrogels play an increasingly important role in a wide range of applications, such as in tissue engineering and smart optical systems *Stuart et al.* (2010). With regards to this kind of interaction, many continuum theories and methods have been developed over the years. In particular *Deng and Pence* (2010); *Baek and Pence* (2011); *Ben Amar and Ciarletta* (2010); *Duda et al.* (2010); *Chester and Anand* (2010); *Duda et al.* (2011); *McMahon et al.* (2010); *Goriely et al.* (2010); *Van der Sman* (2015) treat the emerging problems and capture new behaviors in mechanical responses. Theoretical analysis of residual stresses in growing elastic bodies have shown that swelling-induced stresses can initiate mechanical instabilities such as elastic cavitation *Pence and Tsai* (2006); *McMahon et al.* (2010). The possible role of mechanical stress in the opening of cavities in elastic cylindrical model of aerenchyma tissue has also been considered in *Goriely et al.* (2010). As an another recent example *Baek and Pence* (2011) employed a variational method to obtain governing equations of large deformations of elastomeric gels. Their model was employed to treat both saturated and unsaturated gels in equilibrium and subject to loading at the gel interface. Similar treatments on this kind of gels is found in *Deng and Pence* (2010). Also swelling instability of

surface-attached gels has been studied in *Ben Amar and Ciarletta* (2010) as a model of soft tissue growth. They have proposed a theoretical framework for the mechanical treatment of the growth of soft materials under geometrical constraints.

In the rest of this chapter we review the formulation of swelling in a hyperelastic framework and its implementation in isotropic materials. In this context we also introduce a somewhat broader framework (see Eq. (1.5)) and some new material models (see Eq. (1.12)) to incorporate swelling which involves a straightforward generalization of the conventional hyperelastic theory (*Pence and Tsai* (2005b); *Tsai et al.* (2004)). In this regard, chapters II to V constitute the new contributions of this research.

In Chapter II we focus attention on a class of swellable hyperelastic materials in order to examine how the constitutive theory affects the spherically symmetric expansion of a pressurized hollow sphere. The inflation response of a hyperelastic sphere in the absence of swelling is a classical problem in finite deformation continuum mechanics. As is well known, the resulting pressure-expansion response is not always given by a monotonically increasing graph. The sphere may be thick or thin. The thin wall limit corresponds to a hyperelastic swellable membrane. In the absence of swelling the class of materials corresponds to a classical Mooney-Rivlin material. The inflation response for a hollow sphere composed of the classical Mooney-Rivlin material has been extensively studied. We especially focus on a detailed characterization by *Carroll* (1987) that provides conditions that determine when the inflation response is monotone versus when it is not. We use this characterization to describe the non-swelling response of the sphere problem under consideration here. We then generalize the analysis so as to determine how swelling affects the outcome. In particular, we exhibit swelling induced transitions between monotone and non-monotone

inflation curves. When this happens, various inflation jump events can be triggered. We provide a systematic framework for understanding and predicting these transitions, and we discuss the ramifications of these transitions in terms of a snap-through type bifurcation (a swelling induced burst).

In Chapter III, we again consider a spherical inflation but now under a nonuniform swelling distribution. A family of swelling distributions is defined such that each member of the family has the same added swelling mass. We then examine the stability behavior within a family with common added mass but different spatial distributions of that mass. Numerical analysis of several examples support a hypothesis that the qualitative behavior is independent of the distribution so long as the amount of added mass remains fixed. Numerical analysis of several examples that support this hypothesis are presented. Finally, an inflation instability is demonstrated within a certain range of material parameters.

In Chapter IV we continue to employ a conventional hyperelastic model that considers the impact of swelling for the different geometry of cylindrical deformation. In this regard we obtain the responses of both a solid plug, and of a plug with an internal channel, both of which are confined by a rigid outer wall. Sufficiently large swelling leads to deformation with wall contact in which case the confinement pressure is determined. For the case of a plug with a channel, asymptotic analysis is employed to investigate the channel closure.

It is also the purpose of this thesis to explore the theory of internally balanced elastic materials for describing complex deformational response in solids that are subject to swelling. Hence, in Chapter V, we study the boundary value problem of cylindrical deformation that is laid out in Chapter IV but in the context of internally balanced

material theory. As such, we review the internal balance theory and the incorporation of swelling in order to formulate the problem and investigate the aspects of the theory that accounts for swelling.

In order to plot a picture of the structure of the formulations in this study we should note that the ground framework of this study is in the context of hyperelasticity. The equations are obtained by minimizing the energy functional involving the elastic energy density and thus our framework is based on the equilibrium deformations that are governed by the stress equations of equilibrium. These equations associated with unknown parameters and specific boundary conditions can sometimes be solved analytically and in other cases are solved with the help of numerical treatments although we mainly seek to explore analytical solutions and explanations rather than studying numerical procedures.

1.1 Hyperelastic swelling

As is standard in finite deformation continuum mechanics, let $\mathbf{X}$ be a generic position vector in a reference configuration Ω_X that is regarded as the state of an unloaded body prior to swelling. The deformation under consideration maps the coordinates of the reference configuration to the coordinates $\mathbf{x}$ in the current deformed configuration denoted by Ω_x. The gradient of the map $\mathbf{x} = \chi(\mathbf{X})$ is the tensor

$$\mathbf{F} = \partial\mathbf{x}/\partial\mathbf{X}.$$

The loading is described in the standard way in terms of boundary tractions and body forces. In addition the material expands and contracts, and this is described in terms of change in its natural free volume. This volume change is referred to as *swelling* in this study, and can vary from point to point in the form of a swelling field $v = v(\mathbf{X})$ with $v > 1$ for swelling expansion and $0 < v < 1$ for deswelling. Throughout this thesis, v is treated as a prescribed quantity. In other words it can be viewed as a control parameter. It follows that the appropriate volume constraint on the deformation is

$$\det\mathbf{F} = v, \qquad (\text{with} \quad v > 0). \tag{1.1}$$

A theory that uses (1.1) provides a generalization of the conventional theory for incompressible materials. In the context of hyperelasticity such a framework is demonstrated in *Pence and Tsai* (2005b, 2006); *Tsai et al.* (2004); *Zamani and Pence* (2017) for isotropic material behavior and in *Demirkoparan and Pence* (2007a,b, 2015a,b, 2017) for anisotropic materials. This framework has been utilized to guide the design of actuators *Fang et al.* (2011) and to analyze the behavior of biological soft tissue *Gou and Pence* (2016).

The generality of the condition (1.1) permits the phenomenological modeling of a

variety of physical swelling processes. More specificity as regards the precise swelling mechanism will generally lead to additional conditions on the physical model expressed in terms of additional constraints and equations. For example, an elastomer in a solvent bath that swells due to solvent uptake might take v in (1.1) in the form $v = 1 + \vartheta_{\rm mol}\, c_{\rm ref}$ where $c_{\rm ref}$ is the **c**oncentration of solvent molecules within the elastomer network (per unit **ref**erence volume) and $\vartheta_{\rm mol}$ is the **mol**ecular **v**olume of an individual solvent molecule. In this case our treatment can apply, but subject to $v \geq 1$. Additional equations beyond those that we present here will then enter for the purpose of determining $c_{\rm ref}$ on the basis of poroelastic diffusion. In addition, such a description presumes a completely dry (fully dessicated) reference configuration for the elastomeric constituent (which would in general differ from a natural (stress-free) configuration). Whether or not such a reference configuration description is useful may then be highly problem dependent. For additional discussion on this and other issues with respect to such more specific solute/solvent systems we defer to expert sources such as *Drozdov and Christiansen* (2013).

Complete detail on the general hyperelastic modeling treatment employed here is provided and specialized in Section 1.2 to the case of isotropic solid materials that swell. Generalizations of conventional hyperelastic models, such as the neo-Hookean model, so as to incorporate swelling are given.

The hyperelastic treatment of swelling is based on an elastic energy density W as a function of both $\mathbf{F}$ and v. The hyperelastic energy density is frame-invariant and this requires W to depend on $\mathbf{F}$ only through the right Cauchy-Green deformation tensor $\mathbf{C} = \mathbf{F}^T\mathbf{F}$. Thus $W = W(\mathbf{C}, v)$. In the absence of body forces the equilibrium equation is $\operatorname{div}\mathbf{T} = 0$ where $\mathbf{T}$ is the Cauchy stress tensor,

$$\mathbf{T} = \frac{2}{v}\mathbf{F}\frac{\partial W}{\partial \mathbf{C}}\mathbf{F}^T - p\mathbf{I}. \tag{1.2}$$

Here p is the hydrostatic pressure associated with the volume constraint (1.1). It is to be emphasized that p in (1.2) arises as a Lagrange multiplier associated with the constraint (1.1). In particular, it is not simply related to the type of pore pressure variable that is present in say hyperelastic mixture theory.

In using (1.2) it is important to realize that W gives the stored energy density with respect to a reference frame that is unswollen. Alternatively, one could consider a reference configuration in which the material is uniformly expanded. Such a uniform expansion would have deformation gradient $\mathbf{F}^* = v^{1/3}\mathbf{I}$. Thus the mapping from the unswollen reference configuration to the current configuration that passes through the uniformly swollen reference configuration is given by

$$\mathbf{F} = \hat{\mathbf{F}}\mathbf{F}^*, \tag{1.3}$$

with

$$\mathbf{F}^* = v^{1/3}\mathbf{I}. \tag{1.4}$$

This makes

$$\hat{\mathbf{F}} = v^{-1/3}\mathbf{F} \quad \text{and} \quad \det\hat{\mathbf{F}} = 1.$$

Analysis can now proceed with respect to the deformation gradient $\hat{\mathbf{F}}$ measured from the uniformly swollen reference configuration, and so one can similarly define $\hat{\mathbf{C}} = \hat{\mathbf{F}}^T\hat{\mathbf{F}}$ and hence $\hat{\mathbf{C}} = v^{-2/3}\mathbf{C}$. Let $\hat{W}(\hat{\mathbf{C}}, v)$ be the stored energy density per unit volume with respect to this uniformly swollen reference configuration. The overall stored energy calculated by integrating $\hat{W}$ using the swollen reference frame must be equal to the overall stored energy calculated by integrating W using the unswollen reference frame. This means that $W = v\hat{W}$. The material is incompressible with respect to the uniformly swollen reference configuration, and so the Cauchy stress

calculated using $\hat{W}$ is

$$\mathbf{T} = 2\hat{\mathbf{F}}\frac{\partial \hat{W}}{\partial \hat{\mathbf{C}}}\hat{\mathbf{F}}^T - \hat{p}\mathbf{I} \tag{1.5}$$

where $\hat{p}$ is the hydrostatic pressure associated with the constraint $\det\hat{\mathbf{F}} = 1$. This constraint can now be interpreted as the standard incompressibility constraint that the deformation (as measured from the uniformly swollen reference configuration) is isochoric.

Consistency of these different procedures demands that (1.5) and (1.2) yield the same result for $\mathbf{T}$. This is immediately verified by examining the derivative expression on the right side of (1.2) using $\mathbf{F} = v^{1/3}\hat{\mathbf{F}}$, $\mathbf{C} = v^{2/3}\hat{\mathbf{C}}$, $W(\mathbf{C}, v) = v\,\hat{W}(\hat{\mathbf{C}}, v)$ and invoking the chain rule:

$$\frac{2}{v}\mathbf{F}\frac{\partial W}{\partial \mathbf{C}}\mathbf{F}^T = \frac{2}{v}\Big(v^{1/3}\hat{\mathbf{F}}\Big)\underbrace{\frac{\partial}{\partial \hat{\mathbf{C}}}\Big(v\,\hat{W}(\hat{\mathbf{C}}, v)\Big)}_{v^{1/3}\frac{\partial \hat{W}}{\partial \hat{\mathbf{C}}}}\underbrace{\frac{\partial \hat{\mathbf{C}}}{\partial \mathbf{C}}}_{v^{-2/3}\mathbf{I}\boxtimes\mathbf{I}}\Big(v^{1/3}\hat{\mathbf{F}}\Big)^T = 2\hat{\mathbf{F}}\frac{\partial \hat{W}}{\partial \hat{\mathbf{C}}}\hat{\mathbf{F}}^T. \tag{1.6}$$

From this[1] it follows that taking $\hat{p} = p$ causes (1.5) and (1.2) to yield the same result for $\mathbf{T}$.

As the reader is probably aware, a multiplicative decomposition of the form $\mathbf{F} = \hat{\mathbf{F}}\mathbf{F}^*$ from (1.3) is commonly used in continuum mechanics to describe a variety of physical processes. Having invoked it here to describe swelling by taking the special case $\mathbf{F}^* = v^{1/3}\mathbf{I}$ and requiring $\det\hat{\mathbf{F}} = 1$ retrieves the well known formulation attributed to Flory (see e.g., the discussion in *Chester and Anand* (2010)). In addition, one can now contemplate other descriptions for swelling that invoke $\mathbf{F} = \hat{\mathbf{F}}\mathbf{F}^*$ with $\det\hat{\mathbf{F}} = 1$ but which weakens the condition $\mathbf{F}^* = v^{1/3}\mathbf{I}$ to something less restrictive, such as $\det\mathbf{F}^* = v$. This could offer a route to the consideration of swelling processes in which a uniform expansion in all directions is not energetically preferred, such as might be the case if there are microstructural processes that would serve to

[1] $\mathbf{I}\boxtimes\mathbf{I}$ in (1.6) is the fourth order identity tensor, i.e., $(\mathbf{I}\boxtimes\mathbf{I})_{ijkl} = \delta_{ik}\delta_{jl}$.

favor a non equi-axial expansion. Such considerations are formulated in and explained by the internal balance theory in chapter V.

1.2 Isotropic material behavior subject to swelling

The equivalent equations (1.2) and (1.5) apply to both isotropic and anisotropic behavior. The latter includes fiber reinforced materials, in which case especially designed patterns of fiber stiffening can elicit specialized deformation modes as the material swells. This study focuses solely on isotropic behavior, in which case the dependence of W on $\mathbf{C}$ can only be through the invariants of $\mathbf{C}$,

$$I_1 = \mathbf{C} : \mathbf{I} = \operatorname{tr} \mathbf{C}, \quad I_2 = \tfrac{1}{2}\big((\mathbf{C} : \mathbf{I})(\mathbf{C} : \mathbf{I}) - \mathbf{C} : \mathbf{C}\big) = \tfrac{1}{2}\big((\operatorname{tr} \mathbf{C})^2 - \operatorname{tr} \mathbf{C}^2\big). \tag{1.7}$$

The third invariant $I_3 = \det \mathbf{C}$ is equal to v^2 by virtue of (1.1) and thus $W = W(I_1, I_2, v)$. This causes the Cauchy stress tensor in (1.2) to take the form

$$\mathbf{T} = \frac{2}{v}\left(\frac{\partial W}{\partial I_1} + I_1 \frac{\partial W}{\partial I_2}\right)\mathbf{B} - \frac{2}{v}\frac{\partial W}{\partial I_2}\mathbf{B}^2 - p\mathbf{I} \tag{1.8}$$

where $\mathbf{B}$ is the left Cauchy-Green deformation tensor $\mathbf{B} = \mathbf{F}\mathbf{F}^T$. The tensor $\mathbf{B}$ is symmetric positive definite and so has positive eigenvalues, say λ_1^2, λ_2^2 and λ_3^2. Then $\lambda_1 \geq 0$, $\lambda_2 \geq 0$, $\lambda_3 \geq 0$ are the principal stretches as measured from the unswollen reference configuration. The tensors $\mathbf{B}$ and $\mathbf{C}$ have the same eigenvalues and it therefore follows from (1.7) that $I_1 = \lambda_1^2 + \lambda_2^2 + \lambda_3^2$, $I_2 = \lambda_1^2\lambda_2^2 + \lambda_2^2\lambda_3^2 + \lambda_3^2\lambda_1^2$ and $\lambda_1\lambda_2\lambda_3 = v$. For a general isotropic hyperelastic material subject to the swelling constraint (1.1), the stored energy density can equivalently be taken as a function of these stretches. In this case we shall write $W = \bar{W}(\lambda_1, \lambda_2, \lambda_3, v)$.

The Cauchy stress tensor $\mathbf{T}$ is symmetric and its eigenvalues are the principle stresses, denoted by T_1, T_2 and T_3. In the absence of swelling a standard requirement on any isotropic hyperelastic constitutive model is the well known Baker-Ericksen

inequality

$$(T_i - T_j)(\lambda_i - \lambda_j) > 0, \qquad (i \neq j, \lambda_i \neq \lambda_j, \text{no sum}). \tag{1.9}$$

This is a requirement that the maximum (minimum) principle stress direction correlates with the maximum (minimum) stretch direction. For a swellable isotropic material the same logic continues to apply and so we presume that (1.9) holds for the materials under consideration here.

The corresponding result that follows from (1.5) is that $\hat{W} = \hat{W}(\hat{I}_1, \hat{I}_2, v)$ with

$$\mathbf{T} = 2\left(\frac{\partial \hat{W}}{\partial \hat{I}_1} + \hat{I}_1 \frac{\partial \hat{W}}{\partial \hat{I}_2}\right)\hat{\mathbf{B}} - 2\frac{\partial \hat{W}}{\partial \hat{I}_2}\hat{\mathbf{B}}^2 - p\mathbf{I} \tag{1.10}$$

and $\hat{\mathbf{B}} = \hat{\mathbf{F}}\hat{\mathbf{F}}^T = v^{-2/3}\mathbf{B}$, $\hat{I}_1 = v^{-2/3}I_1$, $\hat{I}_2 = v^{-4/3}I_2$. Note in particular, that there is no obvious concept here of needing to place a $\hat{}$ over the $\mathbf{T}$ since the Cauchy traction is uniquely defined irrespective of reference configuration.

As will be discussed in what follows, the use of the unswollen reference configuration is often preferred when dealing with complex geometry, loads or swelling fields, which argues for a development based on (1.8). On the other hand, use of (1.10) corresponds more directly to the classical incompressible theory (because $\det\hat{\mathbf{F}} = 1$), with its familiar hyperelastic models (corresponding now to $\hat{W}$). Such familiar models can be pulled back to the unswollen reference configuration using $W = v\,\hat{W}$. Thus for a familiar form $\hat{W} = \hat{W}(\hat{I}_1, \hat{I}_2, v)$ it becomes natural to consider

$$W(I_1, I_2, v) = v\hat{W}(v^{-2/3}I_1, v^{-4/3}I_2, v), \tag{1.11}$$

where also any material parameters in the familiar $\hat{W}$ are allowed to become dependent upon v. For example, the conventional Mooney-Rivlin form $\hat{W}(\hat{I}_1, \hat{I}_2) = a_1(\hat{I}_1 - 3) + a_2(\hat{I}_2 - 3)$ with non-negative a_1 and a_2 becomes, under this transforma-

tion,

$$W(I_1, I_2, v) = v\, a_1(v) \left(\frac{I_1}{v^{2/3}} - 3 \right) + v\, a_2(v) \left(\frac{I_2}{v^{4/3}} - 3 \right) \tag{1.12}$$

where the notation $a_1(v)$ and $a_2(v)$ is because these parameters can now be dependent upon v. Constitutive laws similar to (1.12) have previously been used to study a variety of boundary value problems involving mass addition and volumetric change. This includes the studies of Pence and Tsai on swelling induced cavity formation in tubes *Pence and Tsai* (2005a) and spheres *Pence and Tsai* (2006). Amar and Goriely *Ben Amar and Goriely* (2005) make use of a constant material parameter version of (1.12) in the context of more generalized processes of growth to investigate instabilities in the inflation response of spherical shells when the shell wall experiences anisotropic growth. The study *Demirkoparan and Pence* (2008) analyzes swelling induced twist in fiber reinforced composites for materials where the matrix constituent swells (and is described by (1.12)) but the fibrous constituent does not swell and so admits to an alternative constitutive law. In the current and next chapter we will ultimately make use of (1.12) to study the interaction of swelling and a mechanical response when the material parameters d_2 and d_2 are also swelling dependent. Specifically, this model is considered in the next chapter and in *Zamani and Pence* (2017) for the case $a_1(v) = c_1 v^{m_0}$ and $a_2(v) = c_2 v^{n_0}$ with fixed values $c_1 \geq 0$, $c_2 \geq 0$, m_0 and n_0.

The mathematical equivalent to the constitutive law (1.12) can be expressed in the form

$$W(I_1, I_2, v) = \frac{1}{2}\mu_o \alpha v^m \left(\frac{I_1}{v^{2/3}} - 3 \right) + \frac{1}{2}\mu_o (1-\alpha) v^n \left(\frac{I_2}{v^{4/3}} - 3 \right),$$

with $\mu_o > 0$ and $0 \leq \alpha \leq 1$. Here, m and n are the material parameters and identified empirically. In this way μ_o becomes the infinitesimal shear modulus in the unswollen

reference configuration. The focus in the next chapter will be on the influence of m and n in various instability phenomena in balloons and pressurized spherical shells as such a material swells. The pure I_1 special case is found by taking $\alpha = 1$, yielding

$$W(I_1, v) = \tfrac{1}{2}\mu_o v^{(m-2/3)}(I_1 - 3v^{2/3}), \qquad \mathbf{T} = \mu_o v^{(m-5/3)}\mathbf{B} - p\mathbf{I}. \tag{1.14}$$

The no-swelling case ($v = 1$) then retrieves a neo-Hookean treatment. For later purposes of numerical demonstration we shall consider $m = 2/3$ in (1.14), giving

$$W(I_1, v) = \tfrac{1}{2}\mu_o(I_1 - 3v^{2/3}), \qquad \mathbf{T} = \frac{\mu_o}{v}\mathbf{B} - p\mathbf{I}. \tag{1.15}$$

The particular constitutive model that will be used for specific examples in next chapter is motivated by the well known Mooney-Rivlin model

$$W_{\text{MR}}(I_1, I_2) = d_1(I_1 - 3) + d_2(I_2 - 3), \tag{1.16}$$

in the classical incompressible theory where the positive constants d_1 and d_2 are empirically determined material parameters. The generalization of the Mooney-Rivlin model for swelling is to keep the basic form (1.16) while now letting d_1 and d_2 depend upon v. For this purpose we shall in what follows consider examples using the constitutive model (1.12)

$$W(I_1, I_2, v) = d_1\left(\frac{I_1}{v^{2/3}} - 3\right) + d_2\left(\frac{I_2}{v^{4/3}} - 3\right), \;\; d_1 = va_1(v), \;\; d_2 = va_2(v), \tag{1.17}$$

with $d_1 \geq 0$, $d_2 \geq 0$ and $d_1 + d_2 > 0$. Recall that the reason for the scaling $I_1/v^{2/3}$ and $I_2/v^{4/3}$ in (1.17) is that $I_1/v^{2/3} = I_2/v^{4/3} = 3$ for an equiaxial free expansion $\mathbf{F} = v^{1/3}\mathbf{I}$. This enables certain algebraic simplifications. When (1.17) holds the

Cauchy stress tensor (1.2) becomes

$$\mathbf{T} = 2\left(\frac{d_1}{v^{5/3}} + I_1\frac{d_2}{v^{7/3}}\right)\mathbf{B} - 2\frac{d_2}{v^{7/3}}\mathbf{B}^2 - p\mathbf{I}, \qquad \mathbf{B} = \mathbf{F}\mathbf{F}^T. \tag{1.18}$$

Calculating T_i and T_j from (1.18) one then obtains

$$T_i = 2\left(\frac{d_1}{v^{5/3}} + (\lambda_j^2 + \lambda_k^2)\frac{d_2}{v^{7/3}}\right)\lambda_i^2 - p, \qquad (i \neq j \neq k \neq i). \tag{1.19}$$

Using this result it follows for the material model (1.17) that

$$(T_i - T_j)(\lambda_i - \lambda_j) = 2\left(\frac{d_1}{v^{5/3}} + \lambda_k^2\frac{d_2}{v^{7/3}}\right)(\lambda_i - \lambda_j)^2(\lambda_i + \lambda_j) \tag{1.20}$$

Thus the Baker-Ericksen type condition (1.9) is automatically satisfied when W is given by (1.17) because $d_1 \geq 0$ and $d_2 \geq 0$.

CHAPTER II

Burst Instability in Uniform Swelling of Hyperelastic Spherical Shells

In chapters II and III we consider spherical symmetric deformation in a general Mooney-Rivlin type material in which swelling is taken into account. The types of Mooney-Rivlin materials that are distinguished with respect to the response to applied internal and external pressure (inflation) is central to this study. In the classical hyperelastic setting (no swelling) a basic classification of materials with regard to their qualitative pressure-inflation behavior is given in *Carroll* (1987). *Pence and Tsai* (2006) generalize Carroll's procedure so as to account for swelling and show that when swelling is uniform the basic qualitative response is preserved. I briefly review those results and then make use of the literature as a base to generalize the classification for the material types that were given by Carroll. Consequently, in this thesis, the more general type of materials are studied for which even homogeneous swelling field can cause instability to the type of behavior that they exhibit in response to the pressure-swelling interaction. Then in chapter III the effects of a non-homogeneous swelling field are investigated where it is shown that the precise way in which an overall fixed amount of swelling is distributed spatially can alter the quantitative response while preserving key features of the qualitative response.

2.1 Kinematics for radial inflation of a spherical shell

Using the framework just described in Section 1.1 we consider a finite thickness spherical shell with inner radius $R_i > 0$ and outer radius $R_o > R_i$ prior to any loading or any swelling. Attention is restricted to radially symmetric swelling $v = v(R)$. The loading is taken to consist of applied pressures P_i and P_o on the inner and outer boundaries. These symmetric conditions motivate the consideration of the symmetric deformation for *radial inflation*

$$r = r(R), \quad \theta = \Theta, \quad \phi = \Phi \tag{2.1}$$

on $R_i \leq R \leq R_o$, $0 \leq \Theta < 2\pi$, $0 \leq \Phi \leq \pi$ where the radial inflation function $r(R)$ is to be determined. Thus (2.1) is a map from reference spherical coordinates (R, Θ, Φ) to deformed spherical coordinates (r, θ, ϕ). Let $\{\mathbf{e}_R, \mathbf{e}_\Theta, \mathbf{e}_\Phi\}$ represent the unit basis vectors in the reference configuration and let $\{\mathbf{e}_r, \mathbf{e}_\theta, \mathbf{e}_\phi\}$ represent the unit basis vectors in the deformed configuration. It follows from (2.1) that the deformation gradient is given by

$$\mathbf{F} = \lambda_r(\mathbf{e}_r \otimes \mathbf{e}_R) + \lambda_\theta \mathbf{e}_\theta \otimes \mathbf{e}_\Theta + \lambda_\phi \mathbf{e}_\phi \otimes \mathbf{e}_\Phi \tag{2.2}$$

with $\lambda_r = r'$ and $\lambda_\theta = \lambda_\phi = r/R$ in which prime $'$ denotes the differentiation with respect to R ($r' = dr/dR$). Hence

$$\mathbf{C} = \mathbf{F}^T\mathbf{F} = \lambda_r^2(\mathbf{e}_R \otimes \mathbf{e}_R) + \lambda_\theta^2(\mathbf{e}_\Theta \otimes \mathbf{e}_\Theta + \mathbf{e}_\Phi \otimes \mathbf{e}_\Phi), \tag{2.3}$$

$$\mathbf{B} = \mathbf{F}\mathbf{F}^T = \lambda_r^2(\mathbf{e}_r \otimes \mathbf{e}_r) + \lambda_\theta^2(\mathbf{e}_\theta \otimes \mathbf{e}_\theta + \mathbf{e}_\phi \otimes \mathbf{e}_\phi), \tag{2.4}$$

and we observe that λ_r and $\lambda_\theta = \lambda_\phi$ are the principal stretches.

in which prime $'$ denotes the differentiation with respect to R ($r' = dr/dR$). The

swelling constraint (1.1) is

$$v = \frac{r^2 r'}{R^2}, \tag{2.5}$$

Integrating (2.5) from the inner radius R_i to a generic radial value R gives

$$r^3 = r_i^3 + 3\int_{R_i}^{R} v(\xi)\xi^2 d\xi \tag{2.6}$$

where $r_i = r(R_i)$. More generally (2.6) provides the map $r = r(R)$ in terms of the single parameter r_i which still needs to be determined. The Cauchy stress tensor takes the form

$$\mathbf{T} = T_{rr}(\mathbf{e}_r \otimes \mathbf{e}_r) + T_{\theta\theta}(\mathbf{e}_\theta \otimes \mathbf{e}_\theta + \mathbf{e}_\phi \otimes \mathbf{e}_\phi) \tag{2.7}$$

with

$$\begin{aligned} T_{rr} &= \frac{2}{v}\frac{\partial W}{\partial I_1}\lambda_r^2 + \frac{4}{v}\frac{\partial W}{\partial I_2}\lambda_r^2\lambda_\theta^2 - p, \\ T_{\theta\theta} &= \frac{2}{v}\frac{\partial W}{\partial I_1}\lambda_\theta^2 + \frac{2}{v}\frac{\partial W}{\partial I_2}(\lambda_r^2 + \lambda_\theta^2)\lambda_\theta^2 - p. \end{aligned} \tag{2.8}$$

The equilibrium equations $div\mathbf{T} = 0$ gives that $p = p(R)$ along with the requirement

$$\frac{dT_{rr}}{dr} + \frac{2}{r}(T_{rr} - T_{\theta\theta}) = 0. \tag{2.9}$$

The specified pressures P_i and P_o at the inner and outer surfaces yield the boundary conditions

$$T_{rr}\big|_{r_i} = -P_i, \quad T_{rr}\big|_{r_o} = -P_o, \tag{2.10}$$

where $r_o = r(R_o)$.

Using (2.5) and (2.8) the equilibrium equation (2.9) provides an ordinary differential equation for $p(R)$ which can be integrated. The two boundary conditions (2.10) determine the integration constant that emerges from this integration as well as the

scalar r_i. Once r_i is so determined the whole kinematics $r = r(R)$ then follows from (2.6) and consequently the deformation gradient tensor $\mathbf{F}$ is fully known. This constitutes the most obvious solution procedure for determining the output response $r(R)$ as a function of the input swelling field $v(R)$ and the input pressure values P_i and P_o.

There is however a shortcut that gets to the same result by making direct use of the stored energy density in terms of the principle stretches $\bar{W}(\lambda_r, \lambda_\theta, \lambda_\phi, v)$. It is based on a straight forward adaptation of a well known procedure from hyperelasticity when no swelling is present. This earlier procedure corresponds to the special case $v \equiv 1$ in the present treatment. Because $W(I_1, I_2, v) = \bar{W}(\lambda_r, \lambda_\theta, \lambda_\phi, v)$ with $\lambda_\theta = \lambda_\phi$ one may employ the chain rule for the differentiation in (2.8) in the form

$$\frac{\partial W}{\partial I_1} = \frac{\partial \bar{W}}{\partial \lambda_r}\frac{\partial \lambda_r}{\partial I_1} + 2\frac{\partial \bar{W}}{\partial \lambda_\theta}\frac{\partial \lambda_\theta}{\partial I_1}, \tag{2.11}$$

with

$$\frac{\partial \lambda_r}{\partial I_1} = \frac{\lambda_r^2 + \lambda_\theta^2}{2\lambda_r(\lambda_r^2 - \lambda_\theta^2)}, \qquad \frac{\partial \lambda_\theta}{\partial I_1} = \frac{\lambda_\theta}{2(\lambda_\theta^2 - \lambda_r^2)}. \tag{2.12}$$

A similar differentiation applies with respect to I_2 and on this basis one confirms that

$$T_{rr} = \frac{\lambda_r}{v}\frac{\partial \bar{W}}{\partial \lambda_r} - p, \qquad T_{\theta\theta} = T_{\phi\phi} = \frac{\lambda_\theta}{v}\frac{\partial \bar{W}}{\partial \lambda_\theta} - p. \tag{2.13}$$

Introduce the variable

$$s = r/R, \tag{2.14}$$

which, in view of (2.2), is the biaxial stretch $\lambda_\theta = \lambda_\phi$. Also let $s_i = r_i/R_i$ and $s_o = r_o/R_o$ and note that (2.6) gives

$$s_o^3 = \left(\frac{R_i}{R_o}\right)^3 s_i^3 + \frac{3}{R_o^3}\int_{R_i}^{R_o} v(R)R^2 dR. \tag{2.15}$$

In this regard, the following derivation will be useful for the formulations in the next

section

$$\frac{ds}{dr} = \frac{ds/dR}{dr/dR} = \frac{Rr^{'} - r}{R^2 r'} = \frac{v - s^3}{Rv}, \tag{2.16}$$

where the last step from the above chain of equations is due to (2.5). The relation (2.16) together with (2.5) gives

$$\lambda_r = r^{'} = v/s^2, \qquad \lambda_\theta = \lambda_\phi = r/R = s, \tag{2.17}$$

and hence $\bar{W}(\lambda_r, \lambda_\theta, \lambda_\phi, v) = \bar{W}(v/s^2, s, s, v)$. Now define

$$w(s, v) = \bar{W}(v/s^2, s, s, v) \tag{2.18}$$

and calculate the derivative

$$\frac{\partial w(s,v)}{\partial s} = \frac{\partial \bar{W}}{\partial \lambda_r}\frac{\partial \lambda_r}{\partial s} + 2\frac{\partial \bar{W}}{\partial \lambda_\theta}\frac{\partial \lambda_\theta}{\partial s} = -\frac{2v}{s^3}\frac{\partial \bar{W}}{\partial \lambda_r} + 2\frac{\partial \bar{W}}{\partial \lambda_\theta}. \tag{2.19}$$

The combination of (2.17), (2.19) and (2.13) gives $T_{rr} - T_{\theta\theta} = -(s/2v)\partial w(s,v)/\partial s$ so that the equilibrium equation (2.9) can be expressed as

$$\frac{dT_{rr}}{dr} = \frac{s}{rv}\frac{\partial w(s,v)}{\partial s}. \tag{2.20}$$

This is now integrated with the aid of (2.10) and (2.16) to yield

$$\Delta P \equiv P_i - P_o = \int_{s_i}^{s_o} \frac{1}{v - s^3}\frac{\partial w(s,v)}{\partial s} ds. \tag{2.21}$$

Because s_o is determined by s_i from (2.15) it follows that ΔP from (2.21) is indeed a function of s_i. In the absence of swelling, meaning that $v = 1$ identically, (2.21) retrieves a standard expression from conventional incompressible, isotropic hyperelasticity (see (7.18) of *Green and Shield* (1950) and (5.3.21) of *Ogden* (1997)). The

above swelling generalization is equivalent to that given in (22) of *Pence and Tsai* (2006).

In general the swelling field v could depend on position within the shell wall, i.e., $v = v(R)$. This would then require v to be treated as a function of s for the purpose of the integration in (2.21), say $v(R) = \hat{v}(s)$. Such a treatment will be developed later in chapter III but not do so in this chapter. *In this chapter we restrict attention to homogeneous swelling in the shell wall. This means that v is constant as a function of R, however such a v could vary with time in a quasi-static fashion.* Thus in this chapter we now restrict attention to homogeneous swelling where v is a time-dependent parameter. However, note that throughout this work, ΔP *and v serve as independent control variables* in both cases of uniform and varying swelling fields.

It now follows from (2.6) that

$$r = \left(r_i^3 + v(R^3 - R_i^3)\right)^{1/3}. \tag{2.22}$$

For the case of material model (1.17), one obtains that

$$w(s, v) = \left(\frac{v^2/s^4 + 2s^2}{v^{2/3}} - 3\right) d_1 + \left(\frac{s^4 + 2v^2/s^2}{v^{4/3}} - 3\right) d_2 \tag{2.23}$$

and this in turn puts (2.21) in the form

$$\Delta P = \int_{s_i}^{s_o} \frac{4}{v - s^3} \left[\left(\frac{s}{v^{2/3}} - \frac{v^{4/3}}{s^5}\right) d_1 + \left(\frac{s^3}{v^{4/3}} - \frac{v^{2/3}}{s^3}\right) d_2 \right] ds. \tag{2.24}$$

Note that (2.24) continues to allow for the possibility of $d_1 = d_1(v)$ and $d_2 = d_2(v)$. Equation (2.24) in conjunction with

$$s_o = \frac{1}{R_o} \left(R_i^3 \; s_i^3 + v(R_o^3 - R_i^3)\right)^{1/3} \tag{2.25}$$

provides the general relation between: amount of swelling v, applied pressure ΔP, and inner radius expansion $r_i = s_i\ R_i$ for a material with swelling dependent stored energy density (1.17). Although the integration associated with (2.24) could certainly be performed, the resulting lengthy analytical expression does not provide much insight. Instead, we obtain results by generalizing ideas put forward by Carroll in the context of the incompressible theory (in which there is no swelling concept).

2.2 The role of swelling in the pressure-inflation relation

In the absence of swelling, the inflation of a pressurized spherical shell is a classical problem that has been widely studied within the theory of incompressible finite hyperelasticity, i.e., with the constraint $\det\mathbf{F} = 1$. As first discussed in detail by *Green and Shield* (1950), a radially symmetric spherical inflation is possible in every isotropic homogeneous incompressible hyperelastic material. Ultimately, it is given by the $v = 1$ version of (2.21) and (2.23). This permits the construction of an *inflation graph*, which is a plot of ΔP as a function of r_i. A basic discussion on different qualitative forms for the inflation graph is given by *Carroll* (1987). This in turn allows one to identify different material classes. As we now show, these concepts readily generalize so as to provide similarly useful organizing concepts when swelling takes place.

2.2.1 Uniform expansion occurs for homogeneous swelling in the absence of pressure

While the discussion in *Carroll* (1987) made no reference to the swelling concept, the concept is easily introduced into the treatment. Namely, there is now a separate inflation graph for each value of v. As v is increased continuously, it generates a family of inflation graphs in a continuous fashion. We consider the basic features of this family of graphs for a material obeying the Baker-Ericksen type condition (1.9). Using (2.17) this condition, henceforth referred to as the *B-E* condition, becomes

$$(T_{rr} - T_{\theta\theta})(\lambda_r - \lambda_\theta) = \frac{s^3 - v}{2v\,s}\frac{\partial w}{\partial s} = \underbrace{-\frac{(v - s^3)^2}{2vs}}_{\leq 0}\ \underbrace{\frac{1}{v - s^3}\frac{\partial w}{\partial s}}_{\text{integrand of (2.21)}} \quad . \tag{2.26}$$

Thus the B-E condition (1.9) gives that the integrand in (2.21) is negative at all locations where $\lambda_r \neq \lambda_\theta$. What happens if $\lambda_r = \lambda_\theta$? Isolated locations where λ_r and λ_θ coincide have no effect on the overall integral. This leaves a case in which λ_r and

λ_θ coincide on some interval in s. In that case $r' = r/R = v^{1/3}$ on that interval. Then, because $s = r/R = v^{1/3}$ which is a single value, the interval is in fact just a single point. We conclude that (1.9) ensures that the integrand of (2.21) is negative except at possible isolated locations that do not effect the evaluation of the integral.

It is useful to remark upon the special case for which $\lambda_r = \lambda_\theta$ for all R within the shell wall. This corresponds to $r' = r/R = v^{1/3}$ for all R, i.e., $r^3 = vR^3$ throughout the spherical shell. This represents a *uniform expansion*. For a uniform expansion it follows that $s = r/R = v^{1/3}$ for all R so that $s_o = s_i = v^{1/3}$. Consequently the limits of integration in (2.21) are identical and thus $\Delta P = 0$. This gives the baseline result:

- In the absence of pressurization ($\Delta P = 0$), homogeneous swelling causes the sphere to undergo uniform expansion ($r^3 = vR^3$). This gives $\lambda_\theta = \lambda_r$ and $T_{rr} = T_{\theta\theta}$ for all R.

Such a homogeneous swelling expansion is represented by the point $(s_i, \Delta P) = (v^{1/3}, 0)$ on the inflation graph.

Suppose now that $r^3 > vR^3$, i.e., an amount of inflation that exceeds uniform expansion. This will be the case if $r_i > v^{1/3}R_i$. Then $s^3 = r^3/R^3 > v$ and it follows from (2.16) that $ds/dr < 0$ and hence $s_o < s_i$. Thus the integral in (2.21), because the integrand is negative, gives $\Delta P > 0$. Furthermore $\lambda_\theta = r/R > v^{1/3}$, $\lambda_r = r' = vR^2/r^2 < v^{1/3}$ and hence $T_{\theta\theta} > T_{rr}$ for all R. Consequently one obtains another useful result, the first part of which is also intuitive:

- A positive pressurization $\Delta P > 0$ causes the inflation to exceed that of the uniform expansion due to the swelling alone. Then $\lambda_r < v^{1/3} < \lambda_\theta$ and $T_{rr} < T_{\theta\theta}$ for all R.

In a similar fashion, it follows that $\Delta P < 0$ gives an inflation that is less than that of a swelling induced uniform expansion. In such a case one might also expect various

wrinkling type instabilities that break the spherical symmetry. For this reason we restrict attention to $\Delta P \geq 0$. For the same reason we also avoid the consideration of de-swelling ($0 < v < 1$).

2.2.2 Qualitative behavior in the absence of swelling

For a specified value of v the form of the pressure-inflation graph is determined by the stored energy density W using (2.21). The resulting relation between ΔP and $s_i = r_i/R_i$ is dependent on the shell thickness. This shell thickness will be characterized by the thickness ratio parameter

$$\xi \stackrel{\text{def}}{=} R_i/R_o, \qquad 0 < \xi < 1. \tag{2.27}$$

The *thin shell limit* is then $\xi \to 1$. The other limit of $\xi \to 0$ can be viewed either as a microvoid in a finite body or as a spherical hole in an infinite body.

If $v = 1$, i.e. no swelling at all, then we are in the domain of conventional incompressible hyperelasticity and the problem reduces to one that has been extensively studied. In this conventional incompressible hyperelastic context, *Carroll* (1987) identifies three different types of behavior which he names type (a), type (b) and type (c). These three types are diagrammed in Figure 2.1 and are described as follows:

- type (a) behavior: ΔP increases monotonically with increasing r_i;
- type (b) behavior: ΔP increases to a maximum value and then decreases to a nonnegative asymptotic value;
- type (c) behavior: ΔP first increases to a local maximum, then decreases to a local positive minimum before again monotonically increasing.

In the hyperelastic theory without swelling, certain stored energy forms W always give an inflation graph with type (a) behavior. The Mooney-Rivlin material (1.16) specialized to $d_1 = 0$ and $d_2 > 0$ is such a material.

Other stored energy forms always give an inflation graph with type (b) behavior; the neo-Hookean material, meaning a Mooney-Rivlin material (1.16) with $d_2 = 0$ and $d_1 > 0$, is such a material.

Finally there are certain stored energy forms that give type (a) behavior if ξ is relatively small but give type (c) behavior if ξ is relatively large (close to one). The Mooney-Rivlin material (1.16) with $d_1 = 10d_2$ is such a material. For these materials there is a transitional value of the thickness ratio $R_i/R_o = \xi$, say $\xi_{a/c}$, such that $\xi < \xi_{a/c}$ implies type (a) behavior and $\xi > \xi_{a/c}$ implies type (c) behavior. Alternatively stated, these materials have a type (c) inflation graph for thin shell geometries but have a type (a) inflation graph for thick shell geometries. While the above classification framework was established by *Carroll* (1987) for the incompressible theory ($v \equiv 1$) we now use it to describe the swelling materials under consideration.

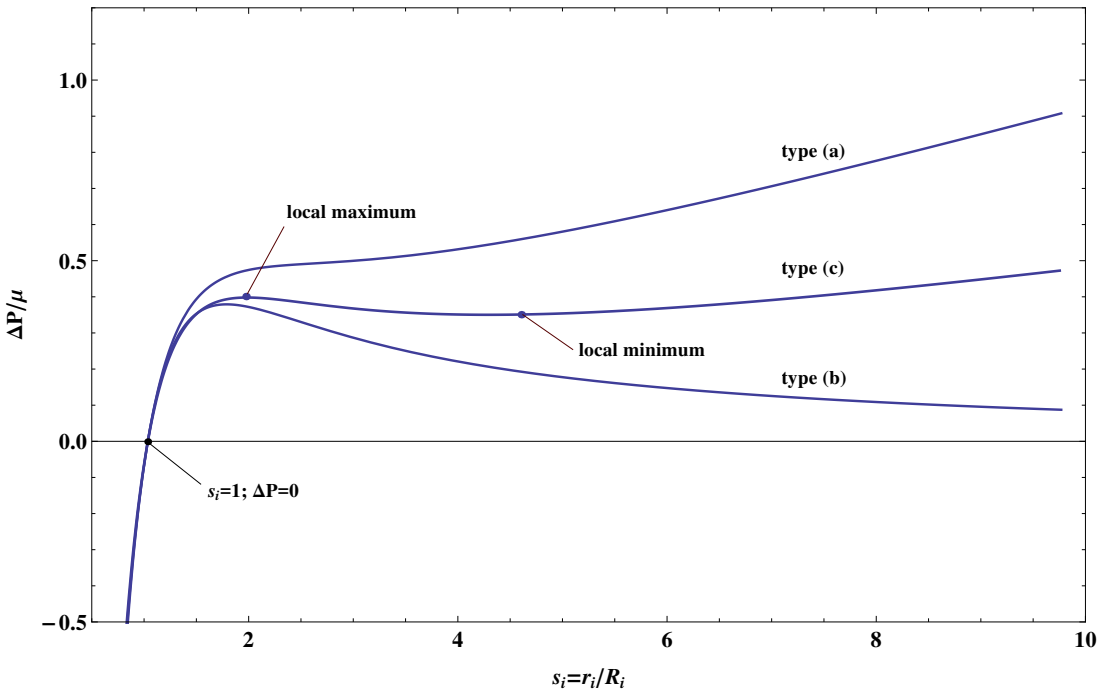

Figure 2.1 Inflation graphs showing three qualitatively different types of behavior (a)-(c) in the absence of swelling. These particular graphs correspond to W given by (1.16), all with thickness ratio $\xi = 0.5$. The differences are due to the values of d_1 and d_2. Here: $d_1 = 4d_2$ (top); $d_1 = 9d_2$ (middle); and $d_2 = 0$ (bottom).

2.2.3 Quantitative determination of the inflation behavior type

For any fixed value $v > 1$ the inflation graph will continue to display one of the various behaviors shown in Figure 2.1. However changes in v could cause a transition from one behavior type to another. For this reason it is useful to obtain a more quantitative characterization of the conditions that distinguish the different graph behaviors. The presence of either a local maximum or a local minimum in the inflation graph is dependent on whether the derivative $\dfrac{d}{ds_i}(\Delta P)$ vanishes for some value of s_i. It follows from (2.21) that this derivative is given by

$$\frac{d}{ds_i}(\Delta P) = \frac{s_i^2}{v - s_i^3}\left(\frac{1}{s_o^2}\frac{\partial w}{\partial s}\bigg|_{s_o} - \frac{1}{s_i^2}\frac{\partial w}{\partial s}\bigg|_{s_i}\right), \tag{2.28}$$

where use has been made of (2.6) and the connections

$$s_o^3 = s_i^3\xi^3 + v(1-\xi^3), \qquad \frac{ds_o}{ds_i} = \xi^3\frac{s_i^2}{s_o^2}. \tag{2.29}$$

Equation (2.28) shows that the inflation graph will have a zero slope location only if the following condition is met:

$$\frac{d}{ds_i}(\Delta P) = 0 \qquad \Leftrightarrow \qquad \frac{1}{s_o^2}\frac{\partial w}{\partial s}\bigg|_{s_o} = \frac{1}{s_i^2}\frac{\partial w}{\partial s}\bigg|_{s_i}. \tag{2.30}$$

To make use of this condition let η be the similarity variable v/s^3. Because we restrict attention to $\Delta P \geq 0$ it then follows that $r \geq v^{1/3}R$ and hence

$$0 < \eta = v/s^3 \leq 1. \tag{2.31}$$

Next define the auxiliary function

$$G(\eta, v) \stackrel{\text{def}}{=} \tfrac{1}{2}v^{1/3}\eta^{2/3}\frac{\partial w(s,v)}{\partial s}\bigg|_{s=(\eta/v)^{-1/3}}. \tag{2.32}$$

Using (2.32) it follows that condition (2.30) is equivalently expressed as

$$\frac{d}{ds_i}(\Delta P) = 0 \qquad \Leftrightarrow \qquad G(\eta_i, v) = G(\eta_o, v), \tag{2.33}$$

with

$$\eta_i = v/s_i^3, \qquad \eta_o = v/s_o^3. \tag{2.34}$$

Conditions (2.13), (2.19) and (2.32) enable a physical interpretation for the function G in terms of swelling v, stretch $s = \lambda_\theta$, and stresses $T_{\theta\theta}, T_{rr}$, namely

$$G(\eta, v)\Big|_{\eta = vR^3/r^3} = \frac{v^2}{\lambda_\theta^3}(T_{\theta\theta} - T_{rr}). \tag{2.35}$$

Now for any fixed value v, the development in Section (2.2.2) showed that a uniform expansion takes place if $\Delta P = 0$. This means that $s = r/R = v^{1/3}$ for all R so that, in particular, $s_o = s_i = v^{1/3}$ and hence $\eta_i = \eta_o = 1$. Because all of the principle stretches are then coincident one also obtains from (2.13) that $T_{\theta\theta} = T_{rr}$. Consequently (2.35) indicates that

$$G(1, v) = 0. \tag{2.36}$$

Conversely, $\Delta P > 0$ gives $s_i > s_o > v^{1/3}$ which in turn implies $s_i^3 > s_o^3 > v$ and hence $0 < v/s_i^3 < v/s_o^3 < 1$. It follows that the first arguments of G in (2.33) are ordered

$$0 < \eta_i < \eta_o < 1 \quad \text{when} \quad \Delta P > 0. \tag{2.37}$$

Also in this case the B-E inequality (1.9) gives $T_{\theta\theta} > 0 > T_{rr}$ at each location R of the nonuniform spherical expansion. Hence (2.35) yields

$$G(\eta, v) > 0 \quad \text{ for } 0 < \eta < 1. \tag{2.38}$$

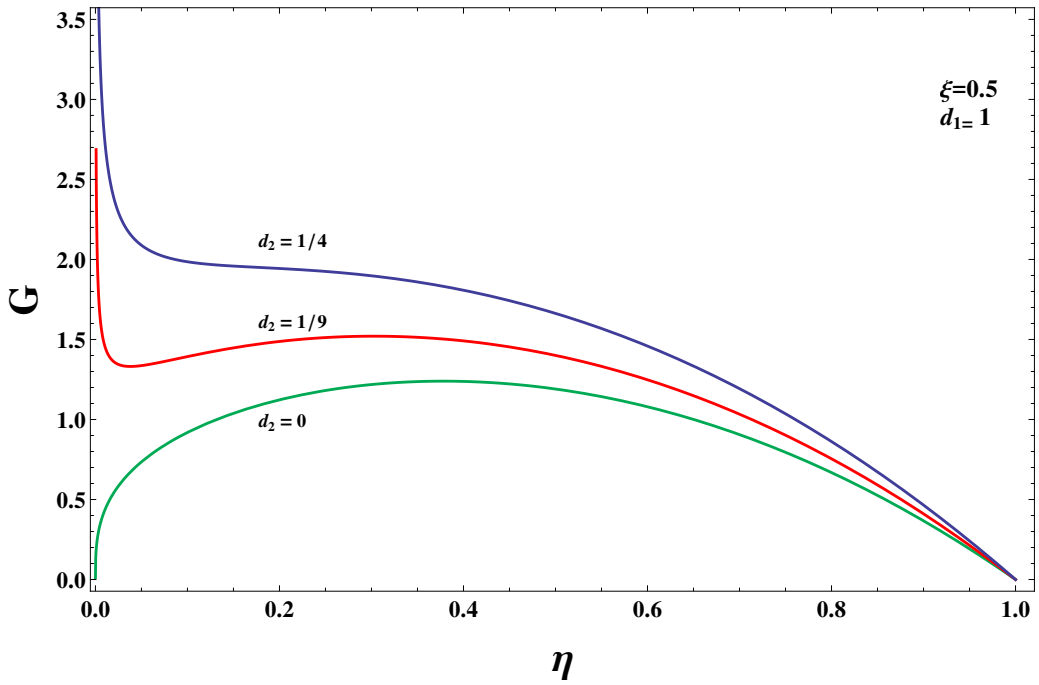

Figure 2.2 Graphs for $G(\eta, v)$ corresponding to the three inflation curves in Figure 2.1. The function $G(\eta, v)$ is computed on the basis of (2.32) using (1.17) and taking $v = 1$. This is equivalent to using (1.16) and ultimately gives the expression (2.43) that we examine in more detail later.

Figure 2.2 shows graphs for $G(\eta, v)$ corresponding to each of the three inflation curves displayed in Figure 2.1 computed on the basis of (2.32) taking $v = 1$. The three graphs are ordered from top to bottom in the same way as the graphs in Figure 2.1. Note that each of the three graphs in Fig. 2.2 obey both of the conditions (2.36) and (2.38). The two top curves tend to ∞ as $\eta \to 0$ while the bottom curve goes to zero at $\eta = 0$. The top curve is monotone decreasing, the middle curve is decreasing-increasing-decreasing, and the bottom curve is increasing-decreasing. As we discuss next, these behaviors correlate with the type (a), type (c) and type (b) behaviors exhibited in Figure 2.1.

To make direct contact with condition (2.33) we define the function that maps η_i to η_o for the specific thickness ratio ξ under consideration. In view of (2.29) this function is

$$\hat{\eta}_o(\eta_i, \xi) \stackrel{\text{def}}{=} \frac{\eta_i}{\xi^3 + \eta_i(1 - \xi^3)}. \tag{2.39}$$

The function $\hat{\eta}_o$ is now used to define the composite function $H \stackrel{\text{def}}{=} \{G \circ \hat{\eta}_o\}$, i.e.,

$$H(\eta, v, \xi) \stackrel{\text{def}}{=} G\big(\hat{\eta}_o(\eta, \xi), v\big). \tag{2.40}$$

We now have two functions: $G(\eta, v)$ defined in (2.32) and $H(\eta, v, \xi)$ defined in (2.40). In general these are different functions of their first argument η. An exception occurs when $\xi = 1$. This is because (2.39) gives $\hat{\eta}_o(\eta_i, 1) = \eta_i$ which in turn provides $G(\eta_i, v) = H(\eta_i, v, 1)$.

The stationary value characterization (2.33) is now expressed as

$$\frac{d}{ds_i}(\Delta P) = 0 \qquad \Leftrightarrow \qquad G(\eta_i, v) = H(\eta_i, v, \xi). \tag{2.41}$$

We seek to determine under what circumstances, namely for what values (η_i, v, ξ), the condition (2.41) is met. For this reason we now, for the rest of this section, use η_i for the first argument of both G and H. The previous result (2.38) establishes that $G(\eta_i, v)$ is a strictly positive function of η_i on $0 < \eta_i < 1$. The function $H(\eta_i, v, \xi)$ is similarly strictly positive on $0 < \eta_i < 1$. Also (2.36) gives that $H(1, v, \xi) = G(1, v) = 0$.

Fix the value v and consider the graphs of $G(\eta_i, v)$ and $H(\eta_i, v, \xi)$ as a function of η_i on the interval $0 < \eta_i \leq 1$ for different values of ξ. Because $G(1, v) = H(1, v, \xi) = 0$ these graphs meet at the endpoint $\eta_i = 1$. However because of inequality (2.37):

> *The graph of H is shifted to the left of the graph of G on the interval $0 < \eta_i < 1$. The amount of this shift is nonuniform in η_i and is dependent upon ξ.*

In the thin shell limit $\xi \to 1$ this shift becomes vanishingly small. Figure 2.3 shows such a leftward shift for each of the three G graphs from Figure 2.2. In particular, each of the Fig. 2.2 graphs is redisplayed as solid curve. The left shifted graphs are displayed as dashed curves of the same color. We take $\xi = 0.5$ because this gives the

thickness ratio associated with the curves from Figure 2.1. Because $\xi = 0.5$ is not close to one (i.e., the shell is thick) the amount of leftward shift is large and this causes the H curves to become distorted relative to the original G curves. However, what is not changed for each same color pair is the monotonicity properties: decreasing for the blue pair, decreasing-increasing-decreasing for the red pair, increasing-decreasing for the green pair. In other words the monotonicity properties of H as a function of η_i do not vary with ξ and so can be regarded as inherited from the original function G.

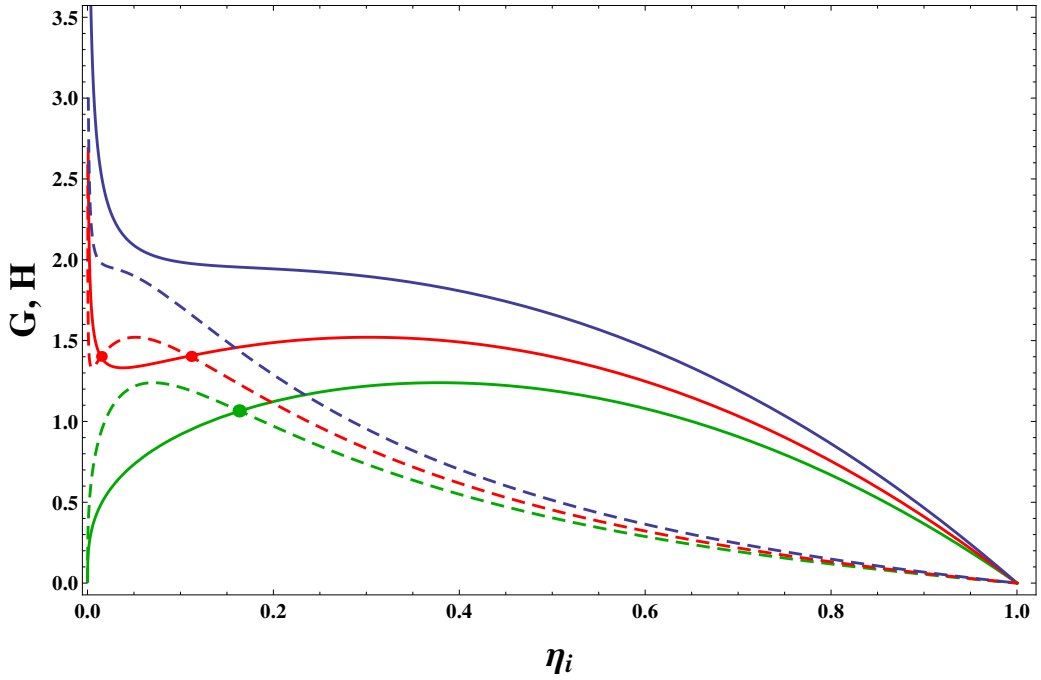

Figure 2.3 G graphs from Fig. 2.2 (solid) along with the corresponding H graphs (dashed) for thickness ratio $\xi = 0.5$. Each point on a G graph is shifted to the left to give a corresponding point on the H graph. This shift is small if ξ is close to one (a thin shell). Here, because ξ is not very close to one, the nonuniform shift distorts the curves, however the basic monotonicity properties do not change.

Condition (2.41) holds if and only if the graph of G intersects the graph of H somewhere on the interval $0 < \eta_i < 1$. If such an intersection occurs, then the associated value of η_i locates either a maximum or a minimum in the corresponding inflation graph. We now consider the consequences of this observation for each of the

three different forms of G shown in Figure 2.2:

The first and simplest G graph form is one that is monotonically decreasing as a function of η_i. In this case the graph of G cannot intersect its shifted image H. Consequently,

- forms for W that generate a monotonically decreasing G as a function of η_i always give a type (a) inflation graph.

This case is represented by the pair of blue curves in Figure 2.3. The solid and dashed blue curves do not intersect, and consequently the corresponding inflation graph in Figure 2.1 is monotone.

The second graph form for G is one in which it is decreasing-increasing-decreasing as a function of η_i as represented by the red curve of Figure 2.2. It then follows that a small shift to the left of this graph will result in two intersections of the original graph with its shifted image. The associated inflation graph will then have a local maximum followed by a local minimum, in other words type (c) behavior. In this graphical construction the amount of shift increases as ξ decreases from $\xi = 1$, i.e., as the shell gets thicker. This is represented by the pair of red curves in Figure 2.3. There are two points of intersection, and these correspond to the local maximum and local minimum of the middle curve in Figure 2.1.

Eventually however, the amount of shift will be sufficient to cause the shifted graph to clear itself of any intersection with the original graph. The specific shift associated with just losing this intersection involves the two intersection points coming together at a single special intersection point where the two graphs now have a common tangent. At this special shift, not only does (2.41) hold, but also

$$\frac{\partial}{\partial \eta_i} G(\eta_i, v) = \frac{\partial}{\partial \eta_i} H(\eta_i, v, \xi). \tag{2.42}$$

This now becomes an equation for the value of ξ associated with a transition from

type (c) behavior to type (a) behavior. Consequently:

- forms for W that generate a G function that is decreasing-increasing-decreasing on $0 < \eta_i < 1$ give type (c) inflation behavior for thin shells and type (a) inflation behavior for thick shells. The special transition value $\xi = \xi_{a/c}$ is found by simultaneous solution of (2.41) and (2.42) for η_i and ξ.

The third and final graph form for G is one that obeys $G = 0$ at $\eta_i = 0$ and which then increases with η_i before decreasing back to zero at $\eta_i = 1$. In this case all left shifted curves for H will have exactly one intersection with the original G curve. Hence there will be a type (b) inflation graph for all values of ξ. Consequently:

- forms for W that generate a G function that is increasing-decreasing on $0 < \eta_i < 1$ always give a type (b) inflation graph.

It is important to realize that the above inflation graph characterization in terms of G has focused on the effect of η_i and ξ irrespective of the value of v. In other words the homogeneous swelling value v has been regarded as a fixed parameter in all of the above discussion. However, for a given stored energy density $W(I_1, I_2, v)$ the conclusions based on the above G graph treatment for one value of v could differ from the conclusions obtained for a different value of v. For example, the graph of G could be monotonically decreasing with η_i for values of v at and near $v = 1$, but could be decreasing-increasing-decreasing for relatively larger values of v. In such a case, if the shell is sufficiently thin, such a W would lead to a type (a) inflation graph when the material is unswollen but would give a type (c) inflation graph when the material is swollen. It is this issue of swelling induced changes in qualitative behavior to which we now turn our attention.

2.3 The swellable Mooney-Rivlin material

We illustrate the effect of a changing amount of swelling using the material constitutive law (1.17). Thus for $v = 1$ this retrieves the familiar Mooney-Rivlin form (1.16).

2.3.1 Inflation behavior prior to swelling

Setting $v = 1$ in $G(\eta, v)$ gives a function that shall be denoted by $g(\eta)$, i.e., $g(\eta) \stackrel{\text{def}}{=} G(\eta, 1)$. This removes v from consideration and effectively reduces the analysis procedure to that described by *Carroll* (1987) for conventional incompressible isotropic hyperelastic materials (i.e., no volume change). For the conventional Mooney-Rivlin material (1.16) this function is given by

$$g(\eta) = 2d_1(\eta^{1/3} - \eta^{7/3}) + 2d_2(\eta^{-1/3} - \eta^{5/3}). \tag{2.43}$$

Note that $g(1) = 0$. Also $g(\eta) \to \infty$ as $\eta \to 0$ provided that $d_2 > 0$. However if $d_2 = 0$ then $g(0) = 0$. Indeed the cases used in generating the graphs in Figures 2.1 - 2.3 all corresponded to this specific example.

By considering the equivalent of the derivative of g, *Carroll* (1987) shows how the monotonicity of this g is dependent upon the parameter ratio d_2/d_1. In particular, the following critical value

$$(d_2/d_1)|_{cr} \stackrel{\text{def}}{=} \max_{0<\eta<1} \left[\frac{\eta^{-2/3} - 7\eta^{4/3}}{5\eta^{2/3} + \eta^{-4/3}} \right] \approx 0.215 \tag{2.44}$$

has special significance. Carroll shows that if d_2/d_1 is greater than this critical value then $g(\eta)$ is monotone decreasing on $0 < \eta \leq 1$, but if d_2/d_1 is less than this critical value then $g(\eta)$ is decreasing-increasing-decreasing.

For our purposes it is convenient to examine the resulting consequences after

expressing d_1 and d_2 in the form

$$d_1 = \tfrac{1}{2}\alpha\mu, \qquad d_2 = \tfrac{1}{2}(1-\alpha)\mu \tag{2.45}$$

which in turn gives

$$\frac{d_2}{d_1} = \frac{1-\alpha}{\alpha}, \qquad \alpha = \frac{d_1}{d_1+d_2}. \tag{2.46}$$

The reason for introducing (2.45) and (2.46) is that it makes $\mu > 0$ the shear modulus. Indeed using (2.45) in (1.16) gives an alternative standard way of writing the Mooney-Rivlin energy form. The parameter α is in the interval $0 \leq \alpha \leq 1$. The special ratio of d_2/d_1 given in (2.44) corresponds to the critical value

$$\alpha_{cr} = \left.\frac{d_1}{d_1+d_2}\right|_{cr} = \left.\frac{1}{1+(d_2/d_1)}\right|_{cr} \approx 0.823. \tag{2.47}$$

The derivative $dg/d\eta = g^{'}(\eta)$ that is computed from (2.43) has two roots if α is in the range $\alpha_{cr} < \alpha < 1$ and has no roots if α is in the range $0 \leq \alpha < \alpha_{cr}$. This identifies the behavior of the inflation graph as follows:

- If $0 \leq \alpha < \alpha_{cr}$ then the function g is monotonically decreasing with η. The inflation graph has no stationary value and so gives type (a) behavior for all ξ.

- If $\alpha_{cr} < \alpha < 1$ then the function g is decreasing-increasing-decreasing. The behavior is either type (a) or type (c) depending on whether ξ is greater or less than a transitional value $\xi_{a/c} = \xi_{a/c}(\alpha)$. If $\xi > \xi_{a/c}$ then the behavior is type (c). If $\xi < \xi_{a/c}$ then the behavior is type (a).

- If $\alpha = 1$ then $d_2 = 0$ and $g(0) = 0$. This is the neo-Hookean special case and the function g has only one stationary value. The behavior is then type (b) for all ξ.

As described in the discussion following (2.42), the transition value of ξ when $\alpha_{cr} <$

$\alpha < 1$ can be obtained by simultaneous solution of (2.41) and (2.42). This gives a value $\xi_{a/c} = \xi_{a/c}(\alpha)$ for each value of α in the range $\alpha_{cr} < \alpha < 1$ when $v = 1$. The curve $\xi = \xi_{a/c}(\alpha)$ is plotted in Figure 2.4. Any ordered pair (ξ,α) that is above the curve $\xi = \xi_{a/c}$ corresponds to a structure (characterized by ξ) composed of a material (characterized by α) that gives an inflation graph having type (c) behavior. Conversely, ordered pairs (ξ,α) below the curve $\xi = \xi_{a/c}$ correspond to a structure-material combination with a type (a) inflation graph. All of this follows directly from Carroll's work in *Carroll* (1987).

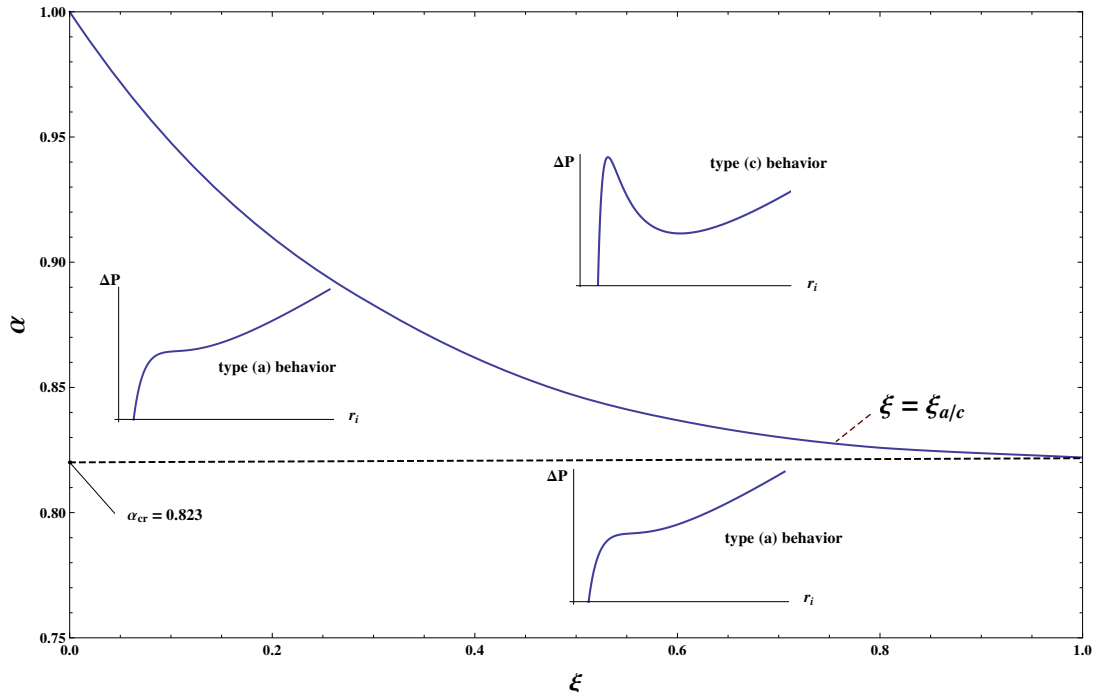

Figure 2.4 Qualitative behavior of the inflation graph for the Mooney-Rivlin model $W = d_1(I_1 - 3) + d_2(I_2 - 3)$ as a function of material parameter $\alpha = d_1/(d_1 + d_2)$ and thickness ratio $\xi = R_i/R_o$. The curve $\xi = \xi_{a/c}$ provides a transition between type (c) and type (a)-behavior.

2.3.2 Inflation graph sequences for increasing swelling

When swelling is present we consider the generalization of (1.16) that is given by (1.17). Then g as given by (2.43) generalizes to

$$G(\eta, v) = 2(\eta^{1/3} - \eta^{7/3})d_1(v) + 2(\eta^{-1/3} - \eta^{5/3})d_2(v). \tag{2.48}$$

The direct correspondence between (2.48) and (2.43) is due to the scalings $I_1/v^{2/3}$ and $I_2/v^{4/3}$ in (1.17). This allows the analysis of G in (2.48) to proceed in a similar fashion to the previous analysis of (2.43). The main difference is that now we must account for the possible dependence of the ratio d_2/d_1 upon v.

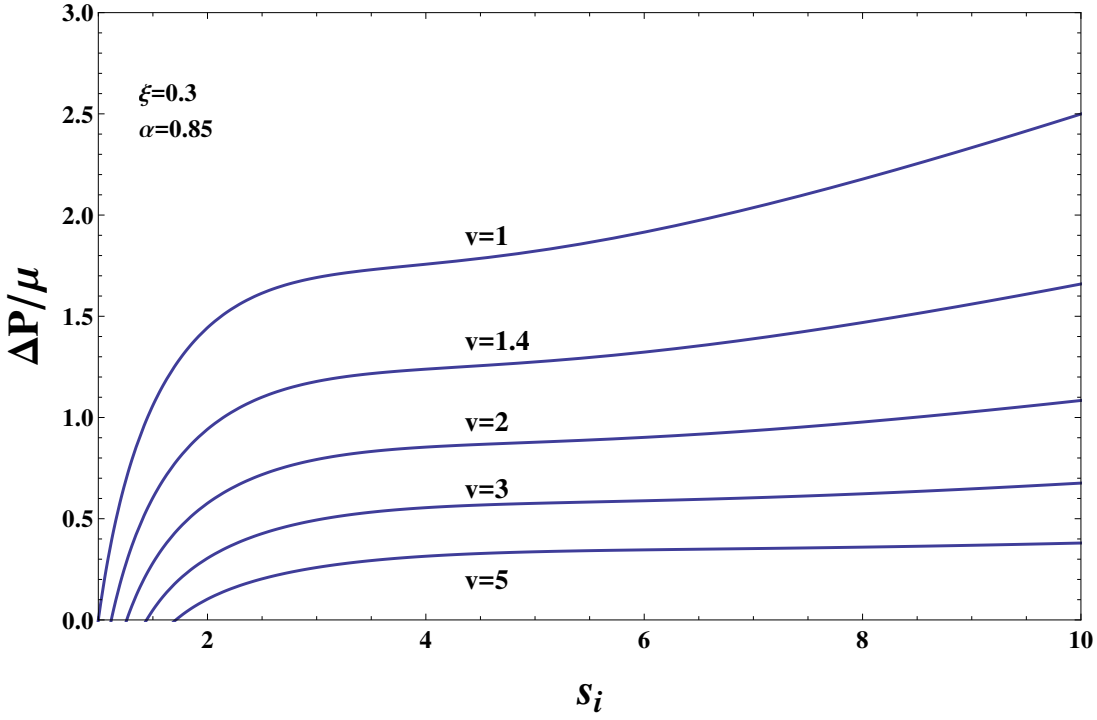

Figure 2.5 Inflation graphs for the Mooney-Rivlin-type model (1.17) using (2.45) with $\alpha = 0.85$, and thickness ratio $\xi = R_i/R_o = 0.3$. All the inflation graphs exhibit type (a) behavior.

We begin by considering the case where d_1 and d_2 are independent of v. According to (2.46) this is equivalent to α being independent of v. In this case homogeneous swelling has no effect on the type of inflation graph. Such a result is consistent with

remarks given in *Pence and Tsai* (2006). As a first example, consider the material parameter $\alpha = 0.85$. Then, because $\alpha = 0.85 > \alpha_{cr}$, there is a transition value of $\xi_{a/c}$ which, according to Figure 2.4, is given by $\xi_{a/c} = 0.47$. We now separately consider $\xi = 0.3 < \xi_{a/c}$ (a relatively thick walled structure) and $\xi = 0.7 > \xi_{a/c}$ (a relatively thin walled structure). The pair $(\xi, \alpha) = (0.3, 0.85)$ is in the type (a) behavior region of Figure 2.4, and so the $v = 1$ inflation graph for $\xi = 0.3$ displays type (a) behavior. This inflation graph is shown in Figure 2.5 along with the inflation graphs for an increasing sequence of v values. Because d_2/d_1 is independent of v all of the inflation graphs are monotonic. Turning to the pair $(\xi, \alpha) = (0.7, 0.85)$, which is in the type (c) behavior region of Figure 2.4, it follows that the $v = 1$ inflation graph for $\xi = 0.7$ displays type (c) behavior. Figure 2.6 shows this inflation graph along with those for a similarly increasing sequence of swelling values v. Because d_2/d_1 is again independent of v all of these graphs exhibit type (c) behavior.

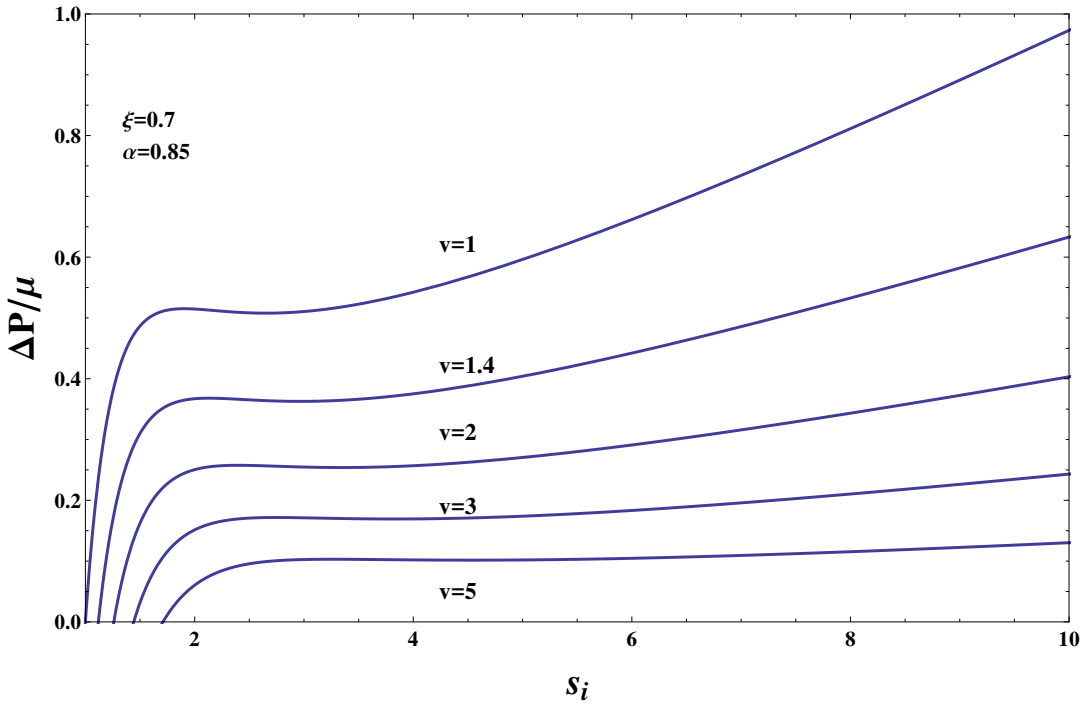

Figure 2.6 Inflation graphs for the same material as in Fig. 2.5 (i.e., (1.17) and (2.45) with $\alpha = 0.85$), but now the thickness ratio $\xi = 0.7$. This corresponds to a relatively thinner walled structure. All the inflation graphs now exhibit type (c) behavior.

2.3.3 Swelling dependent material stiffness parameters

More generally the parameters d_1 and d_2 may be swelling dependent, i.e., $d_1 = d_1(v)$ and $d_2 = d_2(v)$. It then follows that the ratio $d_1(v)/d_2(v)$ changes with the amount of swelling. This can lead to the inflation graph behavior changing its type as v increases. To demonstrate consider materials for which the Mooney-Rivlin parameters $d_1(v)$ and $d_2(v)$ in (1.17) have the form

$$d_1 = \tfrac{1}{2}\mu\alpha\, v^m \quad \text{and} \quad d_2 = \tfrac{1}{2}\mu(1-\alpha)\, v^n, \tag{2.49}$$

where $\mu > 0$ and $0 \leq \alpha \leq 1$ are fixed material constants. This is consistent with (2.45) as can be seen by taking $v = 1$. Equation (2.49) introduces the additional exponent parameters m and n. The choice $m = 0$ and $n = 0$ then formally retrieves the case that was just examined in Section 2.3.2 with both d_1 and d_2 independent of v.

For $m \neq 0$ and $n \neq 0$ the material behavior remains dependent on the ratio

$$\frac{d_2}{d_1} = \frac{1-\alpha}{\alpha} v^{n-m}. \tag{2.50}$$

Thus if $m = n$ then the ratio d_2/d_1 is independent of v and the inflation graph behavior does not change with v. However if $m \neq n$ then the behavior of the function G, which is now determined by d_2/d_1, depends on the amount of swelling v.

The critical value of $(d_2/d_1)_{cr} = 0.215$ from (2.44) continues to distinguish between monotonic and non-monotonic graphs G. In this regard, for any fixed material parameter α, one may solve (2.50) for the special swelling value v that is associated with $(d_2/d_1)_{cr}$. Define this special value of v as $v_{A\leftrightarrow C}$. Making the replacements $d_2/d_1 \to (d_2/d_1)_{cr}$ and $v \to v_{A\leftrightarrow C}$ in (2.50) and solving for $v_{A\leftrightarrow C}$ yields

$v_{A\leftrightarrow C} = v_{A\leftrightarrow C}(m-n,\alpha)$ with

$$v_{A\leftrightarrow C}(m-n,\alpha) \stackrel{\text{def}}{=} \left(\frac{\alpha}{1-\alpha}\,(d_2/d_1)_{cr}\right)^{\frac{1}{n-m}} = (0.215)^{\frac{1}{n-m}}\big(\frac{\alpha}{1-\alpha}\big)^{\frac{1}{n-m}}. \qquad (2.51)$$

Now working through the various possibilities it follows that:

$$\text{if } m<n \text{ then the graph of } G \text{ is } \begin{cases} \text{monotone whenever} \quad v > v_{A\leftrightarrow C}, \\ \\ \text{non-monotone whenever} \quad v < v_{A\leftrightarrow C}, \end{cases} \qquad (2.52)$$

and:

$$\text{if } m>n \text{ then the graph of } G \text{ is } \begin{cases} \text{monotone whenever} \quad v < v_{A\leftrightarrow C}, \\ \\ \text{non-monotone whenever} \quad v > v_{A\leftrightarrow C}. \end{cases} \qquad (2.53)$$

For the case of a non-monotone G graph, as discussed in Sections 2.2.2 and 2.3.1, there is a special value $\xi_{a/c}$ of the thickness ratio ξ that gives the transition between type (a) and type (c) behavior. It is obtained by solving simultaneously the two equations (2.41) and (2.42). For given α, m and n, this value is a function of the swelling amount, hence we can write $\xi_{a/c} = \xi_{a/c}(v)$. Such a function is directly useful if one seeks to determine the effect of a fixed amount of swelling as applied to a range of different structures, each with a different shell thickness.

However the more practical problem involves a fixed structure that is subject to a changing amount of swelling. This motivates an inverting of the relation $\xi = \xi_{a/c}(v)$

to obtain $v = v_{a/c}(\xi)$. The value of swelling $v_{a/c} = v_{a/c}(\xi)$ demarcates the transition between type (a) behavior and type (c) behavior for the given shell geometry. From the material perspective, $v_{a/c}(\xi)$ will depend on α, m and n. In fact, like $v_{A\leftrightarrow C}$ as given in (2.51), the dependence of $v_{a/c}$ upon m and n will be in terms of $m-n$, i.e., $v_{a/c} = v_{a/c}(\xi, m-n, \alpha)$. However, unlike $v_{A\leftrightarrow C}$ which is independent of ξ and given by the simple form (2.51), the function $v_{a/c}$ is dependent upon ξ and not given by a similarly simple expression. In fact the connection between these two is that

$$v_{a/c}(\xi, m-n, \alpha)\Big|_{\xi=1} = v_{A\leftrightarrow C}(m-n, \alpha). \tag{2.54}$$

The qualitative form of the curves $v_{a/c}$ as a function of ξ depends on whether $m > n$ or $m < n$. This is thoroughly discussed in the next section 2.3.4. In particular, it explains why (2.54) holds, and how this leads to the conclusions (2.52) and (2.53). This allows a detailed accounting for how the inflation graph varies with v beginning from the originally unswollen value $v = 1$ and then predicting if and when the inflation graph changes its behavior type as v increases.

2.3.4 Effect of the constitutive exponents m and n on the transitional swelling value $v_{a/c}$

The inflation graph of ΔP vs. s_i for the Mooney-Rivlin swelling model that combines (1.17) with (2.49) displays either type (a) or type (c) behavior depending on the thickness ratio $\xi = R_i/R_o$ and the swelling value v. If for fixed ξ it is possible that v alone can cause such a transition, then this transition happens when $v = v_{a/c}$. The transition value $v_{a/c}$ is sensitive to the constitutive parameters α, m and n in (2.49), however it is not sensitive to μ.

In (2.54) it is stated that the connection between the function $v_{a/c}$ and the function

$v_{A\leftrightarrow C}$ is

$$v_{a/c}(\xi, m-n, \alpha)\Big|_{\xi=1} = v_{A\leftrightarrow C}(m-n, \alpha). \tag{2.54}$$

This can be understood as follows: type (c) behavior is associated with a graph for G that is not monotonic. Any transition from a monotonic graph to a nonmonotonic graph for G must take place at a value of v for which the graph develops an inflection point with zero slope. The condition for this determines $v_{A\leftrightarrow C}$. On the other hand for a finite thickness shell the condition that determines $v_{a/c}$ is the simultaneous solution of (2.41) and (2.42). The conditions (2.41) and (2.42) depend on the thickness ratio ξ because this dictates the amount that the graph of G shifts to the left in order to generate the H graph. This shift becomes vanishingly small in the thin shell limit $\xi \to 1$. In order for the match condition (2.41) to hold under a vanishingly small shift it is required that any such location is one at which the graph of G has zero slope. Similarly, for the matching slope condition (2.42) to hold under a vanishingly small shift requires a zero curvature location. A location with both zero slope and zero curvature is the defining condition for $v_{A\leftrightarrow C}$. Consequently, $v_{A\leftrightarrow C}$ is the same as $v_{a/c}$ in the thin shell limit $\xi = 1$.

For a finite thickness shell ($\xi < 1$) the values of $v_{A\leftrightarrow C}$ and $v_{a/c}$ will no longer be the same. Here it is useful to recall the diagram in Figure 2.4 which, for $v = 1$, served to determine the specific thickness ratio ξ associated with the (a) to (c) behavior transition for values of α that were in the special range permitting both behaviors. When swelling is present any such transition is sensitive to both ξ and v. It is then useful to construct curves of $v_{a/c}$ as a function of the structural parameter ξ for fixed material parameters α, m, n. Given a particular shell geometry constructed of a specific material, one can then locate the appropriate point on such a $v_{a/c}$ curve for the purpose of determining the transitional swelling value. The form of these curves are qualitatively different depending on whether $m > n$ or $m < n$. We now describe in more detail these two separate cases.

2.3.4.1 Dependence of $v_{a/c}$ on ξ for $m > n$

If $m > n$ then the Mooney-Rivlin swelling model (1.17) with (2.49) gives $v_{a/c} > v_{A\leftrightarrow C}$. The sphere exhibits type (a) behavior for $v < v_{a/c}$ and type (c) behavior for $v > v_{a/c}$. For fixed constitutive parameters α, m, n the difference $|v_{a/c} - v_{A\leftrightarrow C}|$ decreases for relatively thinner shells (i.e., as $\xi = R_i/R_o$ increases). In particular, $v_{a/c} \to v_{A\leftrightarrow C}$ as $\xi \to 1$.

These features are apparent in Figure 2.7 which plots the dependence of $v_{a/c}$ upon ξ for exponent choices $m = 2/3$ and $n = 0$. Because $v_{a/c}$ depends on m and n only through their difference, the Fig. 2.7 plots apply more generally to any m and n values obeying $m - n = 2/3$. The different curves correspond to different values of α. Each curve is monotonically decreasing from infinity (as $\xi \to 0$) to the value of $v_{A\leftrightarrow C}$ at $\xi = 1$. Curves for values of $\alpha > 0.823$ are everywhere above the line $v_{a/c} = 1$. This is because $v_{A\leftrightarrow C} > 1$ when $\alpha > 0.823$. In contrast, because $\alpha < 0.823$ makes $v_{A\leftrightarrow C} < 1$ it follows that the curves for $\alpha < 0.823$ cut the line $v = 1$. Because we limit attention to $v \geq 1$ the portions that continue into $v < 1$ are shown as dashed.

The α value of 0.823 *is the value of α_{cr} that was first introduced in (2.47) in the context of the standard neo-Hookean model.* By virtue of (2.54) it also serves to make $v_{A\leftrightarrow C}(m-n, \alpha_{cr}) = 1$ because of the direct way in which the standard incompressible model ((1.16) with (2.45)) was generalized to the swelling model ((1.17) with (2.49)).

The curves shown in Figure 2.7 correspond to $m - n = 2/3$. Curves with similar qualitative behavior are obtained provided that $m > n$. In particular, the α value of 0.823 is always associated with $v_{A\leftrightarrow C} = 1$. Spherical shells with $m > n$ and $\alpha > 0.823$ have $v_{a/c} > 1$. They exhibit type (a) behavior for $1 \leq v < v_{a/c}$ and exhibit type (c) behavior for for $v > v_{a/c}$.

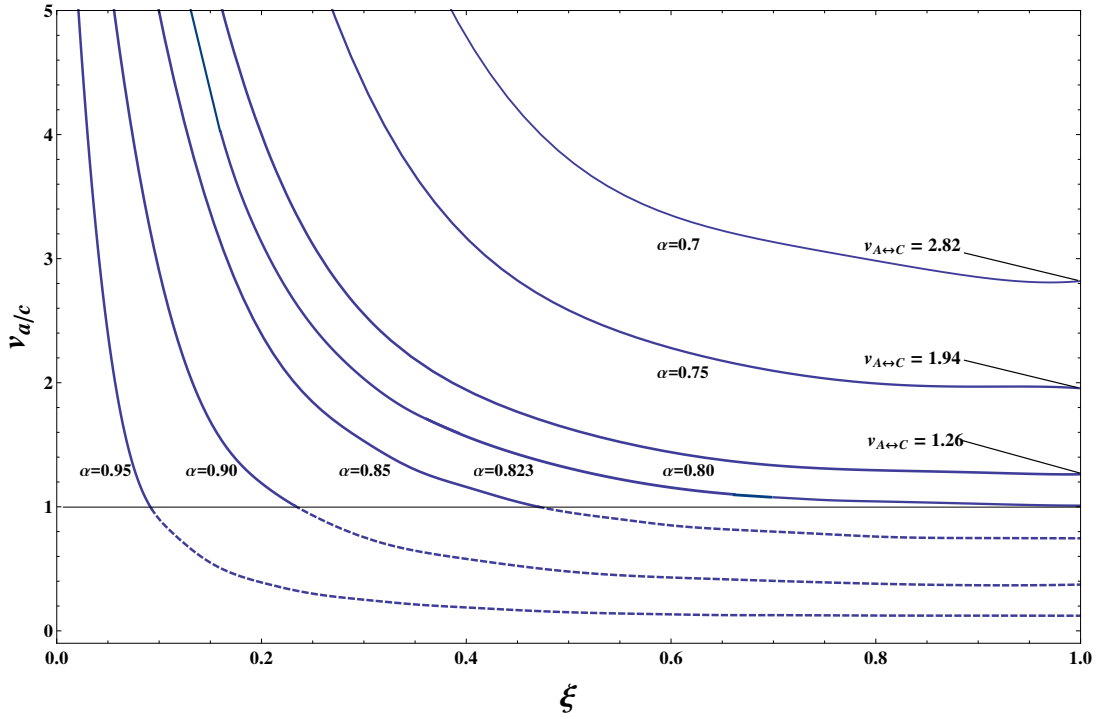

Figure 2.7 Transitional swelling value $v_{a/c}$ versus $\xi = R_i/R_o$ for the Mooney-Rivlin-type model (1.17) with parameters μ, α, m and n in (2.49). The transitional swelling value $v_{a/c}$ is independent of μ and is dependent on n and m only via the difference $m - n$. These plots are for $m - n = 2/3$. For a given α-curve the inflation graph exhibits type (c) behavior if (ξ, v) is in the region above the curve and type (a) behavior if (ξ, v) is in the region below the curve.

2.3.4.2 Dependence of $v_{a/c}$ on ξ for $m < n$

One may similarly construct curves of $v_{a/c}$ vs. ξ for the case in which $m < n$. Now the curves are increasing with ξ instead of decreasing. Each curve continues to approach the value $v_{A\leftrightarrow C}$ as $\xi \to 1$, however now they increase from the value zero at $\xi = 0$. The other major difference is in the significance of these curves. Namely, the spherical shells now have a type (a) behavior in the region *above* the curves ($v > v_{a/c}$) and have a type (c) behavior in the region *below* the curves ($v < v_{a/c}$).

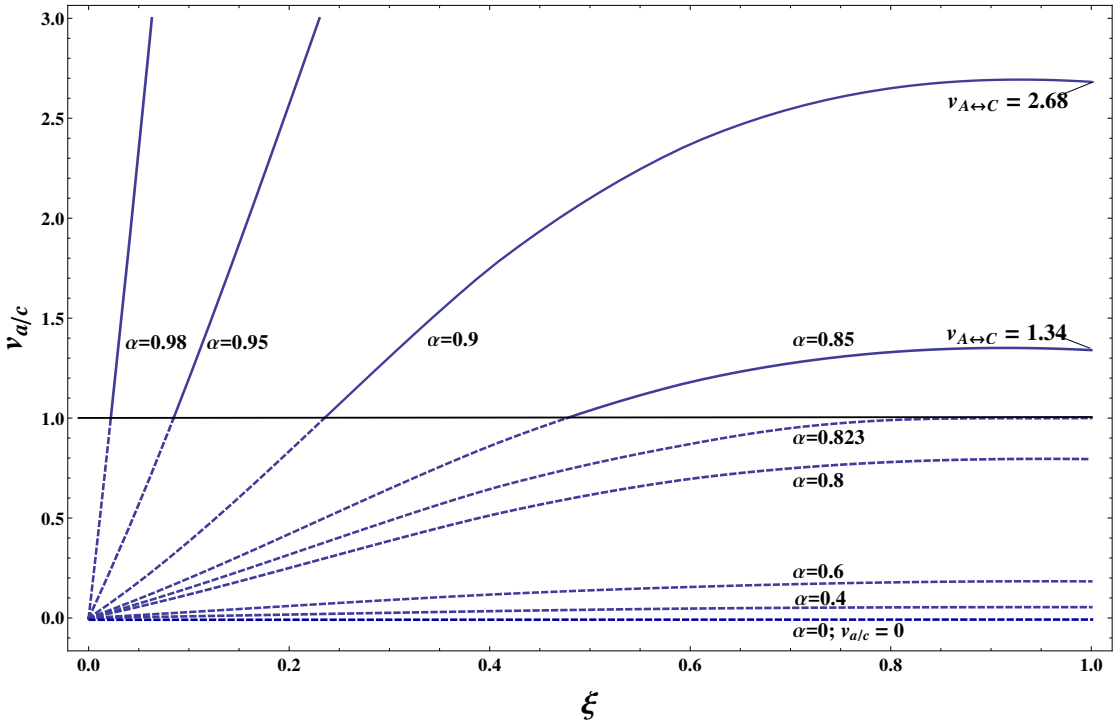

Figure 2.8 Transitional values for swelling $v_{a/c}$ versus $\xi = R_i/R_o$ for Mooney-Rivlin-type model (1.17) with parameters μ, α, m and n in (2.49). The transitional swelling value $v_{a/c}$ is dependent on α as shown but is independent of μ. The curves are dependent on m and n only via the difference $m-n$. This figure is for $m-n = -2/3$. For a given α-curve the inflation graph exhibits type (c) behavior when (ξ, v) is in the region that is below the curve and type (a) behavior in the region that is above the curve.

Such curves are displayed in Figure 2.8 which plots the dependence of $v_{a/c}$ upon ξ for exponent choices $m = 0$ and $n = 2/3$. More generally this figure also applies to any m and n values obeying $m - n = -2/3$. Qualitatively similar curves hold for

any m and n obeying $m < n$. The value $\alpha = 0.823$ continues to retain its special significance because of its continued association with the condition $v_{A\leftrightarrow C} = 1$. It is now the case that curves for $\alpha < 0.823$ are always confined to the region $v_{a/c} < 1$. Because the condition $v < 1$ is not being considered, the $\alpha < 0.823$ curves are shown as dashed over their entire length. Thus if $\alpha < 0.823$ (and $m < n$) then any spherical shell has type (a) behavior for $v \geq 1$.

Conversely curves for $\alpha > 0.823$ cut the line $v = 1$. The portions of these curves that are below the value $v = 1$ are again shown as dashed. If $\alpha > 0.823$ and the shell is sufficiently thick then it has a type (a) inflation graph for all $v \geq 1$; this is because $v_{a/c} < 1$. However if the shell is sufficiently thin then $v_{a/c} > 1$; this means that it has a type (c) inflation graph for $1 \leq v < v_{a/c}$ and a type (a) inflation graph for $v > v_{a/c}$. Consequently in such a case a quasi-static increase in v from the unswollen state $v = 1$ will generate a transition from type (c) to type (a) behavior as v passes through the special value $v_{a/c}$.

2.3.5 Numerical illustration with swelling-dependent material stiffness parameters

The inflation behavior of the sphere with swelling dependent material stiffness can be illustrated by considering the same α and ξ values associated with Figures 2.5 and 2.6 but now allowing for $m \neq 0$ and $n \neq 0$. For this purpose we first consider the case $m < n$ that is obtained by taking $m = 0$ and $n = 2/3$. In particular, consider two subcases corresponding respectively to a thick shell ($\xi = 0.3$) and to a relatively thinner shell ($\xi = 0.7$). Thus the two subcases correspond to $(\xi, \alpha, m, n) = (0.3, 0.85, 0, 2/3)$ and to $(\xi, \alpha, m, n) = (0.7, 0.85, 0, 2/3)$. The $v = 1$ curve for the first subcase is identical to the $v = 1$ type (a) curve from Figure 2.5. Similarly, the $v = 1$ curve in the second subcase matches the $v = 1$ type (c) curve from Figure 2.6. However the curves for $v > 1$ will no longer match the curves shown in these respective figures. One finds

for the first subcase, that with $\xi = 0.3$, the type (a) inflation graph that is present for $v = 1$ persists for all increasing v. This aspect mirrors the situation in Figure 2.5 even though the individual curves for $v > 1$ are different. In the second subcase of $\xi = 0.7$ one finds that the inflation graph is originally type (c) for $v = 1$ but it eventually transitions to type (a) behavior as v increases. This transition occurs at $v = 1.27$, a result that can be predicted on the basis of the procedure for determining $v_{a/c}$ that is described in the appendix.

The case $m > n$ can be handled similarly. For this purpose consider $m = 2/3$ and $n = 0$, again for the respective thick and thin shell values $\xi = 0.3$ and $\xi = 0.7$. Once again the $v = 1$ curves match the $v = 1$ curves from Figures 2.5 and 2.6 respectively. Once again the $v > 1$ curves do not match the curves in these two figures. In fact, Figures 2.9 and 2.10 show a $v > 1$ curve sequence for these two respective cases. For the subcase of $\xi = 0.7$ one finds that the original type (c) behavior at $v = 1$ will persist as v increases (Fig. 2.10). In contrast, for the case of $\xi = 0.3$ one finds that the original type (a) behavior at $v = 1$ will transition to type (c) behavior as v increases (Fig. 2.9). This transition occurs at $v = 1.54$, where, again, such a result can be understood in detail on the basis of the treatment given in the appendix.

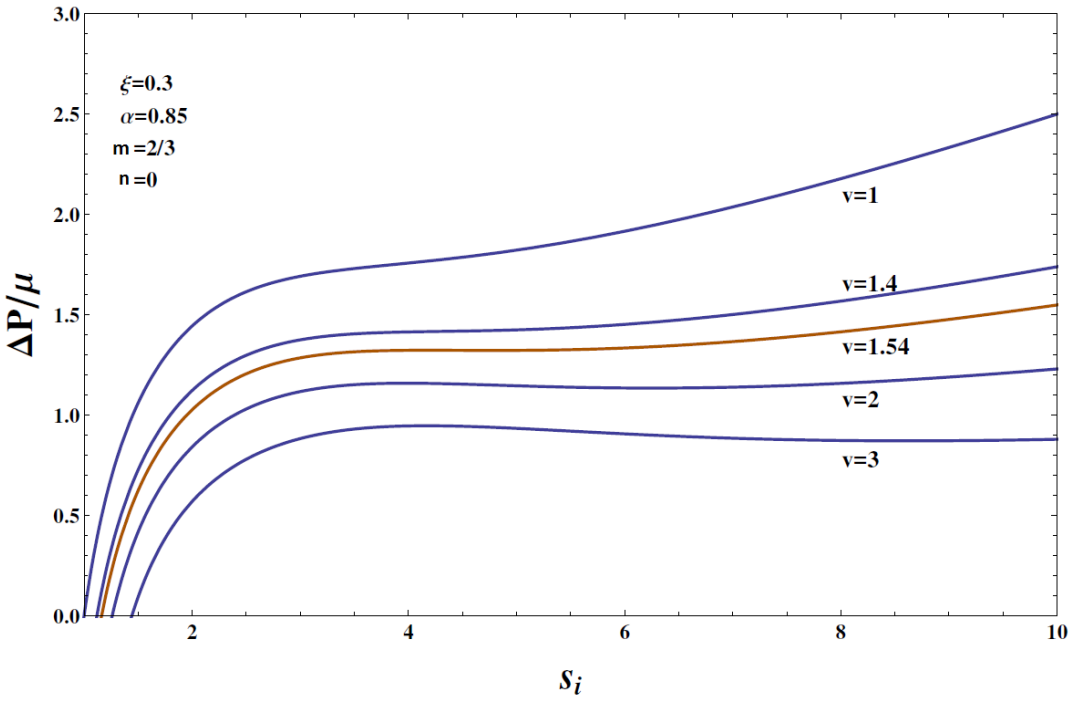

Figure 2.9 Inflation graphs for the Mooney-Rivlin-type model (1.17) using (2.49) with $\alpha = 0.85, m = 2/3, n = 0$, and thickness ratio $\xi = 0.3$. The inflation graphs exhibit the type (a) behavior for $1 \leq v < 1.54$ and type (c) behavior for $v > 1.54$.

2.4 Swelling induced burst

Each of the previous Figures 2.5 - 2.10 shows a sequence of inflation graphs for a given shell thickness ratio ξ composed of a given model material (α, m, n). Such a figure can be used to gauge how the sphere expands as a function of increasing swelling v. If the pressurization is fixed during the swelling, then a quasi-static increase in v corresponds to moving between different curves on the same figure along the horizontal line determined by the stipulated ΔP. For continuously increasing v the associated increase in s_i will also be continuous so long as all of the curves in the sequence are monotonically increasing. However if the curves are not all monotone increasing then there is clearly the possibility of a discontinuity in s_i.

For example, consider again Figure 2.6. The inflation graphs for all v are non-monotone (type (c)) and the s_i interval of graphical decrease varies with v. Figure 2.11

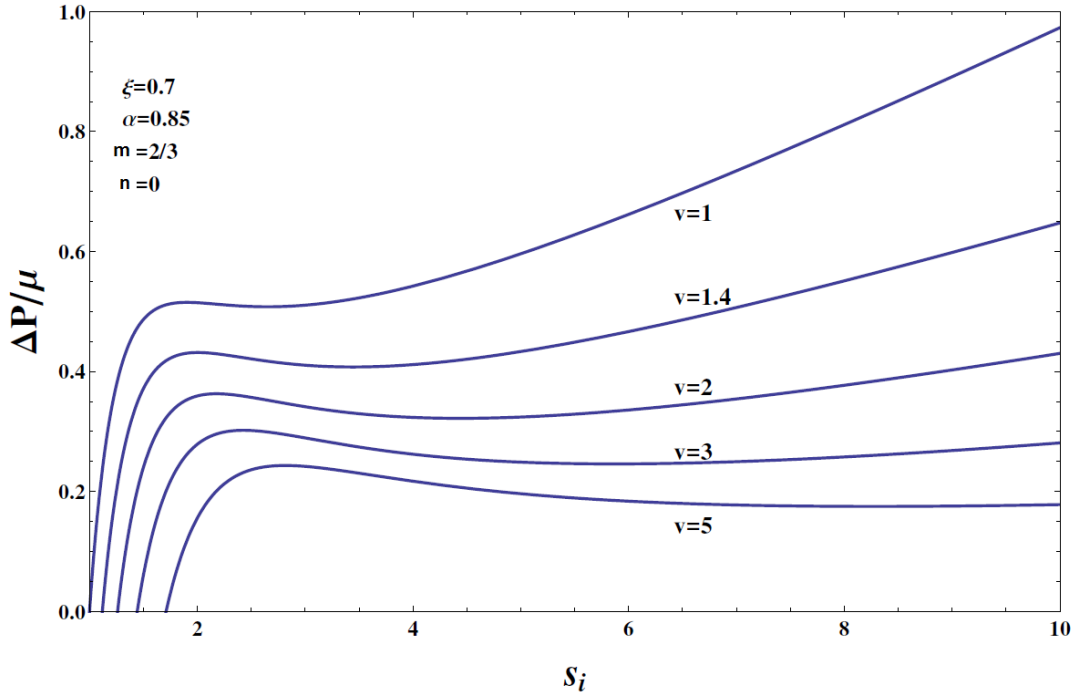

Figure 2.10 Inflation graphs for the Mooney-Rivlin-type model (1.17) using (2.49) with $\alpha = 0.85, m = 2/3, n = 0$, and thickness ratio $\xi = 0.7$. The inflation graphs exhibit type (c) behavior for all $v \geq 1$.

identifies the specific pressurization ΔP that corresponds to the local maximum for $v = 2$. Its value is $\Delta P = 0.258\mu$. Starting with an unswollen and unpressurized sphere $(v = 1, \Delta P = 0)$ consider first an increase in pressure from $\Delta P = 0$ to $\Delta P = 0.258\mu$ while the sphere remains unswollen. The inflation response corresponds to climbing the $v = 1$ curve to $\Delta P = 0.258\mu$ with a relatively small increase in s_i from $s_i = 1$ to $s_i = 1.14$.

Now holding this pressurization fixed let v increase. Then one may proceed in sequence through all of the curves from the original $v = 1$ curve to the curve for $v = 2$. During this sequence there is a corresponding continuous increase in s_i. However, increasing v beyond $v = 2$ cannot proceed with a continuous increase in s_i because the local maximum signals the onset of an interval in s_i corresponding to $v < 2$. This interval proceeds from $s_i = 2.37$ to $s_i = 4.32$. While this interval precludes a continuous increase in s_i as v increases through $v = 2$ it does permit a discontinuous increase

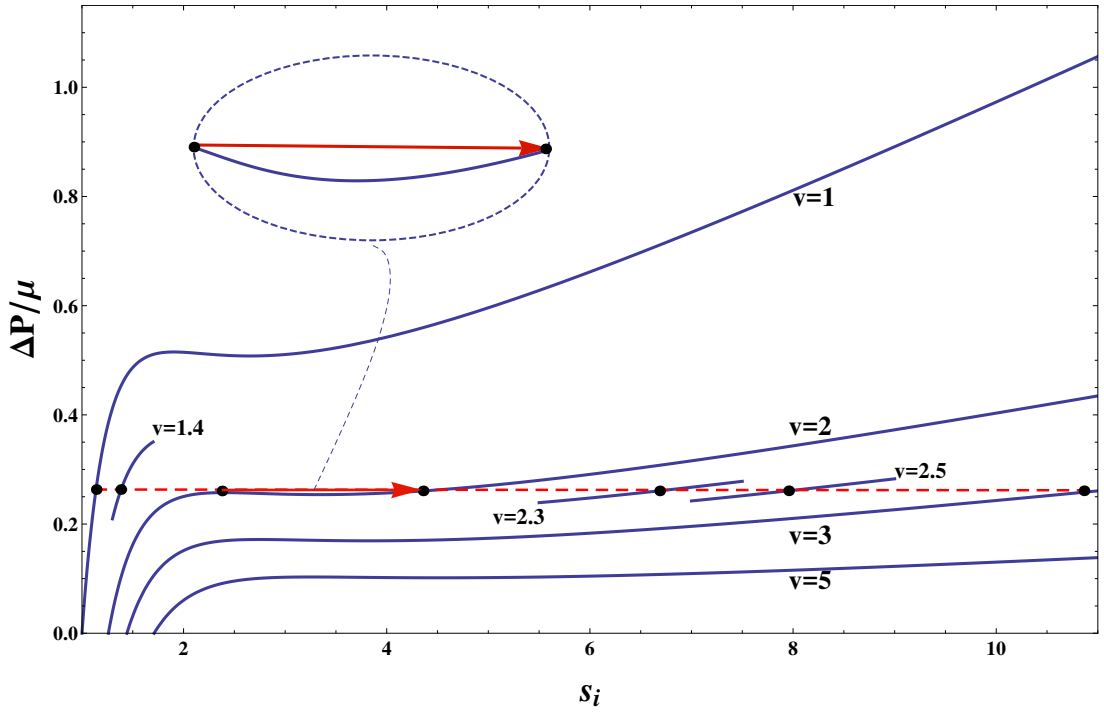

Figure 2.11 Inflation burst caused by increasing v at fixed $\Delta P = 0.258\mu$ for the inflation graphs from Fig. 2.6. Prior to swelling the pressurization $\Delta P = 0.258\mu$ has given a mild radial increase (from $s_i = r_i/R_i = 1$ to $s_i = r_i/R_i = 1.14$ on the $v = 1$ curve). Now increasing v at this fixed ΔP gives a continuous increase of s_i with v (dashed red line) until encountering the inflation graph for $v = 2$ where there is a local maximum. Further increase of v requires a jump across to the other increasing branch of the $v = 2$ curve (solid red segment). This corresponds to an inflation burst with radial increase from $s_i = 2.37$ to $s_i = 4.32$.

from $s_i = 2.37$ to $s_i = 4.32$ at $v = 2$. After such a jump in s_i it is then again possible for s_i to increase continuously because the inflation graphs again become ordered so as permit s_i to increase with v. Figure 2.12 shows directly the corresponding radial increase with swelling (s_i as a function of v).

The jump in s_i corresponds to a "burst of inflation" of limited extent (it concludes at $s_i = 4.32$). Such a burst, which can also be described as a snap-through, is due to the presence of a local maximum in the sequence of inflation graphs. This gives multi-valued choices for s_i when an inflation graph exhibits two increasing branches separated by a decreasing branch.

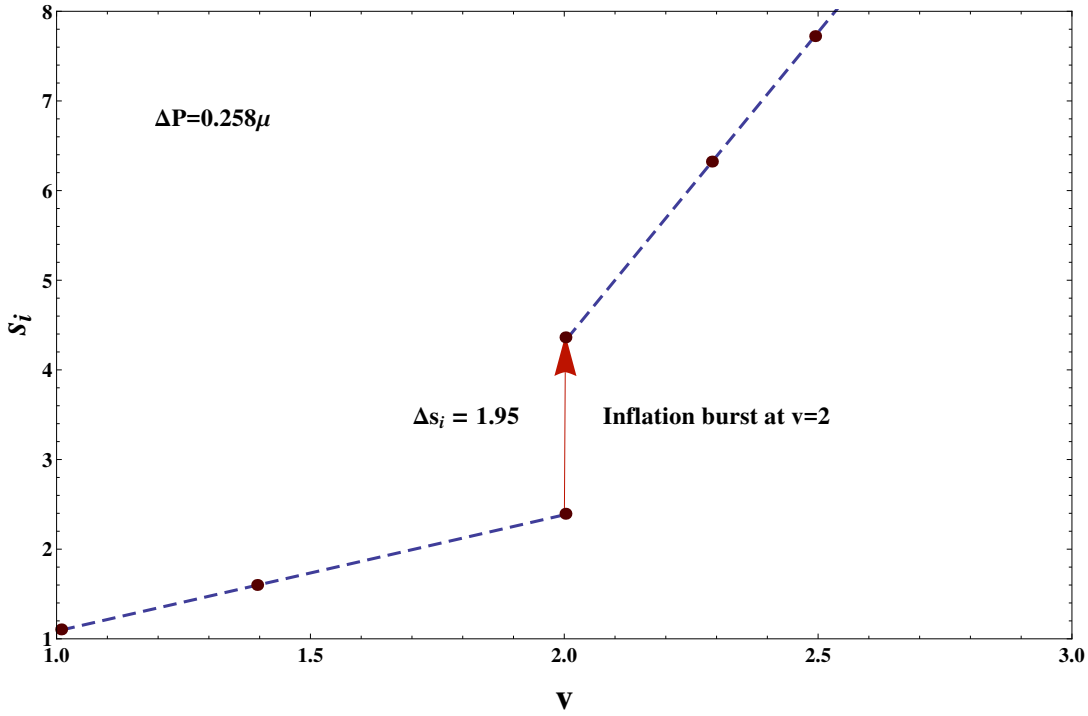

Figure 2.12 Inflation burst showing $s_i = r_i/R_i$ vs. v at $\Delta P = 0.258\mu$ caused by an increase in the swelling parameter v. Locations denoted by • provide correlation with the inflation graphs depicted in Figure 2.11.

Under such circumstances some kind of burst is inherent in the mechanical description. However, the description is potentially ambiguous as regards the value of v at which the jump occurs. For example, we have just described a jump from $s_i = 2.37$ to $s_i = 4.32$ when both $\Delta P = 0.258\mu$ and $v = 2$. However, for $\Delta P = 0.258\mu$ the inflation graphs become multi-valued in s_i for values of $v < 2$ and so the question arises, "why not jump before $v = 2$?". In other words, while $v = 2$ is the maximum value of v that permits one to avoid a discontinuity, there is always the possibility of executing an earlier jump.

Such issues have been extensively studied in conventional hyperelasticity *Müller and Strehlow* (2004) (i.e., no swelling). Then for a single type (c) inflation graph an increase in ΔP eventually provokes a jump to the second increasing branch for the simple reason that the first increasing branch has a maximum permissible ΔP

value. This jump could occur at the local maximum or it could occur before the local maximum. Viewing such jumps as a type of phase transition it can be shown that an energy minimal quasi-static process of ΔP increase predicts that the transition occurs prior to attaining the maximum. Specifically it occurs at the value of ΔP associated with the "Maxwell line" construction *Ericksen* (1975). On the other hand, a transition that occurs at the local maximum upon loading (and at the local minimum upon unloading) is consistent with a notion that the prevailing phase can, under carefully controlled conditions, be preserved even though distantly related states of deformation may now lower the system free energy. In other words, if the system is not subject to large disturbances then jumps will occur at extrema of the inflation graph because it is only then that the inevitable small disturbances provoke a jump to a more energetically favorable configuration.

Such considerations continue to apply to the notion of swelling induced burst that we have been describing. In particular, the sequence of inflation graphs depicted in Figure 2.6 leads to a situation where, at fixed ΔP, a continuous increase in v will give some kind of abrupt change in inflation. Whether this occurs at the local maximum of an inflation graph or whether it occurs prior to such a local maximum is then to be answered on the basis of a more refined treatment. This includes energetic stability analysis such as that described in *Ericksen* (1975) as well as the consideration of less symmetric deformations (such as those with new modes of localized deformation *Kyriakides and Chang* (1990)). More generally, one can employ a broader thermodynamic framework that allows for supplemental physical considerations (e.g., an additional kinetic relation), as well as additional theoretical considerations from the outset (e.g., inertial dynamics, finer scale physics, a statistical physics treatment of fluctuations). Finally, it is worth remarking that the notion of pressure control is itself likely to be an idealization, and that other forms of control, such as one based on controlling a set mass of sealed in gas *Alexander* (1971), can lead to different predictions on how

transitions occur between different points on an inflation graph.

The inflation burst illustrated in Figure 2.11 was based on the inflation graphs for the case that was presented in Figure 2.6. In that case all of the inflation graphs for $v \geq 1$ involved type (c) behavior. Thus one could possibly argue that the swelling induced burst could have been anticipated on the basis of the original unswollen $v = 1$ inflation graph. However, in general it would be premature to draw conclusions on either the presence or absence of swelling induced burst just on the basis of the $v = 1$ inflation graph.

For example, the unswollen $v = 1$ inflation graph in Figure 2.9 exhibits type (a) behavior. Thus if $v = 1$ then a continuous increase in pressure will result in a continuous expansion and so by itself provides no indication of a burst possibility. However swelling induced inflation burst can still occur. This is shown in Figure 2.13 for the example of Figure 2.9. Starting on the $v = 1$ inflation graph with $\Delta P = 1.16\mu$ we consider a subsequent increase in v. The value $\Delta P = 1.16\mu$ is chosen for this discussion because it gives the local maximum on the $v = 2$ inflation graph (other values could similarly be considered). Holding ΔP at this fixed value, an inflation burst is triggered at $v = 2$ in a manner similar to that previously depicted in the example of Figures 2.11 and 2.12. In that previous example the inflation graph behavior was type (c) for all values of ΔP prior to the burst. In the present example, the swelling induced burst involves inflation graphs that transition from "benign" type (a) graphs to "burstible" type (c) graphs as the swelling proceeds.

A converse phenomena is also possible if the $v = 1$ unswollen graph is type (c) and which then transitions to type (a) as the swelling proceeds. This was the case for $(\xi, \alpha, p, q) = (0.7, 0.85, 0, 2/3)$ that was discussed in Section 2.3.3 right after equation (2.54). In such a case it is found that certain loading sequences which alternate pressurization with strategically placed episodes of swelling and deswelling enable *burst avoidance*. This contrasts with the inevitability of burst if all of the pressurization

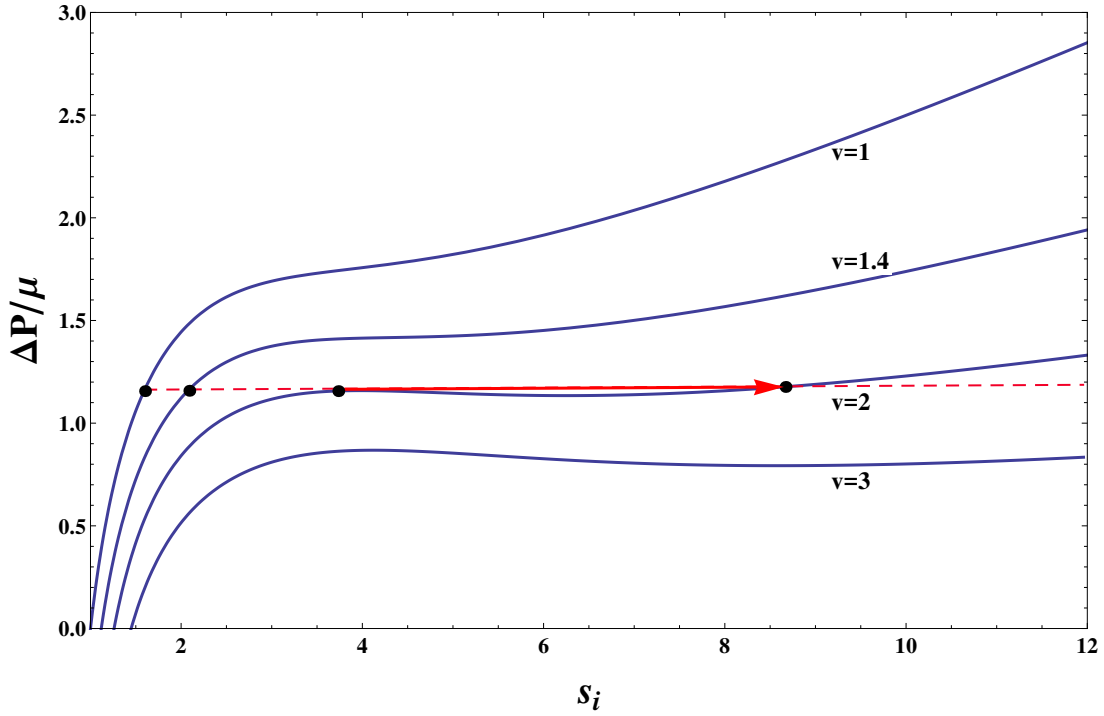

Figure 2.13 Inflation burst caused by increasing v at fixed $\Delta P = 1.16\mu$ for the inflation graphs from Fig. 2.9. Initially, the radius increases continuously, first with $v = 1$ as ΔP increases from zero to 1.16μ and then at this fixed ΔP as v increases to $v = 2$ (dashed red segment). At $v = 2$ there is a jump from the first increasing branch to the second increasing branch after which a continuous increase is again the case.

takes place at fixed v.

CHAPTER III

Non-Uniform Swelling Field of Hyperelastic Spherical Shells

As it was mentioned in chapter II, the swelling field v could in general depend on position within the shell wall, i.e., $v = v(R)$. Such a treatment is developed in this Chapter. In order to make a distinction between the varying (non-uniform) and uniform swelling fields we use the notation v_{uni} for the uniform swelling field in this Chapter. It was shown that for the Mooney-Rivlin-type model (1.17) while the uniform swelling field is present and the material parameters are independent of swelling, only the constant ratio $\kappa = d_2/d_1$ and the thickness ratio $\xi = R_i/R_o$ identify the classification of the inflation behavior (a), (b) or (c) and the material types A, B or C. This is for example presented in Figure 3.29 wherein it is shown that different amounts of uniform swelling field value v_{uni} has no effect on the material and behavior type. Conversely, the uniform swelling field value $v_{uni} > 1$ can change the behavior of the inflation response only when the material parameters d_1 and d_2 are dependent on swelling amount v_{uni} (in the form of different power laws). The question then arises as to how to determine the type of the behavior when the swelling field v is no longer distributed uniformly and varying with R. In this chapter we study the inflation behavior of such fields when the material parameters of the model (1.17) are independent of local volume change $v(R)$. In such an event where $v = v(R)$, it is required to invert the relation $s = r(R)/R$ and write $R = \hat{R}(s)$ and hence $v = \hat{v}(s)$ for the purpose of the integration in (2.21). Additionally, in order to characterize

specific non-uniform swelling fields we introduce a new variable which is the overall added volume or equivalently absorbed mass due to the swelling process. This will allow us to describe family of swelling fields with the same added mass. This in turn enables us to study as how such nonuniform swelling fields will affect the inflation behavior.

3.1 A family of swelling fields with the same added mass

To investigate the characteristics of varying swelling fields we introduce the overall *added swelling volume* ΔV

$$\Delta V = 4\pi \int_{R_i}^{R_o} (v(R) - 1) R^2 dR, \tag{3.1}$$

which is the total amount of volume change due to the mass absorption during the swelling. We limit our attention to consider only swelling fields that are motivated by observation of *steady state distributions* of liquids in porous media. For such swelling fields, the distribution of $v(R)$ is governed by Laplace's equation that in the reference configuration is

$$\nabla^2 v(R) = \frac{1}{R^2} \frac{\partial}{\partial R} \big(R^2 \frac{\partial v(R)}{\partial R} \big) \equiv 0. \tag{3.2}$$

The general distribution of the swelling field that satisfies (3.2) has the form

$$v(R) = \frac{A}{R} + B \tag{3.3}$$

in which A and B are constants. Let

$$v_i \equiv v(R_i) = \frac{A}{R_i} + B, \qquad v_o \equiv v(R_o) = \frac{A}{R_o} + B \tag{3.4}$$

where v_i is the amount of swelling at $R = R_i$ and v_o is the amount of swelling at $R = R_o$. It then follows that

$$A = \frac{v_o - v_i}{1/R_o - 1/R_i}, \quad B = \frac{v_o R_o - v_i R_i}{R_o - R_i}. \tag{3.5}$$

Entering (3.1) with (3.3) one obtains

$$\frac{\Delta V}{R_i^3} = \frac{2\pi}{R_i} (\xi^{-2} - 1) A + \frac{4\pi}{3} (\xi^{-3} - 1)(B - 1). \tag{3.6}$$

Note that for any fixed ΔV and fixed geometry (R_i and ξ) in (3.6), it is seen a linear relation between the parameters A and B. Now imagine any two different mass distributions represented by (A_p,B_p) and (A_q,B_q) but with the same ΔV. The linear relation (3.6) requires that

$$\frac{A_p - A_q}{B_p - B_q} = -\frac{4\pi(\xi^{-3} - 1)/3}{2\pi(\xi^{-2} - 1)/R_i}. \tag{3.7}$$

After some simplification

$$\frac{A_p - A_q}{B_p - B_q} = -\frac{2(\xi^{-3} - 1)}{3(\xi^{-2} - 1)} R_i. \tag{3.8}$$

Now define the radial location R_m as

$$R_m := \frac{2(\xi^{-3} - 1)}{3(\xi^{-2} - 1)} R_i = \frac{2(\xi^3 - 1)}{3(\xi^2 - 1)} R_o \tag{3.9}$$

where it can be easily shown that since $0 < \xi < 1$ then $R_i < R_m < R_o$. It then follows from rearranging (3.8) with (3.9) that

$$\frac{A_p}{R_m} + B_p = \frac{A_q}{R_m} + B_q \tag{3.10}$$

This is in fact the amount of swelling at the radius R_m where according to (3.3) is $v(R_m)$ for both distributions. This means that both distribution have the same amount of swelling at the same radial location R_m. Since the choice of distributions was otherwise arbitrary it is concluded that all swelling distributions $v(R)$ given by (3.3) that absorb the same fixed added mass ΔV have the same amount of swelling at location R_m.

In order to characterize the distributions (3.3) in terms of v_i and v_o instead of A

and B note that plugging (3.5) into (3.6) and solving for v_o gives

$$v_o = \frac{3\Delta V}{2\pi R_i^3}\left(\frac{\xi^3}{2-\xi}\right) + \frac{\xi(\xi-1)(2\xi+1)}{2-\xi}v_i + \frac{2(1-\xi^3)}{2-\xi}. \tag{3.11}$$

It follows that

$$\begin{aligned} A &= \left(\frac{3\Delta V}{2\pi R_i^3}\left(\frac{\xi^3}{-\xi^3+3\xi-2}\right) + v_i\left(\frac{2\xi^3-2}{-\xi^3+3\xi-2}\right) + \frac{2(1-\xi^3)}{-\xi^3+3\xi-2}\right)R_i \\ B &= \frac{3\Delta V}{2\pi R_i^3}\left(\frac{\xi^3}{\xi^3-3\xi+2}\right) + v_i\left(\frac{3\xi-3\xi^3}{\xi^3-3\xi+2}\right) + \frac{2(1-\xi^3)}{\xi^3-3\xi+2} \end{aligned} \tag{3.12}$$

Thus for a given $\Delta V > 0$, R_i, and $R_o = R_i\xi^{-1}$ we may view (3.3) with A and B given by (3.12) as a family of swelling fields for the same added mass but different distributions with tuning parameter v_i. As v_i changes, the same overall added mass ΔV is distributed through the spherical shell in different ways.

We restrict considerations to swelling fields (3.3) such that $v(R) \geq 1$ at all locations. This will be the case if both $v_i \geq 1$ and $v_o \geq 1$. Setting $v_o = 1$ in either (3.6) or (3.11) and solving for v_i we obtain

$$v_i\big|_{v_o=1} = 1 + \frac{3\Delta V}{2\pi R_i^3}\left(\frac{\xi^3(1-\xi)}{2\xi^4-3\xi^3+\xi}\right) \equiv v_i^{max} \tag{3.13}$$

Thus (3.3) with A and B given by (3.12) is parameterized by v_i on the interval $1 \leq v_i \leq v_i^{max}$.

If $v_o = v_i$ then $A = 0$ and we retrieve a uniform distribution of the kind studied in Chapter II. For a given ΔV the uniform distribution is associated with the v_i value that is found by substituting $v_i = v_o = v^{uni}$ in (3.11) and solving for the special value

v^{uni}. This gives

$$v^{uni} = 1 + \frac{3\Delta V}{4\pi R_i^3}\left(\frac{\xi^3}{1-\xi^3}\right). \tag{3.14}$$

If $v_i = v^{uni}$ as given by (3.14) then all of the results from Chapter II apply for the given added mass ΔV. If $1 \leq v_i \leq v^{uni}$ then the added mass is more concentrated near the outer surface. If $v^{uni} \leq v_i \leq v_i^{max}$ then the added mass is more concentrated at the inner surface. Conversely, (3.14) shows that the added mass associated with this uniform distribution is

$$\frac{\Delta V}{R_i^3} = \frac{4}{3}\pi(v^{uni} - 1)\frac{1-\xi^3}{\xi^3}, \tag{3.15}$$

For any fixed amount of ΔV, the amount of v_o is identified from (3.11) in terms of v_i and this defines a family of swelling fields $v(R)$ from (3.3) that can be parameterized only by the amount v_i. One example that will also be used for numerical showcase in the next section is shown in Figure 3.1. The figure shows a family of swelling distributions where they all have the same overall added mass, say 30 percent of the original volume and thus $v^{uni} = 1.3$. In the following section the inflation behavior of such distribution families is studied.

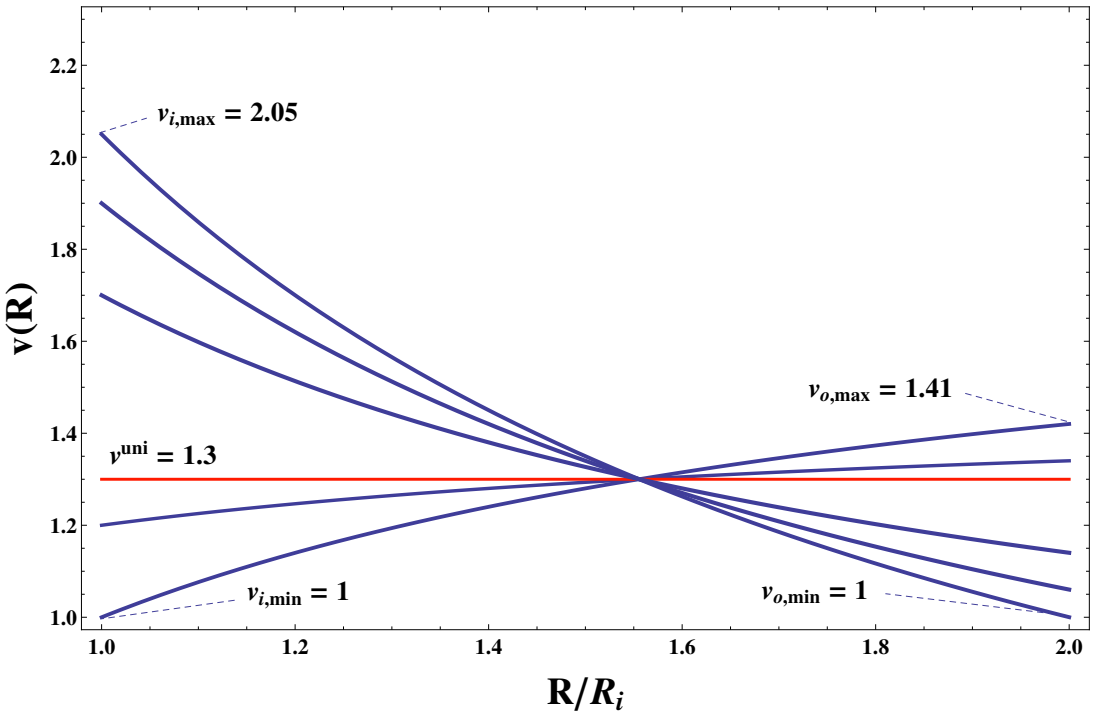

Figure 3.1 The family of swelling distributions (3.3) with constants (3.12) for $\xi = 0.5$ that are parameterized with respect to v_i such that $v(R) \geq 1$. All distributions have the same amount of overall added mass associated with $v^{uni} = 1.3$.

3.2 Kinematics of the spherical deformation with non-uniform swelling field

The symmetric spherical deformation that is described in (2.1) is assumed here as a response to radial inflation that is also subject to the non-uniform swelling field (3.3). In fact, the deformation map (2.6) is now considered with the radial dependent $v = v(R)$. It then follows that

$$r^3 = r_i^3 + 3\int_{R_i}^{R} \left(\frac{A}{\zeta} + B\right) \zeta^2 d\zeta, \tag{3.16}$$

and this simplifies to

$$r^3 = r_i^3 + \frac{3}{2}A(R^2 - R_i^2) + B(R^3 - R_i^3) \tag{3.17}$$

wit A and B given by (3.12).

3.3 Behavior type independent of distribution for fixed added mass

The inflation behavior for varying swelling fields is considered in this section. This makes the use of (2.21) in the form

$$\Delta P = \int_{s_i}^{s_o} \frac{1}{\hat{v}(s) - s^3} \frac{\partial w(s,v)}{\partial s} ds. \tag{3.18}$$

This relation can also be verified by an alternative proof with energy argument to confirm that this relation indeed holds even in the case of non-uniform swelling. The deformation field (2.1) in the absence of body forces is determined by the minimization of the total potential energy

$$\mathbb{E} = \mathbb{E}_{store} - \mathbb{E}_{load}, \tag{3.19}$$

where $\mathbb{E}_{store}$ is the stored energy with respect to reference configuration that includes the effect of elastic deformations and is expressed as

$$\mathbb{E}_{store} = 4\pi \int_{R_i}^{R_o} \bar{W} R^2 dR \tag{3.20}$$

where $\bar{W}$ is the local strain energy density as defined before (2.11). The work functional associated with the prescribed surface tractions is denoted by $\mathbb{E}_{load}$. Hence the work due to the internal pressure loading is given by

$$\mathbb{E}_{load} = \tfrac{4}{3}\pi(r_i^3 - R_i^3)P_i - \tfrac{4}{3}\pi(r_o^3 - R_o^3)P_o \tag{3.21}$$

The requirement of stationary total potential energy $\mathbb{E}$ with respect to the only un-

known r_i provides

$$\frac{\partial}{\partial r_i}(\mathbb{E}_{store} - \mathbb{E}_{load}) = 0. \tag{3.22}$$

Thus it follows that because the radial position R is independent of r_i then

$$\frac{\partial}{\partial r_i}\mathbb{E}_{store} = 4\pi \int_{R_i}^{R_o} \frac{\partial \bar{W}}{\partial r_i} R^2 dR \tag{3.23}$$

and from (3.21)

$$\frac{\partial}{\partial r_i}\mathbb{E}_{load} = 4\pi r_i^2 (P_i - P_o). \tag{3.24}$$

Equating the two relations (3.23) and (5.61) one obtains

$$\Delta P \equiv P_i - P_o = \frac{1}{r_i^2} \int_{R_i}^{R_o} \frac{\partial \bar{W}}{\partial r_i} R^2 dR. \tag{3.25}$$

By recalling (2.16) and using the connections from

$$\frac{dR}{Rs^2} = \frac{ds}{v - s^3}, \qquad \frac{\partial s}{\partial r_i} = \frac{r_i^2}{Rr^2}, \tag{3.26}$$

we convert the relation (3.25) to (3.18). In the event that the relation $s = r(R)/R$ is not explicitly invertible, that is $R = \hat{R}(s)$ is not available, it is required to use (3.18) in the reference configuration and perform the integration with respect to R. For convenience we use this integration in this Chapter. Moreover, instead of converting (3.25) into (3.18) we use the connections (2.5) and (3.26) to rewrite (3.25) with the more convenient derivations of $\bar{W}$ with respect to s that uses the definition (2.18). It

follows that

$$\Delta P = \int_{R_i}^{R_o} \frac{R}{r^2} \frac{\partial w(s,v)}{\partial s}\bigg|_{s=r/R} dR \tag{3.27}$$

Note that from (2.6) we know the map $r = r(R; r_i)$. This provides the integrand in (3.27) in terms of R and the parameter r_i. This in turn makes (3.27) be indeed a relation for the applied pressure and inner deformed radius. In order to employ the inflation relation (3.27) we use the Mooney-Rivlin-type model (1.17) with (2.46). It follows that

$$\frac{\partial w(s,v)}{\partial s}\bigg|_{s=r/R} = 2\alpha\mu\left(\frac{r}{Rv^{2/3}} - \frac{R^5 v^{4/3}}{r^5}\right) + 2(1-\alpha)\mu\left(\frac{r^3}{R^3 v^{4/3}} - \frac{R^3 v^{2/3}}{r^3}\right) \tag{3.28}$$

and thus the inflation relation (3.27) becomes

$$\Delta P/\mu = 2\int_{R_i}^{R_o} \frac{R}{r^2}\Big(\alpha\big(\frac{r}{Rv(R)^{2/3}} - \frac{R^5 v(R)^{4/3}}{r^5}\big) + (1-\alpha)\big(\frac{r^3}{R^3 v(R)^{4/3}} - \frac{R^3 v(R)^{2/3}}{r^3}\big)\Big) dR \tag{3.29}$$

where $r = r(R)$ is from (3.17), $v = v(R)$ is given by the swelling field (3.3) and A and B are according to (3.12). This provides the relation between the applied pressure ΔP and the inner radius r_i. The closed form solution to this integration is not available, however the numerical integration is performed for special cases that are presented in the following.

The varying swelling fields for numerical integration (3.29) will be selected such that they all have one fixed overall added mass ΔV. The choice of swelling fields is the same as was shown in Figure 3.1. As for the first set of numerical result, the other parameters in the integration are set to (ξ, α)=$(0.5, 0.86)$. This is chosen such that,

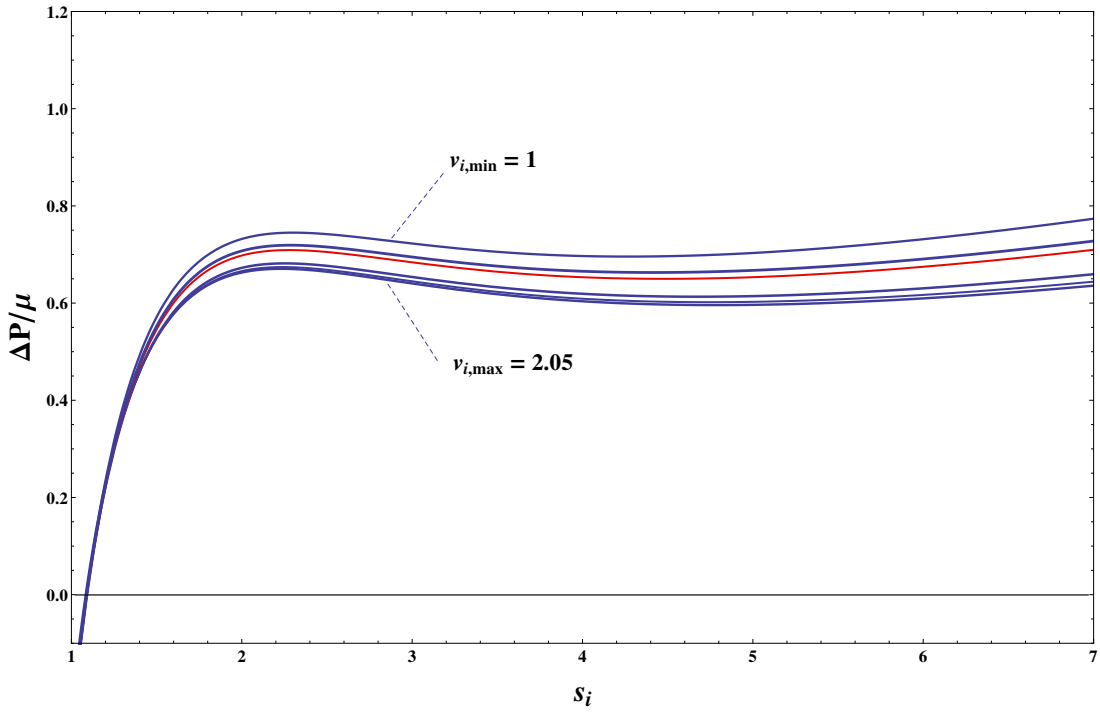

Figure 3.2 Type (c) behavior in response to pressure-inflation for the six different swelling fields in figure 3.1; using fixed properties $(\xi, \alpha) = (0.5, 0.86)$ in the Mooney-Rivlin-type material model (1.17) and (2.46).

with respect to $v_{uni} = 1.3$, type (c) behavior is expected from the results plotted in Figure 2.4. Also note that this is associated with the added mass of $(\Delta V/R_i^3) \simeq 8.8$ given by (3.15). This set is considered in Figure 3.2 in which the solution to (3.29) for the material model (1.17) with (2.46) is plotted. As it is presented in this figure, all of the family of different distributions with fixed added mass showing type (c) behavior consistent with the type (c) behavior that is identified for the uniform swelling of this family with $v_{uni} = 1.3$. For the same family of swelling distribution represented in Figure 3.1 we now consider the second set of parameters of $(\xi, \alpha) = (0.5, 0.83)$ such that type (a) behavior is expected for the uniform swelling $v_{uni} = 1.3$ according to Figure 2.4. As it is seen in Figure 3.3 the solution shows type (a) behavior for the whole distribution family.

The two above numerical examples show that the distribution family of the fixed

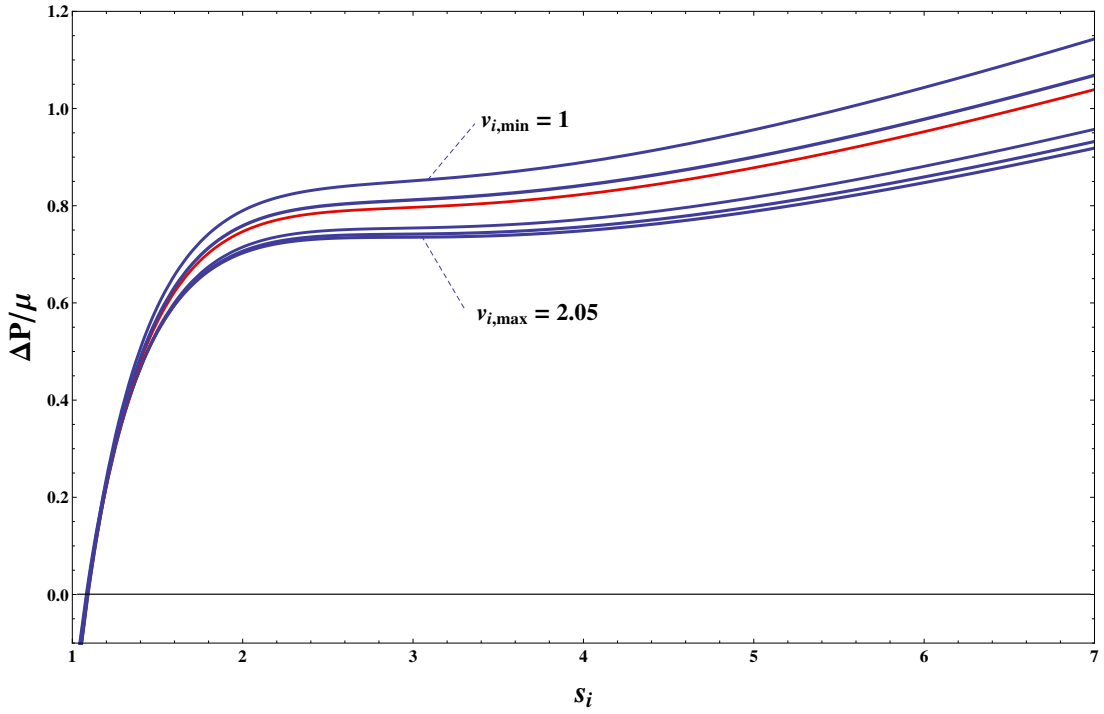

Figure 3.3 Type (a) behavior in response to pressure-inflation for the six different swelling fields in figure 3.1; using fixed properties $(\xi, \alpha) = (0.5, 0.83)$ in the Mooney-Rivlin-type material model (1.17) and (2.46).

added volume with the representative uniform swelling $v_{uni} = 1.3$ followed the same behavior type as the uniform swelling field depicted, depending on the parameters (ξ, α). The latter case was proved in Chapter II to be identified from Figure 2.4. Our hypothesis is that the same type of behavior occurs for all (A, B)-pairs that forms a family of yielding same added volume ΔV and the type of behavior of the family is identified based on the behavior of v_{uni} with (ξ, α). To test this hypothesis we consider 18 additional cases chosen so as to be close to transition curve shown in Figure 3.4. In each case we calculated the response for $v_i = 1$ and $v_i = v_{i,max}$. The numerical results of the inflation curves with the two circled dots in the middle of this figure have been already shown in Figs. 3.2 and 3.3. The numerical results of the inflation curves are showcasing in Figs. 3.5 and 3.6 with four other circled dots from Figure 3.4 as additional examples. For any parameter-point that was chosen above the transition curve both of the representative distributions ($v_i = 1$ and $v_i = v_{i,max}$)

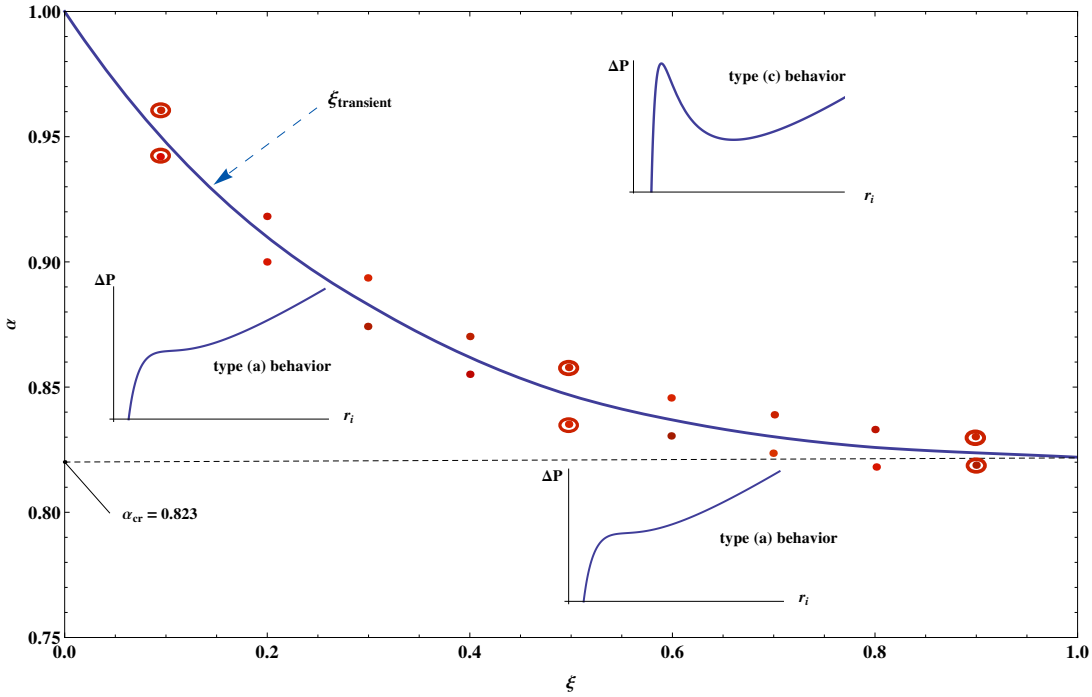

Figure 3.4 Qualitative behavior of the inflation graph for the Mooney-Rivlin model with uniform swelling fields, previously shown in Figure 2.4. Here 18 points are chosen along the transition curve (red dots) to be used in (3.29) for numerical integration. The inflation graphs with the circled parameter choices are shown in Figs. 3.2, 3.3, 3.5 and 3.6.

show type (c) behavior. In contrast, for any parameters chosen below the transition curve both distributions ($v_i = 1$ and $v_i = v_{i,max}$) show type (a) behavior. It is seen that at least these numerical cases support our hypothesis.

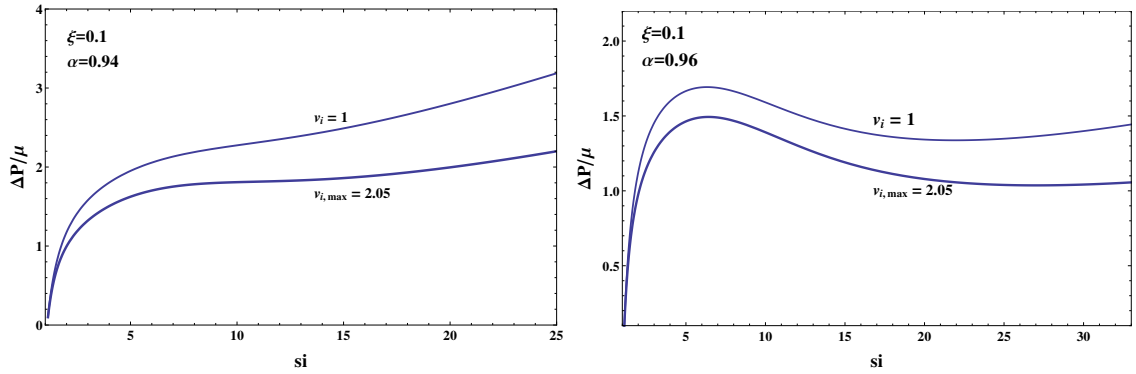

Figure 3.5 Inflation behavior for the two limits of swelling distribution $(v_{i,min}, v_{i,max})$ in figure 3.1; using fixed parameters chosen from Figure 3.4 with $(\xi, \alpha) = (0.1, 0.94)$ (on the left) showing type (a) behavior and $(\xi, \alpha) = (0.1, 0.96)$ (on the right) showing type (c) behavior. The Mooney-Rivlin-type material model is based on (1.17) and (2.46).

3.4 Inflation behavior instability due to mass redistribution

The inflation response (3.29) is numerically obtained for the swelling distributions family (3.3) and A and B given by (3.12) with fixed added mass corresponding to $v^{uni} = 1.3$ (Figure 3.1), in which the family is parameterized by inner amount of swelling according to $1 \leq v_i \leq v_i^{max} = 2.05$. For the material model (1.17) with constant parameters, the inflation graphs of this solution to (3.29) show behavior of type (c) for the set $\xi = 0.5$ and $\alpha = 0.86$ and this is graphed in Figure 3.2. Hence the family shows type (c) behavior for the range from $v_i = 1$, where the added mass is more concentrated on the outer layer of shell, to $v_i = v_i^{max} = 2.05$ where the added mass is more absorbed toward the inner layer of the shell. Thus for all of these distributions the inflation graph shows type (c) behavior independent of the swelling field. Here, the possibility of an inflation instability in inner radius can be captured of the same kind that was illustrated in Figure 2.11 for the case of uniform swelling. However, in the current case the redistribution of the swelling field can cause the burst. For the case of uniform swelling with constant material parameters the quasi-static increase in swelling amount led to the movement of the inflation curves of type (c) behavior such that for a fixed applied pressure it provided the jump in the inner

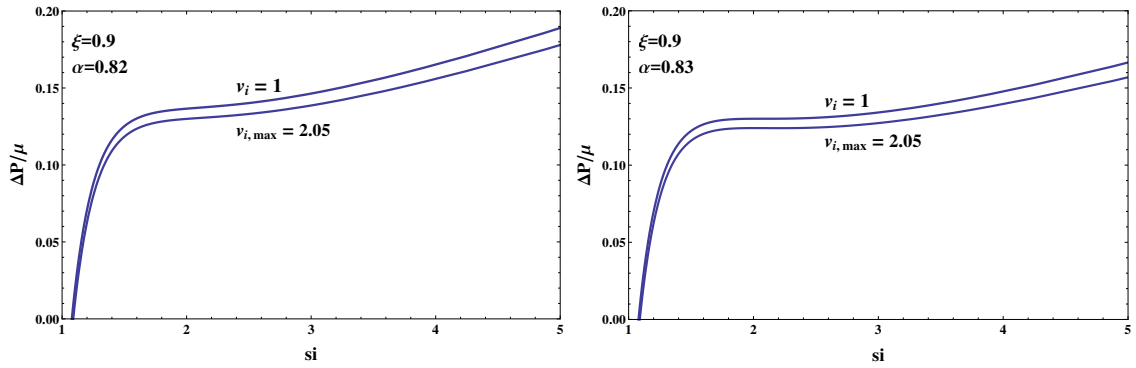

Figure 3.6 Inflation behavior for the two limits of swelling distribution $(v_{i,min}, v_{i,max})$ in figure 3.1; using fixed parameters chosen from Figure 3.4 with $(\xi, \alpha) = (0.9, 0.82)$ (on the left) showing type (a) behavior and $(\xi, \alpha) = (0.9, 0.83)$ (on the right) showing type (c) behavior. The Mooney-Rivlin-type material model is based on (1.17) and (2.46).

radius. Similarly, for the case of a nonuniform swelling fields that generate a family of type (c) behavior it is the redistribution of the field that provides the movements of the inflation curves and this can causes the inflation jump.

The procedure of the inflation instability is represented numerically where one aspect of Figure 3.2 is plotted in Figure 3.7. It is seen that the maximum pressure associated with the branch $v_i = 1$ is $\Delta P/\mu = 0.74$ and the maximum pressure reached on the curve for $v_i = 2.05$ is $\Delta P/\mu = 0.67$. Remaining on the branch $v_i = 1$, the increase of pressure from $\Delta P = 0$ to slightly higher pressures cause the radius to increase continuously. Now the pressure continues to increase and then remains fixed at some value between $0.67 < \Delta P/\mu < 0.74$ and here we choose $\Delta P/\mu = 0.71$ for showing the example of inner radius jump. At this fixed pressure if the total added mass starts to redistribute such that it is more absorbed towards the inner layer it means that inner amount of swelling increases from $v_i = 1$ to some amount $v_i > 1$. This increase in v_i moves the corresponding inflation graph to the right and down at the fixed pressure. This in turns moves the solution to $s_i = r_i/R_i$ closer to the top of the corresponding curve until it eventually reaches to the top of the

inflation graph where $v_i = 1.25$ which corresponds to the maximum value for the pressure $\Delta P = 0.71$. At this point spherical shell experiences a sudden expansion burst and a rapid jump in the inner radius. It follows that, at a fixed pressure, the redistribution of a fixed added mass can cause a shell expansion instability that is similar to that which was previously displayed in Figure 2.11. The important point is that now the overall amount of swelling does not change, just the way it is distributed.

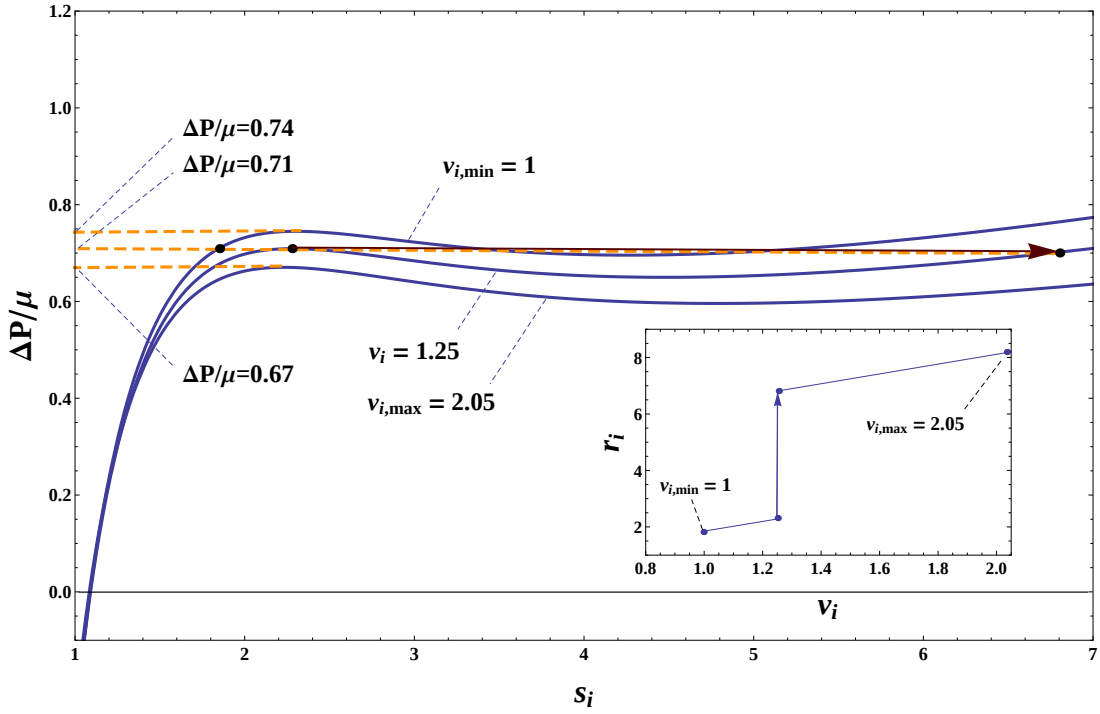

Figure 3.7 Inflation burst due to redistribution of the fixed added mass in type (c) behaviors; using fixed properties $(\xi, \alpha) = (0.5, 0.86)$ in the Mooney-Rivlin-type material model (1.17).

CHAPTER IV

Channel Confinement Swelling of Hyperelastic Plugs and Tubes

4.1 Introduction

The swelling of highly deformable gels and other soft rubbery materials within a confined space will exert forces on the walls of their container. Conversely, the confining walls will act on the soft solid, causing it to distort as it continues to expand. Understanding these effects are important for the design of soft material actuation devices. Similarly, certain biological processes, either of long term growth, or of short term swelling, give rise to tissue distortion as organs and vessels impinge.

In this chapter we model this type of process in a simple setting where the containment is due to an open ended rigid cylinder with circular cross-section – an open tube – within which an initially unswollen soft solid expands. As one might anticipate, this leads to a formulation in cylindrical coordinates (unlike the spherical coordinate considered in chapters II and III). Free swelling, which is a simple homogeneous deformation, takes place until the solid makes contact with the confining tube wall. After contact, we seek to determine the shape of the expanding solid as it continues to swell while being confined. At the same time we also seek to determine the traction forces that this expanding solid exerts on the confining tube.

The expansion of a solid cylindrical plug of original radius R_o within a rigid cylindrical tube of radius $R_c > R_o$ is studied in Section 4.2 where pressure-swelling response graphs are obtained for a conventional hyperelastic model. In Section 4.3 we consider the effect of a plug that has an internal channel, i.e., an annular plug. Now the deformation after wall contact is no longer one of homogeneous deformation. The associated boundary value problem is formulated, and in Section 4.4 this boundary value problem is solved for the case of a neo-Hookean type swelling model. Wall contact now gives a deformation in which swelling combines axial lengthening with internal channel narrowing. Of particular interest is the closing behavior of the internal channel as the swelling proceeds. Treating the associated boundary value problem provides asymptotic expressions for the channel radius closing and the contact pressure in the large swelling regime.

4.2 The homogeneous deformation of laterally confined swelling

We first examine the case in which the swelling material is a solid cylindrical plug prior to swelling. Subsequent expansion takes place freely inside a rigid pipe until it makes contact with the pipe wall (Figure 4.1). After so plugging the pipe all further expansion is necessarily along the pipe axis, whereupon the associated wall contact pressure is of particular interest.

With respect to a common origin, take circular cylindrical coordinates (R, Θ, Z) in the reference configuration and (r, θ, z) in the current configuration. Let $\{\mathbf{e}_R, \mathbf{e}_\Theta, \mathbf{e}_Z\}$ and $\{\mathbf{e}_r, \mathbf{e}_\theta, \mathbf{e}_z\}$ denote unit basis vectors in the reference and deformed configurations, respectively. Consider a circular disk of the material with original (i.e. unswollen) radius R_o and original length L when $v = 1$. Swelling is then described by an increase in v. In this chapter we restrict attention to spatially uniform swelling, so that v is independent of $\mathbf{X}$.

Free swelling $\mathbf{F} = v^{1/3}\mathbf{I}$ can then be expressed in the above radial coordinates as $r = v^{1/3}R$, $\theta = \Theta$, $z = v^{1/3}Z$. Moreover, $I_1 = 3v^{2/3}$, $I_2 = 3v^{4/3}$, $\mathbf{B} = v^{2/3}\mathbf{I}$ so that (1.8) gives

$$\mathbf{T} = \left(2v^{-1/3}\frac{\partial W}{\partial I_1}\bigg|_{v^{1/3}\mathbf{I}} + 4v^{1/3}\frac{\partial W}{\partial I_2}\bigg|_{v^{1/3}\mathbf{I}} - p\right)\mathbf{I}$$

where the notation $|_{v^{1/3}\mathbf{I}}$ denotes evaluation at the above values for $\mathbf{F} = v^{1/3}\mathbf{I}$. By taking $p = 2v^{-1/3}\dfrac{\partial W}{\partial I_1}\bigg|_{v^{1/3}\mathbf{I}} + 4v^{1/3}\dfrac{\partial W}{\partial I_2}\bigg|_{v^{1/3}\mathbf{I}}$, the stress tensor $\mathbf{T} = \mathbf{0}$ and so all surfaces are traction free.

We now suppose that an original unswollen disk is placed in a rigid pipe with an inner channel radius $R_c > R_o$. Then free swelling may proceed so long as $v < R_c^3/R_o^3$. However for $v > R_c^3/R_o^3$ the pipe provides a lateral confinement and all subsequent volume change must be accommodated by lengthening of the disk in the Z-direction because the disk plugs the pipe as shown in Figures 4.1 and 4.2.

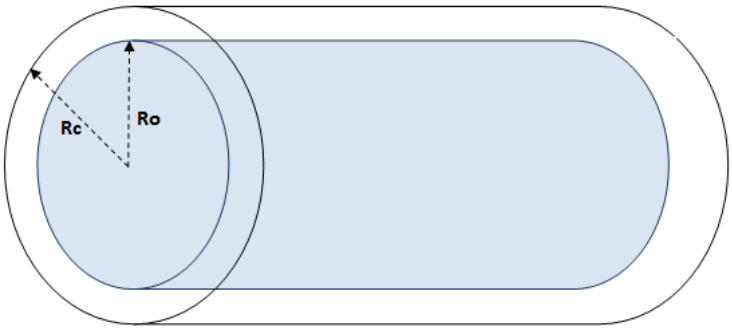

Figure 4.1 Solid cylinder with the radius R_o and the confinement pipe with radius $R_c > R_o$.

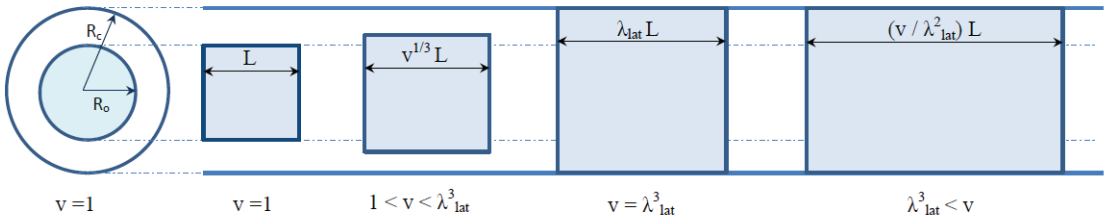

Figure 4.2 Representation of the plug swelling within a rigid pipe. For $v < \lambda_{lat}^3$ the plug has yet to make contact with the pipe wall. Contact first occurs when $v = R_c^3/R_o^3 = \lambda_{lat}^3$. For $v > \lambda_{lat}^3$ all further swelling is directed into Z-direction extension. This generates the pressure P_{lat} between the plug and the pipe wall.

If the contact between the plug and the pipe is frictionless then for $v > R_c^3/R_o^3$ it follows that

$$\mathbf{T} = -P_{lat}(\mathbf{e}_r \otimes \mathbf{e}_r + \mathbf{e}_\theta \otimes \mathbf{e}_\theta), \quad \mathbf{F} = \lambda_{lat}(\mathbf{e}_r \otimes \mathbf{e}_R + \mathbf{e}_\theta \otimes \mathbf{e}_\Theta) + \frac{v}{\lambda_{lat}^2}\mathbf{e}_z \otimes \mathbf{e}_Z, \quad (4.1)$$

where we have defined the *fixed constant*

$$\lambda_{lat} \equiv R_c/R_o. \quad (4.2)$$

This λ_{lat} is the free swelling stretch that just causes all-around contact of the swollen specimen with the pipe's inner wall. This fixed constant (4.2) will appear often in what follows.

Consequently, the condition $v > R_c^3/R_o^3$ will be written as $v > \lambda_{lat}^3$ when the contact condition is met. The P_{lat} appearing in $(4.1)_1$ is the *lateral confining pressure*. In contrast to the known and fixed λ_{lat}, the lateral confining pressure P_{lat} is as yet unknown. Consistency with free swelling ensures that $P_{lat} = 0$ when $v = \lambda_{lat}^3$ (free-swelling that has just made contact with the wall). Our interest is in determining the dependence of P_{lat} upon v for $v > \lambda_{lat}^3$ (see the Fig. 4.2 schematic).

It is useful to note that the problem can also be described with respect to fixed Cartesian coordinates with an orthonormal basis $\{\mathbf{e}_1, \mathbf{e}_2, \mathbf{e}_3\}$. Letting the $\mathbf{e}_3$ direction coincide with the Z-direction of the cylindrical geometry it follows that (4.1) is equivalent to

$$\mathbf{T} = -P_{lat}(\mathbf{e}_1 \otimes \mathbf{e}_1 + \mathbf{e}_2 \otimes \mathbf{e}_2), \quad \mathbf{F} = \lambda_{lat}(\mathbf{e}_1 \otimes \mathbf{e}_1 + \mathbf{e}_2 \otimes \mathbf{e}_2) + \frac{v}{\lambda_{lat}^2}\mathbf{e}_3 \otimes \mathbf{e}_3.$$

This form for $\mathbf{F}$ makes $\mathbf{B} = \lambda_{lat}^2(\mathbf{e}_1 \otimes \mathbf{e}_1 + \mathbf{e}_2 \otimes \mathbf{e}_2) + v^2/\lambda_{lat}^4 \mathbf{e}_3 \otimes \mathbf{e}_3$ so that $I_1 = 2\lambda_{lat}^2 + v^2/\lambda_{lat}^4 \equiv \tilde{I}_1(v)$ and $I_2 = 2v^2/\lambda_{lat}^2 + \lambda_{lat}^4 \equiv \tilde{I}_2(v)$. Thus (1.8) gives $\mathbf{T} = T_{11}(\mathbf{e}_1 \otimes \mathbf{e}_1 + \mathbf{e}_2 \otimes \mathbf{e}_2) + T_{33}\mathbf{e}_3 \otimes \mathbf{e}_3$ with

$$T_{11} = 2\frac{\partial W}{\partial I_1}\Big|_{\tilde{I}_1,\tilde{I}_2} \frac{\lambda_{lat}^2}{v} + 2\frac{\partial W}{\partial I_2}\Big|_{\tilde{I}_1,\tilde{I}_2} \left(\frac{\lambda_{lat}^4}{v} + \frac{v}{\lambda_{lat}^2}\right) - p,$$
$$T_{33} = 2\frac{\partial W}{\partial I_1}\Big|_{\tilde{I}_1,\tilde{I}_2} \frac{v}{\lambda_{lat}^4} + 4\frac{\partial W}{\partial I_2}\Big|_{\tilde{I}_1,\tilde{I}_2} \frac{v}{\lambda_{lat}^2} - p.$$

In polar coordinates $T_{rr} = T_{\theta\theta} = T_{11}$ and $T_{zz} = T_{33}$. Invoking $-P_{lat} = T_{11}$ and $T_{33} = 0$ to eliminate p gives

$$P_{lat} = 2\left(\frac{\partial W}{\partial I_1}\Big|_{\tilde{I}_1,\tilde{I}_2} + \lambda_{lat}^2 \frac{\partial W}{\partial I_2}\Big|_{\tilde{I}_1,\tilde{I}_2}\right)\left(\frac{v}{\lambda_{lat}^4} - \frac{\lambda_{lat}^2}{v}\right).$$

This is the relation of the lateral confining pressure exerted on the solid cylinder due

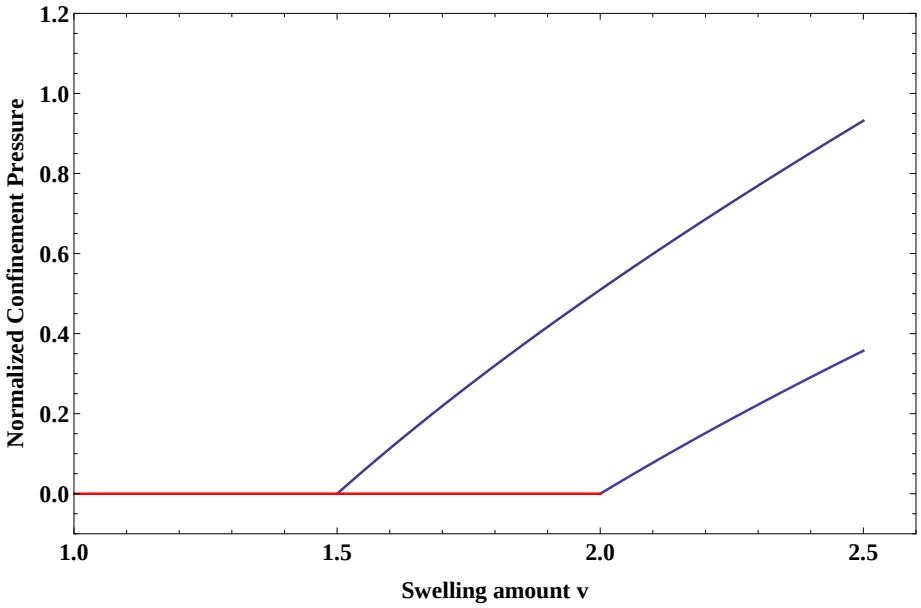

Figure 4.3 Confinement Pressure P_{lat} as a function of swelling v in a solid cylinder taking the outer radius $R_o = 1$ (so that $\lambda_{lat} = R_c$). The graphs are for the pipe radii $R_c = 1.5^{1/3}$ on the left and $R_c = 2^{1/3}$ on the right. Here P_{lat} is normalized by the material modulus μ.

to the all-around contact after the cylinder has plugged the pipe ($v > \lambda_{lat}^3 = R_c^3/R_o^3$). Turning to the specific material model introduced in Section 1.2 this now gives the result of using (1.15) directly, namely,

$$P_{lat} = \mu_o \left(\frac{v}{\lambda_{lat}^4} - \frac{\lambda_{lat}^2}{v} \right). \tag{4.3}$$

We note that for $v = \lambda_{lat}^3$ the lateral pressure (4.3) gives $P_{lat} = 0$ which is consistent with the fact that the cylinder has no lateral pressure when it has just made contact with the surrounding pipe.

Graphs of the confining pressure P_{lat} (normalized by μ_o) as a function of the swelling v for this material model is shown in Figure 4.3. For this figure we take $R_o = 1$ and the two different values $R_c = 1.5^{1/3}$ and $R_c = 2^{1/3}$ so as to initiate contact either at $v = 1.5$ or $v = 2$ (equivalently, we consider $\lambda_{lat} = 1.5^{1/3}$ and $2^{1/3}$).

4.3 The confinement boundary value problem for an annular plug

The problem for laterally confined swelling as just considered in Section 4.2 is a problem for homogeneous deformation. Thus all of the various scalar and tensor quantities: $\mathbf{F}$, $\mathbf{T}$, p, while varying with v in a parametric fashion, were always independent of spatial position $\mathbf{x}$. As such, the equilibrium equation $\operatorname{div}\mathbf{T} = \mathbf{0}$ was automatically satisfied.

The situation changes if we replace the originally unswollen solid disk of radius R_o with an *annular disk* of outer radius R_o and *inner radius* $R_i > 0$. This originally unswollen annular disk is again placed in a channel of radius $R_c > R_o$ and allowed to swell. Under these circumstances there will once again be a period of free swelling, specifically as v increases from its initial value $v = 1$ to the value $v = R_c^3/R_o^3 = \lambda_{lat}^3$ during which the deformation gradient is $\mathbf{F} = v^{1/3}\mathbf{I}$ and this free swelling with the homogeneous deformation generates no stresses and hence $\mathbf{T} = 0$. Note that this free swelling period of deformation is again expressed as $r = v^{1/3}R$, $\theta = \Theta$ and $z = v^{1/3}Z$. The outer radius attains the value $r(R_o) = R_c$ when $v = \lambda_{lat}^3$ and it is again at this point that the solid cylinder makes contact with the pipe wall. Further swelling can now be accommodated not only by axial lengthening but also by continued change in the inner radius of the disk. The resulting *inhomogeneous deformation* will no longer render $\operatorname{div}\mathbf{T} = 0$ in a trivial fashion. It is to this issue that we now turn our attention.

We consider the following somewhat more general symmetric deformation

$$r = r(R), \quad \theta = \Theta, \quad z = \lambda_z Z, \tag{4.4}$$

for $R_i \leq R \leq R_o$, $0 \leq \Theta < 2\pi$, $-\frac{1}{2}L \leq Z \leq \frac{1}{2}L$. With respect to this

deformation define $r_i = r(R_i)$ and $r_o = r(R_o)$. The deformation gradient is given by

$$\mathbf{F} = r'(\mathbf{e}_r \otimes \mathbf{e}_R) + \frac{r}{R}(\mathbf{e}_\theta \otimes \mathbf{e}_\Theta) + \lambda_z(\mathbf{e}_z \otimes \mathbf{e}_Z) \tag{4.5}$$

in which prime ($'$) denotes the derivative with respect to R, i.e., $r' = dr/dR$.

Both $\mathbf{C}$ and $\mathbf{B}$ are diagonal with respect to their polar basis sets. The principal stretch are clearly $\lambda_r = r'$, $\lambda_\theta = r/R$ and λ_z. Because the swelling is prescribed in the amount v it follows from (1.1) that

$$v = \frac{rr'\lambda_z}{R}, \tag{4.6}$$

and because the swelling v is spatially constant, this can be integrated to give

$$r^2 = r_i^2 + \frac{v}{\lambda_z}(R^2 - R_i^2). \tag{4.7}$$

Once contact is made with the rigid pipe wall the outer radius of the plug stays fixed at the radius R_c. Thus once $v \geq \lambda_{lat}^3$ it follows that

$$r_o = r(R_o) = \lambda_{lat} R_o = R_c. \tag{4.8}$$

The inner radius is then determined from (4.7) and (4.8) in terms of λ_z as

$$r_i = \left(R_c^2 - \frac{v}{\lambda_z} R_o^2 + \frac{v}{\lambda_z} R_i^2 \right)^{1/2}. \tag{4.9}$$

The condition $r_i \geq 0$ gives the lower bound

$$\lambda_z \geq \frac{R_o^2 - R_i^2}{R_c^2} v. \tag{4.10}$$

The symmetry of the deformation (4.4) makes the stress tensor take the form

$\mathbf{T} = T_{rr}\mathbf{e}_r \otimes \mathbf{e}_r + T_{\theta\theta}\mathbf{e}_\theta \otimes \mathbf{e}_\theta + T_{zz}\mathbf{e}_z \otimes \mathbf{e}_z$. The contact pressure at the rigid channel wall $R = R_c$ will still be denoted by P_{lat}, giving $T_{rr}|_{r=R_c} = -P_{lat}$ where again P_{lat} needs to be determined. Unlike the spatially constant swelling characterized by (4.1) when no channel is present, it will now be the case that all three quantities T_{rr}, $T_{\theta\theta}$, T_{zz} are functions of r, or, equivalently, of R. It will also generally be the case that T_{rr} is no longer equal to $T_{\theta\theta}$.

The stress equations of equilibrium then give that the hydrostatic pressure p is a function of r (or R), and that T_{rr} and $T_{\theta\theta}$ relate to each other via

$$\frac{\partial T_{rr}}{\partial r} + \frac{1}{r}(T_{rr} - T_{\theta\theta}) = 0. \tag{4.11}$$

The boundary conditions for this problem are (4.8) at the contact surface in conjunction with the traction free conditions on the remaining free surfaces. On the inner radius this gives $T_{rr} = 0$. However there is the possibility that the inner channel completely closes in which case this surface collapses to a line segment and ceases to provide a boundary condition. Thus the original reference inner radius at $R = R_i$ is subject to the condition

$$T_{rr}|_{r_i} = 0 \quad \text{if} \quad r_i > 0. \tag{4.12}$$

The remaining boundaries are the annular caps at $z = -\frac{1}{2}\lambda_z L$ and $z = \frac{1}{2}\lambda_z L$. The traction free condition associated with such a surface then formally requires the vanishing of T_{zz} for all R obeying $R_i < R < R_o$ (equivalently all r obeying $r_i < r < R_c$). However because T_{zz} is no longer constant, such a pointwise condition cannot be met. This reflects the fact that $z = \lambda_z Z$ in (4.4) is too simplistic of an assumption on the detailed nature of the inhomogeneous deformation. We invoke the usual remedy of St. Venant's principle in which (4.4) approximates the deformation away from the caps (in a long cylinder approximation). Consequently, we abandon the point-wise condition $T_{zz} = 0$ and replace it with a condition that the resultant axial force must

vanish i.e.,

$$\int_{r_i}^{R_c} T_{zz} dA = 0 \qquad \Longrightarrow \qquad 2\pi \int_{r_i}^{R_c} T_{zz} r dr = 0. \tag{4.13}$$

We proceed to investigate this boundary value problem for the case in which $W = W(I_4, v)$ as is the case for the material model (1.15). We then have from (1.8), (4.5) and (4.6) that the polar coordinate stress components are

$$T_{rr} = \frac{2}{v} \frac{\partial W}{\partial I_1}\Big|_{I_1^{lat}} \frac{v^2 R^2}{\lambda_z^2 r^2} - p, \tag{4.14}$$

$$T_{\theta\theta} = \frac{2}{v} \frac{\partial W}{\partial I_1}\Big|_{I_1^{lat}} \frac{r^2}{R^2} - p, \tag{4.15}$$

$$T_{zz} = \frac{2}{v} \frac{\partial W}{\partial I_1}\Big|_{I_1^{lat}} \lambda_z^2 - p. \tag{4.16}$$

The notation is to indicate that I_1 is evaluated at the value $I_1^{lat} = I_1^{lat}(R, r_i, \lambda_z, v)$ with

$$I_1^{lat}(R, r_i, \lambda_z, v) = (r')^2 + \frac{r^2}{R^2} + \lambda_z^2 = \frac{v^2 R^4 + (vR^2 - vR_i^2 + \lambda_z r_i^2)^2}{\lambda_z R^2 (vR^2 - vR_i^2 + \lambda_z r_i^2)} + \lambda_z^2$$

where use has been made of (4.6) and (4.7) in arriving at the final expression.

We now integrate the equation of equilibrium (4.11) in the form

$$\underbrace{\int_{r_i}^{r} \frac{\partial T_{rr}}{\partial r}\, dr}_{T_{rr}(r) - T_{rr}(r_i)} = -\int_{r_i}^{r} \frac{1}{r} \left(T_{rr} - T_{\theta\theta}\right) dr.$$

Making use of (4.12), (4.14), (4.15) then gives

$$T_{rr}(r) = -\int_{r_i}^{r} \frac{2}{v} \frac{\partial W}{\partial I_1}\Big|_{I_1^{lat}} \left((r')^2 - \frac{r^2}{R^2}\right) \frac{dr}{r}. \tag{4.17}$$

The integration can be performed with the aid of (4.6), giving T_{rr} as a function of the parameters λ_z, r_i and v. In particular, evaluating this expression at $r = r_o = R_c$ gives P_{lat}, which at this stage is a function of λ_z, r_i and v.

To render everything as a function of v it is necessary to determine r_i and λ_z as functions of v. One equation for this purpose is given by (4.9), however another equation is also needed. This additional equation is provided by (4.13). For this purpose, T_{zz} follows from (4.16) where $p = p(r)$ follows from (4.14) using the explicit form for T_{rr} that has already been obtained from (4.17). In the next section we demonstrate these procedures for the case of material model (1.15).

4.4 Annulus contact for the neo-Hookean type swelling model

The derivative $\partial W/\partial I_1 = \frac{1}{2}\mu_o$ for the material model (1.15) so that (4.17) becomes

$$T_{rr}(R) = -\frac{\mu_o}{v}\underbrace{\int_{r_i}^{r}(r')^2\,\frac{dr}{r}}_{\mathfrak{J}_a} + \frac{\mu_o}{v}\underbrace{\int_{r_i}^{r}\frac{r^2}{R^2}\,\frac{dr}{r}}_{\mathfrak{J}_b} = \frac{\mu_o}{v}\left(-\mathfrak{J}_a + \mathfrak{J}_b\right). \tag{4.18}$$

Examining each integral $\mathfrak{J}_a$ and $\mathfrak{J}_b$ separately using (4.6) and (4.7) we have that

$$\begin{aligned}
\mathfrak{J}_a &= \int_{r_i}^{r}\left(\frac{vR}{r\lambda_z}\right)^2\frac{dr}{r} = \frac{v^2}{\lambda_z^2}\int_{r_i}^{r}\frac{R^2}{r^3}dr = \frac{v^2}{\lambda_z^2}\int_{r_i}^{r}\left(\frac{\lambda_z}{v}(r^2-r_i^2)+R_i^2\right)\frac{dr}{r^3}\\
&= \frac{v}{\lambda_z}\int_{r_i}^{r}\frac{dr}{r} + \frac{v^2}{\lambda_z^2}\left(-\frac{r_i^2\lambda_z}{v}+R_i^2\right)\int_{r_i}^{r}\frac{dr}{r^3}\\
&= \frac{v}{\lambda_z}\ln\left[\frac{r}{r_i}\right] + \frac{v^2}{2\lambda_z^2}\left(-\frac{r_i^2\lambda_z}{v}+R_i^2\right)\left(\frac{1}{r_i^2}-\frac{1}{r^2}\right)\\
&= \frac{v}{\lambda_z}\ln\left[\frac{r}{r_i}\right] + \frac{v^2}{2\lambda_z^2}\left(-\frac{R^2}{r^2}+\frac{R_i^2}{r_i^2}\right)
\end{aligned} \tag{4.19}$$

and

$$\mathfrak{J}_b = \int_{r_i}^{r}\frac{1}{R^2}\overbrace{r\,dr}^{(vR/\lambda_z)\,dR} = \frac{v}{\lambda_z}\int_{R_i}^{R}\frac{dR}{R} = \frac{v}{\lambda_z}\ln\left[\frac{R}{R_i}\right]. \tag{4.20}$$

Combining the previous results (4.18), (4.19), (4.20) now yields

$$T_{rr}(R) = \frac{\mu_o}{\lambda_z}\ln\left[\frac{r_i\,R}{r\,R_i}\right] + \frac{\mu_o v}{2\lambda_z^2}\left(\frac{R^2}{r^2}-\frac{R_i^2}{r_i^2}\right). \tag{4.21}$$

The hydrostatic pressure p now follows from (4.14) and (4.21), whereupon the other

stress components from (4.15) and (4.16) become

$$T_{\theta\theta}(R) = \frac{\mu_o}{v}\left(\frac{r^2}{R^2}\right) - \frac{\mu_o v}{\lambda_z^2}\left(\frac{R^2}{r^2}\right) + \frac{\mu_o}{\lambda_z}\ln\left[\frac{r_i\, R}{r\, R_i}\right] + \frac{\mu_o v}{2\lambda_z^2}\left(\frac{R^2}{r^2} - \frac{R_i^2}{r_i^2}\right),$$
$$T_{zz}(R) = \frac{\mu_o}{v}\lambda_z^2 - \frac{\mu_o v}{\lambda_z^2}\left(\frac{R^2}{r^2}\right) + \frac{\mu_o}{\lambda_z}\ln\left[\frac{r_i\, R}{r\, R_i}\right] + \frac{\mu_o v}{2\lambda_z^2}\left(\frac{R^2}{r^2} - \frac{R_i^2}{r_i^2}\right). \tag{4.22}$$

It remains to determine r_i and λ_z in terms of v.

The axial stress expression (4.22) enables one to express the zero axial load condition (4.13) in the form

$$\left(\frac{1}{v}\lambda_z^2 - \frac{v}{2\lambda_z^2}\frac{R_i^2}{r_i^2}\right)\underbrace{\int_{r_i}^{R_c} r dr}_{\mathfrak{J}_c} - \frac{v}{2\lambda_z^2}\underbrace{\int_{r_i}^{R_c}\left(\frac{R^2}{r^2}\right) r dr}_{\mathfrak{J}_d} - \frac{1}{\lambda_z}\underbrace{\int_{r_i}^{R_c}\left(\ln\left[\frac{rR_i}{r_i R}\right]\right) r dr}_{\mathfrak{J}_e} = 0. \tag{4.23}$$

Here we have defined

$$\mathfrak{J}_c = \int_{r_i}^{R_c} r dr = \frac{1}{2}\left(R_c^2 - r_i^2\right),$$

and

$$\begin{aligned}
\mathfrak{J}_d &= \int_{r_i}^{R_c} R^2\,\frac{dr}{r} = \int_{r_i}^{R_c}\left(\frac{\lambda_z}{v}(r^2 - r_i^2) + R_i^2\right)\frac{dr}{r} \\
&= \frac{\lambda_z}{v}\mathfrak{J}_c + \left(R_i^2 - \frac{\lambda_z}{v}r_i^2\right)\ln\left[\frac{R_c}{r_i}\right] \\
&= \frac{\lambda_z}{2v}\left(R_c^2 - r_i^2\right) + \frac{1}{2}\left(R_i^2 - \frac{\lambda_z}{v}r_i^2\right)\ln\left[\frac{R_c^2}{r_i^2}\right],
\end{aligned}$$

and

$$\begin{aligned}
\mathfrak{J}_e &= \int_{r_i}^{R_c} \left(\ln\left[\frac{rR_i}{r_i R}\right] \right) r\,dr = \int_{r_i}^{R_c} \left(\ln\left[\frac{r}{r_i}\right] \right) r\,dr - \int_{r_i}^{R_c} \left(\ln\left[\frac{R}{R_i}\right] \right) \overbrace{r\,dr}^{(vR/\lambda_z)\,dR} \\
&= \int_{r_i}^{R_c} \left(\ln\left[\frac{r}{r_i}\right] \right) r\,dr - \frac{v}{\lambda_z} \int_{R_i}^{R_o} \left(\ln\left[\frac{R}{R_i}\right] \right) R\,dR \\
&= \left\{ -\frac{1}{4}\left(R_c^2 - r_i^2\right) + \frac{1}{2} R_c^2 \ln\left[\frac{R_c}{r_i}\right] \right\} - \frac{v}{\lambda_z} \left\{ -\frac{1}{4}\left(R_o^2 - R_i^2\right) + \frac{1}{2} R_o^2 \ln\left[\frac{R_o}{R_i}\right] \right\} \\
&= \frac{1}{4}\Big(-R_c^2 + \underbrace{r_i^2 + \frac{v}{\lambda_z}(R_o^2 - R_i^2)}_{R_c^2} + R_c^2 \ln\left[\frac{R_c^2}{r_i^2}\right] - \frac{v}{\lambda_z} R_o^2 \ln\left[\frac{R_o^2}{R_i^2}\right] \Big),
\end{aligned}$$

so that

$$\mathfrak{J}_e = \frac{1}{4} R_c^2 \ln\left[\frac{R_c^2}{r_i^2}\right] - \frac{v}{4\lambda_z} R_o^2 \ln\left[\frac{R_o^2}{R_i^2}\right].$$

The axial force balance (4.23) thus contains terms either with or without $\ln[\cdot]$ functions. Using the expressions for $\mathfrak{J}_c$ and $\mathfrak{J}_d$ in the right side of (4.23) one finds that the terms that do not contain logarithm factors sum to

$$\frac{1}{2}\Big(\underbrace{R_c^2 - r_i^2}_{v(R_o^2 - R_i^2)/\lambda_z} \Big) \left(\frac{\lambda_z^2}{v} - \frac{v}{2\lambda_z^2} \frac{R_i^2}{r_i^2} - \frac{1}{2\lambda_z} \right) = \frac{v}{4\lambda_z^2} (R_o^2 - R_i^2) \left(\frac{2\lambda_z^3}{v} - \frac{v}{\lambda_z} \frac{R_i^2}{r_i^2} - 1 \right).$$

Using the expressions for $\mathfrak{J}_d$ and $\mathfrak{J}_e$ in the right side of (4.23) one finds that the terms that contain the logarithm factors sum to

$$\frac{1}{4\lambda_z} \Bigg(\underbrace{-\frac{v}{\lambda_z} R_i^2 + r_i^2 - R_c^2}_{-vR_o^2/\lambda_z} \Bigg) \ln\left[\frac{R_c^2}{r_i^2}\right] + \frac{v}{4\lambda_z^2} R_o^2 \ln\left[\frac{R_o^2}{R_i^2}\right] = \frac{v}{4\lambda_z^2} R_o^2 \ln\left[\frac{r_i^2 R_o^2}{R_c^2 R_i^2}\right].$$

Combining these results and dividing by $vR_o^2/4\lambda_z^2$ puts the zero axial load condition

into the form

$$\ln\left[\frac{r_i^2 R_o^2}{R_c^2 R_i^2}\right] + \left(1 - \frac{R_i^2}{R_o^2}\right)\left(\frac{2\lambda_z^3}{v} - \frac{vR_i^2}{\lambda_z r_i^2} - 1\right) = 0.$$

We now eliminate r_i in this equation by substituting from (4.9). The various radial distances can be normalized out by introducing the initial thickness ratio $\zeta \equiv R_i/R_o < 1$ and recalling that $\lambda_{lat} = R_c/R_o$.

The result of this long string of calculations that began with (4.23) is:

$$\ln\left[\frac{1}{\zeta^2} - \frac{v}{\lambda_z\lambda_{lat}^2}\left(\frac{1-\zeta^2}{\zeta^2}\right)\right] - (1-\zeta^2)\left(1 - \frac{2\lambda_z^3}{v} + \frac{v\zeta^2}{\lambda_z\lambda_{lat}^2 + v(\zeta^2-1)}\right) = 0. \quad (4.24)$$

Equation (4.24) is a single equation for the determination of $\lambda_z = \lambda_z(v)$ at any swelling value $v \geq \lambda_{lat}^3$ associated with wall contact.

In terms of these normalizations the restriction (4.10) on λ_z now writes itself as

$$\lambda_z \geq (1-\zeta^2)v/\lambda_{lat}^2. \quad (4.25)$$

Once λ_z is known then r_i follows from (4.9). Finally, with the two primary unknowns r_i and λ_z so determined, the lateral confinement pressure P_{lat} follows from the evaluation of (4.21) at $R = R_o$. Specifically, $P_{lat} = P_{lat}(v, \zeta, \lambda_{lat})$ is found to take the form

$$P_{lat} = \frac{\mu_o}{2\lambda_z}\ln\left[\frac{\lambda_z\lambda_{lat}^2\zeta^2}{\lambda_z\lambda_{lat}^2 - v(1-\zeta^2)}\right] + \frac{\mu_o v}{2\lambda_z^2}\left(\frac{\lambda_z\zeta^2}{\lambda_z\lambda_{lat}^2 - v(1-\zeta^2)} - \frac{1}{\lambda_{lat}^2}\right), \quad (4.26)$$

using $\lambda_z = \lambda_z(v)$.

The initial contact value $v = \lambda_{lat}^3$ causes (4.24) to be satisfied with $\lambda_z = \lambda_{lat}$ for all ζ. These values then make $P_{lat} = 0$ thus confirming consistency with all of the conditions associated with first wall contact.

4.4.1 Existence and uniqueness

The natural question that arises is whether (4.24) has a unique solution for λ_z obeying (4.25) for all $v > \lambda_{lat}^3$. For this purpose we define

$$G(\lambda_z; v, \zeta, \lambda_{lat}) \equiv \ln\left[\frac{1}{\zeta^2} - \frac{v}{\lambda_z \lambda_{lat}^2}\left(\frac{1-\zeta^2}{\zeta^2}\right)\right], \tag{4.27}$$

$$H(\lambda_z; v, \zeta, \lambda_{lat}) \equiv (1-\zeta^2)\left(1 - \frac{2\lambda_z^3}{v} + \frac{v\zeta^2}{\lambda_z\lambda_{lat}^2 - v(1-\zeta^2)}\right). \tag{4.28}$$

Now the solution to (4.24) for λ_z is equivalent to the solution of $G = H$. Note that at first wall contact, where $v = \lambda_{lat}^3$ and $\lambda_z = \lambda_{lat}$, one finds that both G and H vanish, i.e.,

$$G(\lambda_{lat}; \lambda_{lat}^3, \zeta, \lambda_{lat}) = 0, \qquad H(\lambda_{lat}; \lambda_{lat}^3, \zeta, \lambda_{lat}) = 0,$$

confirming that $G = H$ at the first wall contact.

The following two lemmas will be used to establish the existence of a solution.

Lemma 1. *If* $\lambda_z \downarrow (1-\zeta^2)\dfrac{v}{\lambda_{lat}^2}$ *then* $G < H$.

Proof. The notation $\downarrow$ means that the approach is from above. We do not simply evaluate λ_z at $(1-\zeta^2)v/\lambda_{lat}^2$ because

$$\lambda_z \downarrow (1-\zeta^2)v/\lambda_{lat}^2 \quad \Rightarrow \quad G \to -\infty, \quad \text{and} \quad H \to \infty,$$

which will be sufficient to establish the result.

To see that indeed $G \to -\infty$ take $\lambda_z = (1-\zeta^2+\delta_1)v/\lambda_{lat}^2$ whereupon $G = \ln[\delta_1/(\zeta^2(1-\zeta^2+\delta_1))] \to -\infty$ as $\delta_1 \downarrow 0$.

To see that indeed $H \to \infty$ take $\lambda_z = \delta_2 + (1-\zeta^2)v/\lambda_{lat}^2$ whereupon

$$H = (1-\zeta^2)\left(\frac{v^2\zeta^2\lambda_{lat}^4 + \delta_2 v\lambda_{lat}^6 - 2\delta_2(v - v\zeta^2 + \delta_2\lambda_{lat}^2)^3}{\delta_2 v\lambda_{lat}^6}\right) \to (1-\zeta^2)\left(\frac{v^2\zeta^2\lambda_{lat}^4}{\delta_2 v\lambda_{lat}^6}\right) \to \infty$$

as $\delta_2 \downarrow 0$. $\square$

Lemma 2. *If $\lambda_z \to \infty$ then $G > H$.*

Proof. It follows that

$$\lim_{\lambda_z \to \infty} G(\lambda_z; v, \zeta, \lambda_{lat}) = \ln\left[\frac{1}{\zeta^2}\right] > 0,$$

since $0 < \zeta < 1$. Also

$$\lim_{\lambda_z \to \infty} H(\lambda_z; v, \zeta, \lambda_{lat}) \to (1-\zeta^2)\left(-\frac{2\lambda_z^3}{v}\right) \to -\infty,$$

thus confirming the result. $\square$

Thus by continuity the graphs of G and H must intersect on $\lambda_z > (1-\zeta^2)v/\lambda_{lat}^2$ thereby ensuring existence. Furthermore, if it is also the case that G is increasing and H is decreasing everywhere on this range, then the intersection will be unique. This is ensured by the next lemma.

Lemma 3. *For fixed $v > 0$, $0 < \zeta < 1$, $\lambda_{lat} > 0$ it follows that*

$$\frac{dG}{d\lambda_z} > 0, \qquad \frac{dH}{d\lambda_z} < 0 \quad \textit{for all} \quad \lambda_z > (1-\zeta^2)\frac{v}{\lambda_{lat}^2}.$$

Proof. The derivative of (4.27) is

$$\frac{dG}{d\lambda_z} = \frac{v\,(1-\zeta^2)}{\lambda_z\,(\lambda_{lat}^2\lambda_z - v\,(1-\zeta^2))}. \tag{4.29}$$

On the right hand side of this equation the numerator $v(1-\zeta^2)$ is positive. The factor in the denominator $(\lambda_{lat}^2\lambda_z - v(1-\zeta^2))$ is positive because $\lambda_z > (1-\zeta^2)v/\lambda_{lat}^2$. Thus this derivative is positive and the first condition is confirmed.

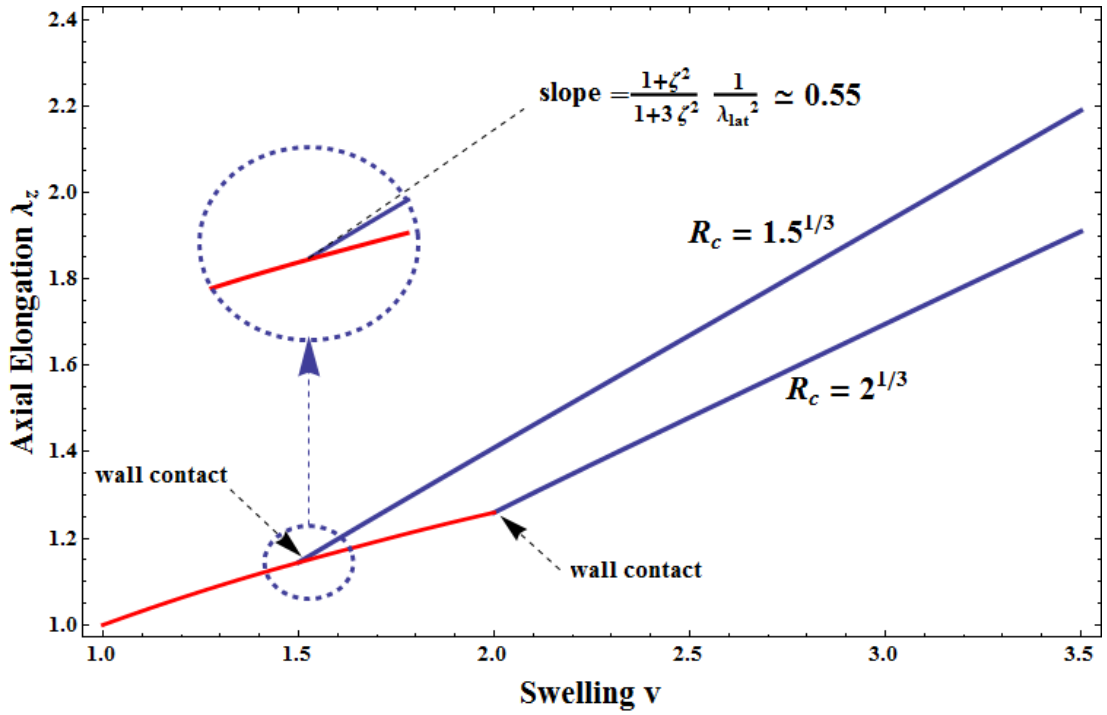

Figure 4.4 Axial elongation λ_z as a function of swelling v for the expanding annular plug with inner radius $R_i = 1/2$ and outer radius $R_o = 1$ (so that $\lambda_{lat} = R_c$ and $\zeta = 1/2$). Wall contact occurs when $v = \lambda_{lat}^3$. The graphs are for two separate cases of outer pipe radius: $R_c = 1.145$ and $R_c = 1.260$, which are chosen so as to give contact v values of 1.5 and 2, respectively. The slope of the curves immediately after contact are given by (4.31).

The derivative of (4.28) is

$$\frac{dH}{d\lambda_z} = -\left[1-\zeta^2\right]\left(\left[\frac{6{\lambda_z}^2}{v}\right] + \left[\frac{v\lambda_{lat}^2\zeta^2}{\left(\lambda_{lat}^2\lambda_z - v\left(1-\zeta^2\right)\right)^2}\right]\right), \tag{4.30}$$

where all of the terms in brackets $[\cdot]$ are positive. Hence this derivative is negative and the lemma is proved. □

4.4.2 Numerical demonstrations

As an example, consider the axial stretch λ_z as determined by (4.24) for a case where $R_i = 1/2$ and $R_o = 1$ (making $\zeta = 0.5$). Figure 4.4 plots λ_z as a function of v for the two different pipe confinement radii considered previously in Section 4.2:

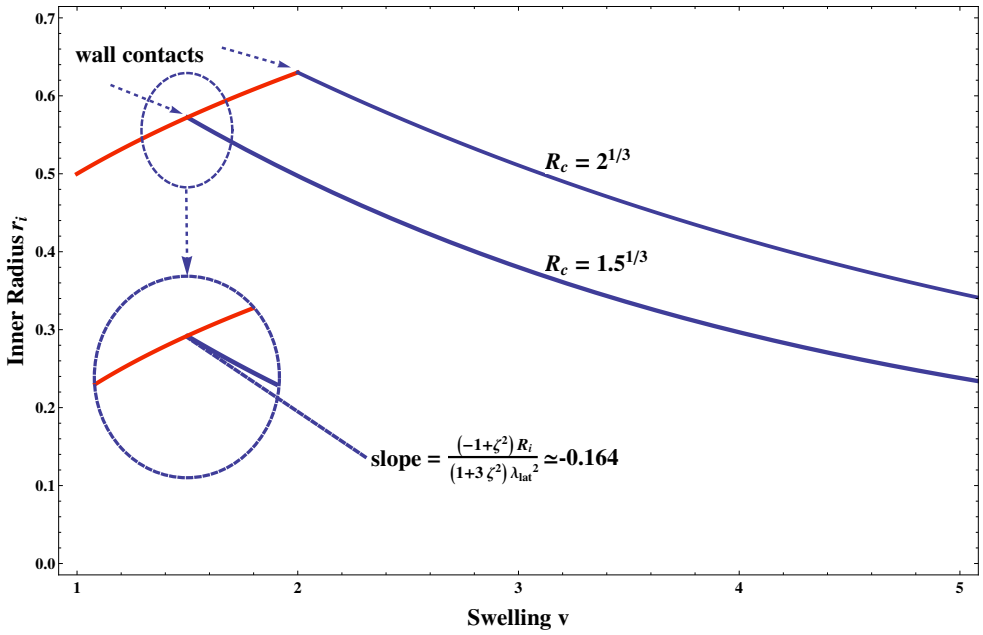

Figure 4.5 Deformed inner radius r_i as a function of swelling v for the wall contact cases from Fig. 4.4. Prior to wall contact the swelling $v < \lambda_{lat}^3$ and the homogeneous deformation causes r_i to increase. After contact, when $v > \lambda_{lat}^3$, the inner radius is monotonically decreasing with swelling.

$R_c = 1.5^{1/3} = 1.145$ and $R_c = 2^{1/3} = 1.260$. Consequently, $\lambda_{lat} = R_c/R_o = R_c$. Wall contact takes place when $v = \lambda_{lat}^3 = R_c^3$ and hence either $v = 1.5$ or $v = 2$. These aspects all mirror the situation considered previously with respect to Figure 4.3, although of course there was no channel in that case (formally $R_i = 0$) whereas now we are taking $R_i = 0.5$.

Prior to wall contact ($v < \lambda_{lat}^3$) the homogeneous free-swelling deformation gives $\lambda_z = v^{1/3}$ and this relation is the first part of the graphs in Figure 4.4. At wall contact the axial elongation noticibly increases. By implicitly differentiating (4.24) with respect to v and evaluating the result at $v = \lambda_{lat}^3$ one obtains the slope immediately after **f**irst **c**ontact

$$\left.\frac{d\lambda_z}{dv}\right|_{fc} = \left(\frac{1+\zeta^2}{1+3\zeta^2}\right)\frac{1}{\lambda_{lat}^2} > \frac{1}{3\lambda_{lat}^2}, \tag{4.31}$$

where the value $\frac{1}{3}\lambda_{lat}^{-2}$ is the slope of the free-swelling part of the curve just before contact with the wall.

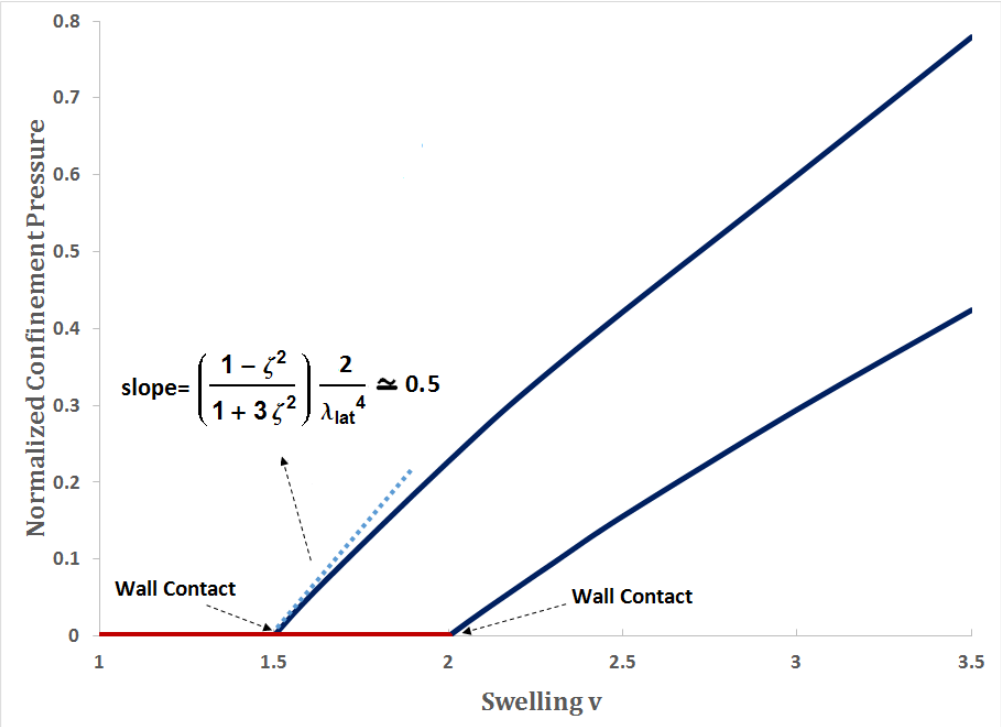

Figure 4.6 Confinement pressure P_{lat} as a function of swelling v for the wall contact cases from Figs. 4.4 and 4.5. Here P_{lat} is normalized by the material modulus μ_o. The slope at first contact is given by (4.32).

Prior to wall contact the inner radius r_i is increasing with v according to the simple homogeneous deformation rule $r_i = v^{1/3}R_i$. At wall contact this increase is reversed so that after wall contact r_i is decreasing with v. These decreasing values are found by using the previously obtained $\lambda_z = \lambda_z(v)$ in the kinematic condition (4.9). Hence the channel achieves a maximum of r_i given by $\lambda_{lat}R_i = R_cR_i/R_o$ at first wall contact when $v = (R_c/R_o)^3$. This is shown in Figure 4.5 for the same cases considered in Fig. 4.4. Differentiating (4.9) and using (4.31) gives the decreasing slope immediately after first contact

$$\frac{dr_i}{dv}\Big|_{fc} = -\left(\frac{1-\zeta^2}{1+3\zeta^2}\right)\frac{R_i}{\lambda_{lat}^2} < 0,$$

thus showing the abrupt turn-around in the radial deformation.

As was the case for the plug without a channel (Section 4.2) the surface $R = R_o$ is traction free until wall contact. After becoming confined by the wall at R_c the contact pressure is given by (4.26). The monotonic increase of this P_{lat} with v is shown in Figure 4.6 for the same cases as considered in Figs. 4.4 and 4.5. Differentiating (4.26) and using (4.31) it is found that the slope of these curves just after contact is given by

$$\frac{dP_{lat}}{dv}\Big|_{fc} = \left(\frac{1-\zeta^2}{1+3\zeta^2}\right)\frac{2\mu}{\lambda_{lat}^4} > 0. \tag{4.32}$$

This can be compared to the slope of P_{lat} at first contact for the plug without a channel that is obtained by differentiation of (4.3) and evaluation at $v = \lambda_{lat}^3$ yielding $2\mu_o/\lambda_{lat}^4$. As one might have anticipated, this matches (4.32) in the $\zeta \to 0$ limit corresponding to zero channel radius. More generally, the initial slope (4.32) of the contact pressure is decreasing with ζ. This is consistent with the expectation that the contact force generated by the expanding annulus would decrease as its wall becomes thinner. One would similarly anticipate that the pressure curves would exhibit this

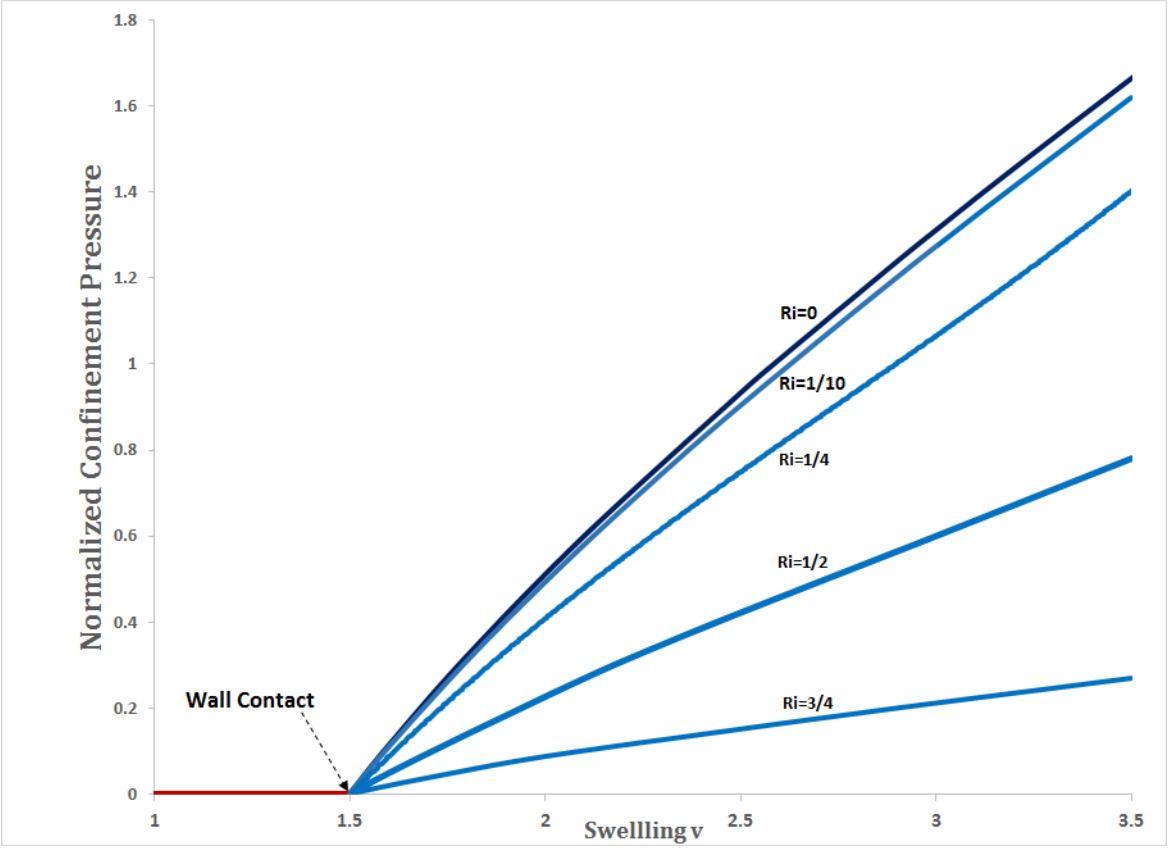

Figure 4.7 Confinement pressure P_{lat} for a solid plug ($R_i = 0$) and for tubes (annulus plugs with $R_i = 1/10, 1/4, 1/2, 3/4$) as a function of swelling v. In all cases $R_o = 1$ (so that $\lambda_{lat} = R_c$). The confining radius is $R_c = 1.5^{1/3}$ so as to be consistent with one of the cases shown previously in Figs. 4.4, 4.5 and 4.6. P_{lat} is again normalized by the material modulus μ_o. The zero channel radius limit ($\zeta = 0$) recovers the neo-Hookean type curves in Fig. 4.3. Thinner walls (larger ζ) give less contact pressure for the same value of swelling.

decreasing contact pressure with wall thickness not only at first contact, but for all values of swelling. This is confirmed in Figure 4.7 where the contact pressure as a function of v is shown for a variety of thicknesses ratios ζ.

4.4.3 Asymptotic behavior for large swelling values

The examples of Section 4.4.2 raise an obvious question as to the channel closing behavior in the large v limit. Specifically, when viewing a graph like that given in Fig. 4.5 one can ask which of the three logical alternatives occurs: (a) the channel closes at some finite v, (b) the channel never fully closes but approaches a zero radius as v tends to infinity, or (c) the channel radius approaches a finite positive asymptote as v tends to infinity?

To answer this question we first perform a $v \to \infty$ asymptotic analysis of the condition $G = H$ in order to extract the large v behavior of λ_z. To this end we first observe from (4.25) that the bound $v/\lambda_z \leq \lambda_{lat}^2/(1-\zeta^2)$ gives that $\lambda_z \to \infty$ as $v \to \infty$. If λ_z is order Cv^m in this limit then $m \geq 1$. Furthermore if $m > 1$ then $C > 0$ and if $m = 1$ then $C \geq (1-\zeta^2)/\lambda_{lat}^2$.

Consider a case in which $\lambda_z \sim Cv^m$ with $m > 1$. It would then follow from (4.27) and (4.28) that

$$G = \ln\left[\frac{1}{\zeta^2}\right] + o(1) \quad \text{and} \quad H = -(1-\zeta^2)\frac{2\lambda_z^3}{v} + O(1) \quad \text{as } v \to \infty. \tag{4.33}$$

This case is now discarded because (4.33) is inconsistent with meeting the condition $G = H$ in the large v limit. It is thus concluded that

$$\lambda_z = Cv + o(v) \quad \text{with } C \geq (1-\zeta^2)/\lambda_{lat}^2 \text{ as } v \to \infty.$$

If the inequality is strict, i.e., if $C > (1-\zeta^2)/\lambda_{lat}^2$, this then makes

$$G = \ln\left[1 - \frac{1-\zeta^2}{C\lambda_{lat}^2} + o(1)\right] + O(1),$$

and

$$H = (1-\zeta^2)\left(1 - 2C^3v^2 + o(v^2) + \frac{\zeta^2}{C\lambda_{lat}^2 - (1-\zeta^2)} + O(1)\right),$$

so that once again it is not possible to meet the condition $G = H$ in the large v limit. Therefore the remaining possibility is that $\lambda_z \sim Cv$ with $C = (1-\zeta^2)/\lambda_{lat}^2$ whereupon we write

$$\lambda_z = Cv\,(1+\epsilon_1(v)) \;\text{ with }\; C = (1-\zeta^2)/\lambda_{lat}^2 \;\text{ and }\; \epsilon_1(v) = o(1) \;\text{ as }\; v \to \infty. \quad (4.34)$$

It then follows that

$$G = \ln\left[\frac{1}{\zeta^2}\right] + \ln\left[\frac{\epsilon_1}{1+\epsilon_1}\right] = \ln[\epsilon_1] + O(1)$$

and

$$\begin{aligned} H &= (1-\zeta^2)\left(1 - \frac{2}{v}C^3v^3(1+3\epsilon_1+O(\epsilon_1^2)) + \frac{v\zeta^2}{v(1-\zeta^2)(1+\epsilon_1) - v(1-\zeta^2)}\right) \\ &= (1-\zeta^2)\left(1 - 2C^3v^2 + O(\epsilon_1 v^2) + \frac{\zeta^2}{1-\zeta^2}\frac{1}{\epsilon_1}\right) \\ &= -2(1-\zeta^2)C^3v^2 + \frac{\zeta^2}{\epsilon_1} + O(1) + o(v^2). \end{aligned}$$

Hence the condition $G = H$ gives

$$\ln[\epsilon_1] + O(1) = -2(1-\zeta^2)C^3v^2 + \frac{\zeta^2}{\epsilon_1} + O(1) + o(v^2), \quad \text{as } v \to \infty. \quad (4.35)$$

There are three main terms in (4.35) and at this stage it is not obvious which two

are dominant, and hence in balance with each other, as $v \to \infty$. We seek the leading order behavior in the function $\epsilon_1(v)$ so as to provide the appropriate balance between whichever two terms are in fact dominant.

There are three possible ways to balance the expression (4.35):

$$\overbrace{\ln[\epsilon_1] = \underbrace{-2(1-\zeta^2)C^3v^2}_{I} + \underbrace{\frac{\zeta^2}{\epsilon_1}}_{III}}^{II}. \tag{4.36}$$

Balance possibility I gives $\epsilon_1 \sim e^{-2(1-\zeta^2)C^3v^2}$, so that the two balanced terms are $O(v^2)$. However, this makes the third (unbalanced) term $\zeta^2/\epsilon_1 \sim \zeta^2 e^{2(1-\zeta^2)C^3v^2}$ which dominates the $O(v^2)$ terms as $v \to \infty$. Hence balance I is inconsistent and so removed from further consideration.

Balance possibility II involves two terms that are of fundamentally different orders and hence cannot balance each other. This balance possibility is therefore also discarded.

Balance possibility III yields

$$\epsilon_1 \sim \frac{\zeta^2}{2(1-\zeta^2)C^3}\frac{1}{v^2}, \qquad \text{as} \quad v \to \infty$$

which is consistent with the requirement that $\epsilon_1(v) = o(1)$ as $v \to \infty$. The remaining unbalanced term in (4.36) is $O(\ln[v])$ and hence satisfies the requirement that it is dominated by the $O(v^2)$ terms that are in balance for this possibility.

Hence III provides a consistent balance, and it is the only consistent balance from among the three possibilities diagrammed in (4.36). Thus the $\epsilon_1(v)$ appearing in (4.34) can now be written as

$$\epsilon_1(v) = \frac{\zeta^2}{2(1-\zeta^2)C^3}\frac{1}{v^2}(1+\epsilon_2(v)) \text{ with } \epsilon_2(v) = o(1) \text{ as } v \to \infty$$

where C continues to be by given $(1-\zeta^2)/\lambda_{lat}^2$. Continuing the analysis now using

$$\lambda_z = Cv\left(1+\frac{\zeta^2}{2(1-\zeta^2)C^3}\frac{1}{v^2}(1+\epsilon_2)\right)$$

it is found that G becomes simply

$$G = -2\ln[v] + O(1).$$

On the other hand, the determination of the leading behavior for H requires a sequence of tedious manipulations that results in

$$H = (1-\zeta^2) - \frac{3(1-\zeta^2)\zeta^2}{\lambda_{lat}^6 C^3} - 2C^3(1-\zeta^2)\epsilon_2 v^2 + O(\epsilon_2) + O(v^{-2}) + O(\epsilon_2^2 v^2).$$

Enforcing the condition $G = H$ now leads to the conclusion that

$$\epsilon_2 \sim \frac{\lambda_{lat}^6}{(1-\zeta^2)^4}\frac{1}{v^2}\ln[v].$$

Consolidating all of these results provides the following asymptotic expression for λ_z as a function of v,

$$\lambda_z = \underbrace{\frac{1-\zeta^2}{\lambda_{lat}^2}}_{C} v + \frac{\lambda_{lat}^4\zeta^2}{2(1-\zeta^2)^3}\left(\frac{1}{v}\right) + \frac{\lambda_{lat}^{10}\zeta^2}{2(1-\zeta^2)^7}\left(\frac{1}{v^3}\ln[v]\right) + o\left(\frac{1}{v^3}\ln[v]\right). \quad (4.37)$$

Employing this expansion of λ_z in the lateral pressure expression (4.26) it is found that $P_{lat} = \mu C^2 v + O(\ln[v]/v) \sim \mu(1-\zeta^2)^2 v/\lambda_{lat}^4$. Employing (4.37) in (4.9) now yields the corresponding expansion for r_i by using

$$r_i = R_o\lambda_{lat}\left(1-\frac{Cv}{\lambda_z}\right)^{1/2} = R_o\lambda_{lat}\left(1-\frac{1}{1+\epsilon_1}\right)^{1/2} = R_o\lambda_{lat}\,\epsilon_1^{1/2}(1+\epsilon_1)^{-1/2},$$

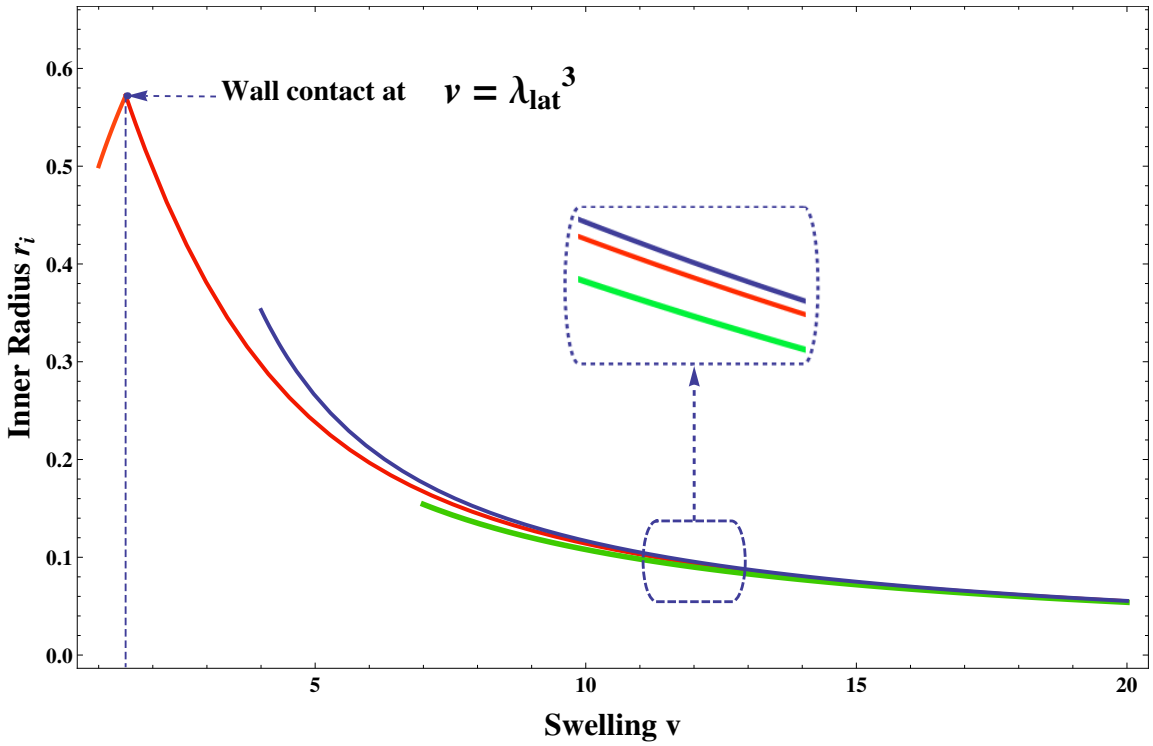

Figure 4.8 Asymptote of the deformed inner radius r_i as a function of swelling v in a hollow tube taking the inner radius $R_i = 1/2$ and the outer radius $R_o = 1$ (so that $\lambda_{lat} = R_c$ and $\zeta = 1/2$) with $R_c = 1.5^{1/3}$. The graphs are for the pure numerical solution (red curve in the middle) and the asymptotic expansion (4.38) with only the leading term (green curve on the bottom) and with the additional first correction term (blue curve on the top).

with ϵ_1 again defined as in (4.34). It follows that

$$\frac{r_i}{R_o} = \frac{\sqrt{2}}{2}\frac{\lambda_{lat}^4\,\zeta}{(1-\zeta^2)^2}\left(\frac{1}{v}\right) + \frac{\sqrt{2}}{4}\frac{\lambda_{lat}^{10}\,\zeta}{(1-\zeta^2)^6}\left(\frac{1}{v^3}\ln[v]\right) + o\left(\frac{1}{v^3}\ln[v]\right), \tag{4.38}$$

which shows for this material model how the channel closes in the large v asymptotic limit. This is depicted in Figure 4.8 where the asymptotic result is compared with the pure numerical treatment.

CHAPTER V

Channel Confinement Swelling of Internally Balanced Material Plugs and Tubes

5.1 Internally balanced elastic materials

Chapters *II* to *IV* considered swelling in the purely hyperelastic context. In this chapter we broaden the material constitutive theory so as to place swelling in the framework of internally balanced materials. The theory of internally balanced elastic materials as described in *Demirkoparan et al.* (2014); *Demirkoparan and Pence* (2015a); *Hadoush et al.* (2017, 2014, 2015) makes use of the general multiplication decomposition of the deformation gradient $\mathbf{F} = \hat{\mathbf{F}}\mathbf{F}^*$ that was also used here in (1.3). Such a decomposition, which was originally invoked in the setting of finite deformation plasticity due to dislocation slip *Kröner* (1959); *Lee* (1969), is now commonly used in other mechanical descriptions of finite deformations, including thermoelastic deformation *Vujošević and Lubarda* (2002), crystallographic transformation plasticity *Havner* (1992); *Forest et al.* (2014) and biological growth *Chen and Hoger* (2000). In such treatments the first factor in (1.3) typically describes the action of the physical effect under consideration and the second factor $\hat{\mathbf{F}}$ corresponds to some sort of elastic recovery or accommodation. This allows $\hat{\mathbf{F}}$ to be described via energy minimization, whereas $\mathbf{F}^*$ need not in general have a corresponding energetic framework. Indeed it may be the case that the phenomena described by $\mathbf{F}^*$ is inherently dissipative. In contrast, the theory of internally balance elastic materials as studied in *Demirkoparan*

et al. (2014); *Demirkoparan and Pence* (2015a); *Hadoush et al.* (2017, 2014, 2015) specifically attributes an energy minimal variational structure to both factors in the decomposition (1.3).

The internally balanced material theory as described in *Hadoush et al.* (2017, 2014, 2015) involved no material constraint whereas the internally balanced material theory as described in *Demirkoparan et al.* (2014); *Demirkoparan and Pence* (2015a) involved the material constraint of incompressibility. It is our purpose here to consider the effect of the constraint (1.1) in the internal balance theory. Recall the discussion in page 10 that indicated the possibility of considering functions $\mathbf{F}^*$ in (1.3) that were not prescribed to be equal to $v^{1/3}\mathbf{I}$. For our purpose we instead specify that the individual factors in (1.3) are to be subject to the individual constraints

$$det\hat{\mathbf{F}} = 1, \qquad det\mathbf{F}^* = v. \tag{5.1}$$

The special case of (5.1) with $v = 1$ then recovers the treatment as given in *Demirkoparan et al.* (2014); *Demirkoparan and Pence* (2015a).

One motivation for the particular constraint choice (5.1) is that it makes the decomposition $\mathbf{F} = \hat{\mathbf{F}}\mathbf{F}^*$ a generalization of the simpler decomposition $\mathbf{F} = v^{1/3}\hat{\mathbf{F}}$ with $\det\hat{\mathbf{F}} = 1$. This simpler decomposition is a special case of $\mathbf{F} = \hat{\mathbf{F}}\mathbf{F}^*$ as can be seen by taking $\mathbf{F}^* = v^{1/3}\mathbf{I}$. The simpler decomposition $\mathbf{F} = v^{1/3}\hat{\mathbf{F}}$ with $\det\hat{\mathbf{F}} = 1$ has served as a useful description of material swelling in a more conventional hyperelastic framework *Tsai et al.* (2004); *Pence and Tsai* (2005b); *Demirkoparan and Pence* (2007a); *Fang et al.* (2011). In contrast the framework presented here does not require that $\mathbf{F}^* = v^{1/3}\mathbf{I}$; hence it offers the possibility of modeling more complicated swelling phenomena.

Mirroring conventional hyperelasticity let W denote the mechanical energy storage density per unit volume in the reference configuration. This W is to depend on both $\hat{\mathbf{F}}$ and $\mathbf{F}^*$ and thus any such W is described in terms of alternative and equivalent constitutive specifications

$$W = \Phi^{(0)}(\mathbf{F}, \mathbf{F}^*, v) = \Phi^{(1)}(\mathbf{F}, \hat{\mathbf{F}}, v) = \Phi^{(2)}(\hat{\mathbf{F}}, \mathbf{F}^*, v), \tag{5.2}$$

with $\mathbf{F}$, $\hat{\mathbf{F}}$ and $\mathbf{F}^*$ related via (1.3). A specification for any one of the energy density functions $\Phi^{(0)}$, $\Phi^{(1)}$ or $\Phi^{(2)}$ permits determination of the other two by simply requiring consistency with (1.3). In what follows we shall omit v in the argument list of these energy density functions in order to provide a simpler notation. Continuum mechanics principles such as material frame indifference and material symmetry place specific restrictions on the way in which these energy densities may depend upon $\mathbf{F}$, $\mathbf{F}^*$, and $\hat{\mathbf{F}}$. The principle of material frame indifference specifically gives that

$$W = \Phi^{(3)}(\mathbf{C}, \mathbf{C}^*), \tag{5.3}$$

with

$$\mathbf{C} = \mathbf{F}^T\mathbf{F}, \qquad \mathbf{C}^* = (\mathbf{F}^*)^T\mathbf{F}^*, \qquad \hat{\mathbf{C}} = \hat{\mathbf{F}}^T\hat{\mathbf{F}}. \tag{5.4}$$

Although $\hat{\mathbf{C}}$ does not appear in (5.3) it is introduced in (5.4) because of subsequent developments. By virtue of (5.1) it follows that $\det\mathbf{C} = \det\mathbf{C}^* = v^2$ and $\det\hat{\mathbf{C}} = 1$. It is to be remarked that $\mathbf{C}$ and $\mathbf{C}^*$ do not determine $\hat{\mathbf{C}}$, and thus one may *not* conclude that W can be written as a function of $\mathbf{C}$ and $\hat{\mathbf{C}}$. The function $\Phi^{(3)}$ can always be expressed as a symmetric function of the tensors $\mathbf{C}$ and $\mathbf{C}^*$, and it is presumed that this is the case in going forward *Demirkoparan et al.* (2014).

As in conventional hyperelasticity, equilibrium deformations minimize the total stored energy minus the work of any body forces and prescribed surface tractions. The total stored energy is computed by the volume integral of W taken with respect to the reference configuration. In terms of $\Phi^{(0)}$ this energy integral is

$$\mathcal{E}(\chi, \mathbf{F}^*) = \int_{\mathcal{B}} \Phi^{(0)}(\nabla\chi, \mathbf{F}^*) dV_R. \tag{5.5}$$

The work functional $\mathcal{W}(\chi)$ is a volume integral over the region that is subject to body forces in conjunction with a surface integral over the portion of the boundary that is subject to prescribed surface tractions. The minimization is both with respect to deformations χ and with respect to the factor $\mathbf{F}^*$. Incorporating the constraints (5.1) by means of Lagrange multiplier fields $p = p(\mathbf{X})$ and $q = q(\mathbf{X})$ the functional that is to remain stationary with respect to variations of χ, $\mathbf{F}^*$, p and q can be taken as

$$\mathcal{I}(\chi, \mathbf{F}^*) = \mathcal{E}(\chi, \mathbf{F}^*) - \mathcal{W}(\chi) - \int_{\mathcal{B}} p(\det\nabla\chi - v) dV_R - \int_{\mathcal{B}} q(\det\mathbf{F}^* - v) dV_R. \tag{5.6}$$

For simplicity in going forward, body forces will be neglected and each boundary point is presumed to be either a free surface or else subject to a prescribed displacement. This makes the work functional $\mathcal{W}(\chi) = 0$. Consideration of body forces and consideration of more general boundary conditions is easily accomplished by specifying an appropriate $\mathcal{W}(\chi)$ *Demirkoparan et al.* (2014).

Minimization of $\mathcal{I}$ with respect to χ leads to

$$div\mathbf{T} = \mathbf{0}, \qquad \mathbf{T} = \frac{2}{v}\mathbf{F}\frac{\partial\Phi^{(3)}}{\partial\mathbf{C}}\mathbf{F}^T - p\mathbf{I}, \tag{5.7}$$

where *div* is the divergence operator with respect to the deformed configuration described by locations $\mathbf{x}$.

Minimization with respect to $\mathbf{F}^*$ provides the new aspect of the treatment. This

leads to the internal balance requirement in the form of the tensor equation

$$\frac{\partial \Phi^{(0)}}{\partial \mathbf{F}^*} - q(\det \mathbf{F}^*)\mathbf{F}^{*-T} = \mathbf{0}. \tag{5.8}$$

By using (5.3), the internal balance (5.8) is manipulated into the form

$$2\frac{\partial \Phi^{(3)}}{\partial \mathbf{C}^*} - qv\mathbf{C}^{*-1} = \mathbf{0}. \tag{5.9}$$

The partial derivatives with respect to $\mathbf{C}$ and $\mathbf{C}^*$ in $(5.7)_2$ and (5.9) involve holding the other tensor fixed (the standard meaning). For the case of no swelling, meaning $v = 1$, the above equations all reduce to those as given previously in *Demirkoparan et al.* (2014); *Demirkoparan and Pence* (2015a).

5.1.1 Retrieving the hyperelastic theory

The purely hyperelastic theory of swelling with $W = W(\mathbf{C}, v)$ and $\mathbf{T}$ given by (1.2) can be recovered form the above framework in which (1.1) is imposed as a constraint. This theory makes no explicit use of the decomposition (1.3), although it can be connected to the present framework by imposing the additional requirement $\mathbf{F}^* = v^{1/3}\mathbf{I}$. In such a case the tensor $\mathbf{C}^*$ in (5.4) becomes a prescribed quantity. As such, the notion of minimizing with respect to either $\mathbf{F}^*$ or $\mathbf{C}^*$ becomes moot so that (5.9) is no longer generated. Alternatively, taking $\mathbf{C}^* = v^{2/3}\mathbf{I}$ and temporarily allowing variation with respect to v we have that

$$\frac{\partial \Phi^{(3)}}{\partial \mathbf{C}^*} = \frac{\partial \Phi^{(3)}}{\partial v}\frac{dv}{d\mathbf{C}^*} \tag{5.10}$$

where, in view of (5.1) and (5.4),

$$\frac{dv}{d\mathbf{C}^*} = \frac{d}{d\mathbf{C}^*}(\det \mathbf{C}^*)^{1/2} = \frac{1}{2}(\det \mathbf{C}^*)^{1/2}\mathbf{C}^{*^{-1}} = \frac{1}{2}v\mathbf{C}^{*^{-1}}, \tag{5.11}$$

so that (5.9) becomes a requirement that

$$v\frac{\partial\Phi^{(3)}}{\partial v}\mathbf{C}^{*-1} - qv\mathbf{C}^{*-1} = \mathbf{0}, \tag{5.12}$$

which is satisfied identically provided that q takes on the pleasing form

$$q = \frac{\partial\Phi^{(3)}}{\partial v}. \tag{5.13}$$

Thus by a variety of arguments it is confirmed that (5.9) plays no role if $\mathbf{F}^*$ is stipulated in the form $\mathbf{F}^* = v^{1/3}\mathbf{I}$. This leaves (5.7) with $\Phi^{(3)} = \Phi^{(3)}(\mathbf{C})$ which retrieves the theory of hyperelasticity as explored in a variety of papers such as *Tsai et al.* (2004); *Pence and Tsai* (2005b); *Demirkoparan and Pence* (2007b); *Fang et al.* (2011); *Demirkoparan and Pence* (2015b); *Gou and Pence* (2016).

5.1.2 Isotropic materials

The framework as summarized in (1.1), (1.3), (5.1), (5.3), (5.7) and (5.9) is a straightforward generalization of a theory of incompressible internally balanced elastic materials, as described in *Demirkoparan and Pence* (2015a), to a theory of internally balanced elastic materials subject to prescribed volumetric change. In *Demirkoparan et al.* (2014) and *Demirkoparan and Pence* (2015a) the incompressible theory is considered in detail where it is shown that the resulting formulation describes a material that is isotropic if

$$W = \Phi^{(4)}(I_1, I_2, I_1^*, I_2^*, \hat{I}_1, \hat{I}_2). \tag{5.14}$$

The same logic continues to apply in the present setting (the change from $\det\mathbf{F}^* = 1$ to $\det\mathbf{F}^* = v$ in (5.1) has no effect on the formal argument) and thus (5.14) provides constitutive description for an isotropic material in the internally balanced treatment when swelling is present. Two questions immediately arise. The first is whether (5.14)

is consistent with (5.3). It is consistent because

$$\hat{I}_1 = \mathbf{C}^{*-1} : \mathbf{C}, \tag{5.15}$$

and

$$\hat{I}_2 = \frac{1}{2}\big((\mathbf{C}^{*-1} : \mathbf{C})(\mathbf{C}^{*-1} : \mathbf{C}) - (\mathbf{C}^{*-1}\mathbf{C}) : (\mathbf{C}\mathbf{C}^{*-1})\big), \tag{5.16}$$

which allows $\hat{I}_1$ and $\hat{I}_2$ to be calculated directly from $\mathbf{C}$ and $\mathbf{C}^*$. The second question is to what extent (5.14) is consistent with the usual isotropy stipulation in terms of a material symmetry group that consists of all proper rotations. This issue is also discussed in *Demirkoparan et al.* (2014) where it is shown that (5.1) is consistent with material isotropy in the standard sense. However because of the decomposition (1.3) one may introduce secondary stipulations on the individual parts, including a notion of interstitial symmetry. As discussed in *Demirkoparan et al.* (2014) the form (5.14) is not generally consistent with the additional notion of isotropic interstitial symmetry. However, the form (5.14) does become consistent with the notion of isotropic interstitial symmetry if the argument list of $\Phi^{(4)}$ in (5.14) is restricted so as to include only $(I_1^*, I_2^*, \hat{I}_1, \hat{I}_2)$.

For the purpose of using $(5.7)_2$ and (5.9) for materials obeying (5.14) it is noted that

$$\begin{aligned}\frac{\partial \Phi^{(3)}}{\partial \mathbf{C}} &= \frac{\partial \Phi^{(4)}}{\partial I_1}\mathbf{I} + \frac{\partial \Phi^{(4)}}{\partial I_2}\big(I_1\mathbf{I} - \mathbf{C}\big) + \frac{\partial \Phi^{(4)}}{\partial \hat{I}_1}\mathbf{C}^{*-1} \\ &\quad + \frac{\partial \Phi^{(4)}}{\partial \hat{I}_2}\big(\hat{I}_1\mathbf{C}^{*-1} - \mathbf{C}^{*-1}\mathbf{C}\mathbf{C}^{*-1}\big)\end{aligned} \tag{5.17}$$

and

$$\frac{\partial\Phi^{(3)}}{\partial\mathbf{C}^*} = \frac{\partial\Phi^{(4)}}{\partial I_1^*}\mathbf{I} + \frac{\partial\Phi^{(4)}}{\partial I_2^*}\big(I_1^*\mathbf{I} - \mathbf{C}^*\big) - \frac{\partial\Phi^{(4)}}{\partial\hat{I}_1}\mathbf{C}^{*-1}\mathbf{C}\mathbf{C}^{*-1}$$

$$-\frac{\partial\Phi^{(4)}}{\partial\hat{I}_2}\big(\hat{I}_1\mathbf{C}^{*-1}\mathbf{C}\mathbf{C}^{*-1} - \mathbf{C}^{*-1}\mathbf{C}\mathbf{C}^{*-1}\mathbf{C}\mathbf{C}^{*-1}\big). \tag{5.18}$$

Alternative expressions may be obtained through use of the connection $\mathbf{C}^{*-1}(\mathbf{C}\mathbf{C}^{*-1})^n = \mathbf{F}^{*-1}\hat{\mathbf{C}}^n\mathbf{F}^{*-T}$. The Cauchy stress tensor $(5.7)_2$ thus becomes

$$\mathbf{T} = \frac{2}{v}\big(\frac{\partial\Phi^{(4)}}{\partial I_1} + I_1\frac{\partial\Phi^{(4)}}{\partial I_2}\big)\mathbf{B} - \frac{2}{v}\frac{\partial\Phi^{(4)}}{\partial I_2}\mathbf{B}^2$$

$$+\frac{2}{v}\big(\frac{\partial\Phi^{(4)}}{\partial\hat{I}_1} + \hat{I}_1\frac{\partial\Phi^{(4)}}{\partial\hat{I}_2}\big)\hat{\mathbf{B}} - \frac{2}{v}\frac{\partial\Phi^{(4)}}{\partial\hat{I}_2}\hat{\mathbf{B}}^2 - p\mathbf{I} \tag{5.19}$$

with

$$\mathbf{B} = \mathbf{F}\mathbf{F}^T, \qquad \mathbf{B}^* = \mathbf{F}^*(\mathbf{F}^*)^T, \qquad \hat{\mathbf{B}} = \hat{\mathbf{F}}\hat{\mathbf{F}}^T. \tag{5.20}$$

Although $\mathbf{B}^*$ does not appear in (5.19) it is introduced in (5.20) because of subsequent developments. Also (5.1) gives $\det\mathbf{B} = \det\mathbf{B}^* = v^2$ and $\det\hat{\mathbf{B}} = 1$.

The internal balance (5.9) is cast into a convenient form by the following sequence of operations: premultiplication by $\mathbf{F}$, postmultiplication by $\mathbf{F}^T$, substitution from (5.18), and use of the Cayley Hamilton theorem to express $\hat{\mathbf{B}}^3$ in terms of lower powers. The result is

$$-2I_1^*\frac{\partial\Phi^{(4)}}{\partial I_2^*}\mathbf{F}\mathbf{C}^*\mathbf{F}^T + 2\big(\frac{\partial\Phi^{(4)}}{\partial I_1^*} + I_1^*\frac{\partial\Phi^{(4)}}{\partial I_2^*}\big)\mathbf{B}$$

$$-\bar{q}v\hat{\mathbf{B}} - 2\frac{\partial\Phi^{(4)}}{\partial\hat{I}_1}\hat{\mathbf{B}}^2 + 2\frac{\partial\Phi^{(4)}}{\partial\hat{I}_2}\mathbf{I} = \mathbf{0}, \tag{5.21}$$

where $\bar{q}$ is a redefined multiplier in place of q (formally $\bar{q}v = qv + 2\hat{I}_2\partial\Phi^{(4)}/\partial\hat{I}_2$).

A *natural configuration* for an unconstrained material is one for which the Cauchy stress vanishes, i.e., $\mathbf{T} = \mathbf{0}$. For a constrained material, a natural configuration is one for which the Cauchy stress is restricted to take the form of the constraint stress. In conventional isotropic incompressible hyperelasticity, the reference configuration is automatically a natural configuration, meaning that the stress tensor takes the form of a hydrostatic pressure. An analogous result holds for the internally balanced material. To see this for a given v we consider the state of uniform (equi-axial) swelling $\mathbf{F} = v^{1/3}\mathbf{I}$. The Cauchy stress (5.19) is then

$$\begin{aligned}\mathbf{T} &= \Big(2v^{-1/3}\frac{\partial\Phi^{(4)}}{\partial I_1} + 4v^{1/3}\frac{\partial\Phi^{(4)}}{\partial I_2} - p\Big)\Big|_{\mathbf{F}=v^{1/3}\mathbf{I}}\mathbf{I} \\ &\quad + \frac{2}{v}\Big(\frac{\partial\Phi^{(4)}}{\partial\hat{I}_1} + \hat{I}_1\frac{\partial\Phi^{(4)}}{\partial\hat{I}_2}\Big)\Big|_{\mathbf{F}=v^{1/3}\mathbf{I}}\hat{\mathbf{B}} - \frac{2}{v}\frac{\partial\Phi^{(4)}}{\partial\hat{I}_2}\Big|_{\mathbf{F}=v^{1/3}\mathbf{I}}\hat{\mathbf{B}}^2. \qquad (5.22)\end{aligned}$$

Here the subscript $\mathbf{F} = v^{1/3}\mathbf{I}$ indicates $I_1 = 3v^{2/3}$ and $I_2 = 3v^{4/3}$ with the four remaining arguments $(\hat{I}_1,\, \hat{I}_2,\, I_1^*,\, I_2^*)$ as yet undetermined. In addition $\mathbf{F} = v^{1/3}\mathbf{I}$ casts the internal balance (5.21) into the form

$$\begin{aligned}&-2v^{2/3}I_1^*\frac{\partial\Phi^{(4)}}{\partial I_2^*}\Big|_{\mathbf{F}=v^{1/3}\mathbf{I}}\mathbf{C}^* - 2\frac{\partial\Phi^{(4)}}{\partial\hat{I}_1}\Big|_{\mathbf{F}=v^{1/3}\mathbf{I}}\hat{\mathbf{B}}^2 - \bar{q}v\hat{\mathbf{B}} \\ &\quad + 2\Big(v^{2/3}\frac{\partial\Phi^{(4)}}{\partial I_1^*} + v^{2/3}I_1^*\frac{\partial\Phi^{(4)}}{\partial I_2^*} + \frac{\partial\Phi^{(4)}}{\partial\hat{I}_2}\Big)\Big|_{\mathbf{F}=v^{1/3}\mathbf{I}}\mathbf{I} = \mathbf{0}. \qquad (5.23)\end{aligned}$$

This internal balance (5.23) in conjunction with $\hat{\mathbf{F}}\mathbf{F}^* = v^{1/3}\mathbf{I}$, $\det\hat{\mathbf{F}} = 1$, and $\det\mathbf{F}^* = v$ is now a set of equations for $\hat{\mathbf{F}}$, $\mathbf{F}^*$ and $\bar{q}$. A solution to this set is given by $\hat{\mathbf{F}} = \mathbf{I}$, $\mathbf{F}^* = v^{1/3}\mathbf{I}$ and

$$\bar{q} = -\frac{2}{v}\Big(\frac{\partial\Phi^{(4)}}{\partial\hat{I}_1} - \frac{\partial\Phi^{(4)}}{\partial\hat{I}_2} - v^{2/3}\frac{\partial\Phi^{(4)}}{\partial I_1^*} + 3(v^2 - v^{4/3})\frac{\partial\Phi^{(4)}}{\partial I_2^*}\Big)\Big|_{(3v^{2/3},3v^{4/3},3,3,3v^{2/3},3v^{4/3})}. \qquad (5.24)$$

The subscript $(3v^{2/3}, 3v^{4/3}, 3, 3, 3v^{2/3}, 3v^{4/3})$ in (5.24) denotes the evaluation $(I_1, I_2, \hat{I}_1, \hat{I}_2, I_1^*, I_2^*) = (3v^{2/3}, 3v^{4/3}, 3, 3, 3v^{2/3}, 3v^{4/3})$. The particular value of $\bar{q}$ as given above plays no formal role other than to show that it allows the satisfaction of the internal balance (5.24). Then entering (5.22) with $\hat{\mathbf{B}} = \mathbf{I}$ and the full evaluation $(I_1, I_2, \hat{I}_1, \hat{I}_2, I_1^*, I_2^*) = (3v^{2/3}, 3v^{4/3}, 3, 3, 3v^{2/3}, 3v^{4/3})$ one obtains

$$\mathbf{T} = -\bar{p}\mathbf{I} \tag{5.25}$$

where $\bar{p}$ is given by a sum of terms where, with the exception of the constraint term containing $-p$, each term involves the evaluation of a derivative of $\Phi^{(4)}$ with respect to one of the six arguments $(I_1, I_2, \hat{I}_1, \hat{I}_2, I_1^*, I_2^*)$. Since the constraint pressure p in this expression is still arbitrary it follows that $\bar{p}$ in (5.25) is similarly arbitrary. Taking $\bar{p} = 0$ one obtains from (5.25) that free swelling $\mathbf{T} = \mathbf{0}$ gives an all-around equiaxial volume change $\mathbf{F} = v^{1/3}\mathbf{I}$. Furthermore since the volume v is determined by constraint, it follows more generally from (5.25) that equiaxial volume change is consistent with an arbitrary hydrostatic pressure $\bar{p}$. All of these results exactly mirror that of conventional isotropic hyperelasticity with a volume constraint. In particular, as in conventional isotropic incompressible hyperelasticity, the reference configuration is automatically a natural configuration.

For the internally balanced theory the hyperelastic energy expression (1.15) suggests consideration of the form

$$\Phi^{(4)}(I_1, I_2, I_1^*, I_2^*, \hat{I}_1, \hat{I}_2) = \frac{\alpha}{2}(I_1 - 3v^{2/3}) + \frac{\alpha^*}{2}(I_1^* - 3v^{2/3}) + \frac{\hat{\alpha}}{2}(\hat{I}_1 - 3) \tag{5.26}$$

where the moduli parameters obey $\alpha \geq 0$, $\alpha^* \geq 0$, $\hat{\alpha} \geq 0$. Just as the modulus μ in the hyperelastic model (1.15) was allowed to depend on v, the moduli in the internally balanced material (5.26) are also allowed to depend upon v.

For the internally balanced material with stored energy density (5.26), the Cauchy

stress follows from (5.19) as

$$\mathbf{T} = \frac{\alpha}{v}\mathbf{B} + \frac{\hat{\alpha}}{v}\hat{\mathbf{B}} - p\mathbf{I}. \tag{5.27}$$

The internal balance condition (5.21) reduces to

$$\alpha^*\mathbf{B} - \hat{\alpha}\hat{\mathbf{B}}^2 - qv\hat{\mathbf{B}} = \mathbf{0}, \tag{5.28}$$

where, recalling that $\bar{q}v = qv + 2\hat{I}_2\partial\Phi^{(4)}/\partial\hat{I}_2$, we return to the use of q for notational ease. Equivalent forms for (5.28) are

$$\alpha^*\mathbf{B}^* - \hat{\alpha}\hat{\mathbf{C}} - qv\mathbf{I} = \mathbf{0}, \tag{5.29}$$

and

$$\alpha^*\mathbf{C}^{*2} - \hat{\alpha}\mathbf{C} - qv\mathbf{C}^* = \mathbf{0}. \tag{5.30}$$

If $\hat{\alpha} = 0$ and $\alpha^* > 0$ it follows from (5.27) that $\mathbf{T} = (\alpha/v)\mathbf{B} - p\mathbf{I}$ so that if $v = 1$ then the model is equivalent to the usual neo-Hookean material model in hyperelasticity with modulus α. The internal balance (5.28) then formally gives $\hat{\mathbf{B}} = v^{-2/3}\mathbf{B}$ and $q = \alpha^* v^{-1/3}$.

If $\alpha^* = 0$ and $\hat{\alpha} > 0$ it follows from (5.28) that $\hat{\mathbf{B}} = \mathbf{I}$ and $q = -\hat{\alpha}/v$. This gives $\mathbf{T} = (\alpha/v)\mathbf{B} + (\hat{\alpha}/v - p)\mathbf{I}$ and $\hat{\alpha}/v$ can be absorbed into p. Hence if $v = 1$ the model with $\alpha^* = 0$ and $\hat{\alpha} > 0$ is also equivalent to a neo-Hookean material with modulus α.

Additional understanding of the range of qualitative behaviors follows from consideration of the three different two-term dominant balances that may occur between the various terms of the internal balance (5.28). For this purpose we rewrite (5.28) as

$$\hat{\alpha}\,\hat{\mathbf{B}}^2 + qv\hat{\mathbf{B}} = \alpha^*\,\mathbf{B}, \tag{5.31}$$

and inquire into the determination of both $\hat{\mathbf{B}}$ (obeying $\det\hat{\mathbf{B}} = 1$) and q for specified $\hat{\alpha}$, α^*, v and $\mathbf{B}$ (obeying $\det\mathbf{B} = v^2$).

Consider first a dominant balance between the second and third terms of (5.31), that is

$$\hat{\alpha}\,\hat{\mathbf{B}}^2 + qv\underbrace{\hat{\mathbf{B}} = \alpha^*}\,\mathbf{B}. \tag{5.32}$$

Such a balance becomes dominant as $\alpha^* >> \hat{\alpha}$. Specifically consider $\alpha^* \to \infty$ at finite $\hat{\alpha}$. Introduce

$$\beta = \hat{\alpha}/\alpha^*, \qquad \rho(\mathbf{X}) = q(\mathbf{X})v(\mathbf{X})/\alpha^*. \tag{5.33}$$

Here we have written q and v as possible functions of $\mathbf{X}$ to emphasize that possibility in the formulation and solution of boundary value problems. We could also have written $\hat{\alpha}$ and α^* as a possible function of $\mathbf{X}$ so as to treat the case of nonuniform and composite materials. In going forward, we shall cease to indicate this possible dependence upon $\mathbf{X}$. Using the notation (5.33) the internal balance equation (5.31) is recast into the form

$$\beta\,\hat{\mathbf{B}}^2 + \rho\,\hat{\mathbf{B}} = \mathbf{B}. \tag{5.34}$$

In the limit $\beta \to 0$ the solution pair $(\rho, \hat{\mathbf{B}})$ such that (5.34) is satisfied with $\det\hat{\mathbf{B}} = 1$ is $\rho = v^{2/3}$ and $\hat{\mathbf{B}} = v^{-2/3}\mathbf{B}$. On the presumption that both ρ and $\hat{\mathbf{B}}$ can be expanded in powers of β it is found from the $O(\beta)$ analysis of (5.34) (using also $\det\hat{\mathbf{B}} = 1$) that the $O(\beta)$ corrections are respectively: $-(v^{-2/3}/3)I_1$ and $-v^{-2}\mathbf{B}^2 + (v^{-2}/3)I_1\mathbf{B}$. Hence returning to original variables it is concluded that

$$\hat{\mathbf{B}} \;=\; v^{-2/3}\mathbf{B} + \frac{\hat{\alpha}}{\alpha^*}\Big(\frac{1}{3}v^{-2}I_1\mathbf{B} - v^{-2}\mathbf{B}^2\Big) + O\Big(\Big(\frac{\hat{\alpha}}{\alpha^*}\Big)^2\Big),$$

$$q \;=\; \alpha^* v^{-1/3} - \frac{1}{3}\hat{\alpha} v^{-5/3} I_1 + \hat{\alpha}\, O\Big(\frac{\hat{\alpha}}{\alpha^*}\Big), \tag{5.35}$$

as $\alpha^* \to \infty$ at finite $\hat{\alpha}$.

Next consider a dominant balance between the first and second terms, that is

$$\hat{\alpha}\, \underbrace{\hat{\mathbf{B}}^2 + qv\, \hat{\mathbf{B}}} = \alpha^*\, \mathbf{B}. \tag{5.36}$$

Such a balance becomes dominant as $\hat{\alpha} >> \alpha^*$. Specifically consider $\hat{\alpha} \to \infty$ at finite α^*. Introduce

$$\gamma = \alpha^*/\hat{\alpha}, \qquad \kappa = qv/\hat{\alpha}, \tag{5.37}$$

to rewrite equations (5.31) in the form

$$\hat{\mathbf{B}}^2 + \kappa\, \hat{\mathbf{B}} = \gamma \mathbf{B}. \tag{5.38}$$

In the limit $\gamma \to 0$ the solution pair $(\kappa, \hat{\mathbf{B}})$ such that (5.38) is satisfied with $\det\hat{\mathbf{B}} = 1$ is $\kappa = -1$ and $\hat{\mathbf{B}} = \mathbf{I}$. On the presumption that both κ and $\hat{\mathbf{B}}$ can be expanded in powers of γ it is found from the $O(\gamma)$ analysis of (5.38) (using also $\det\hat{\mathbf{B}} = 1$) that the $O(\gamma)$ corrections are respectively: $(1/3)I_1$ and $\mathbf{B} - (1/3)I_1\mathbf{I}$. Hence returning to original variables it is concluded that

$$\hat{\mathbf{B}} \;=\; \mathbf{I} + \frac{\alpha^*}{\hat{\alpha}}\Big(\mathbf{B} - \frac{1}{3} I_1 \mathbf{I}\Big) + O\Big(\Big(\frac{\alpha^*}{\hat{\alpha}}\Big)^2\Big),$$

$$q \;=\; -\frac{\hat{\alpha}}{v} + \frac{1}{3}\frac{\alpha^*}{v} I_1 + \alpha^*\, O\Big(\frac{\alpha^*}{\hat{\alpha}}\Big), \tag{5.39}$$

as $\hat{\alpha} \to \infty$ at finite α^*.

Finally, consider a dominant balance between the first and third terms, that is

$$\underbrace{\hat{\alpha}\ \hat{\mathbf{B}}^2 + qv\ \hat{\mathbf{B}} = \alpha^*\ \mathbf{B}}. \tag{5.40}$$

This balance gives $\hat{\mathbf{B}} \sim \sqrt{(\alpha^*/\hat{\alpha})\mathbf{B}}$ where it is recalled that symmetric positive-definite tensors have a unique symmetric positive-definite square root (the symbol $\sqrt{\cdot}$ denotes this unique tensor square-root). The scalar q drops out of the balance, and this loss has as a consequence that the condition $\det\hat{\mathbf{B}} = 1$ is met if and only if $\alpha^*/\hat{\alpha} = v^{-2/3}$. More formally, this balance becomes dominant as $\alpha^* \to \hat{\alpha}v^{-2/3}$ and it is an exact balance for $\alpha^* = \hat{\alpha}v^{-2/3}$. Specifically, it follows that

$$\hat{\mathbf{B}} = v^{-1/3}\sqrt{\mathbf{B}}, \qquad q = 0, \tag{5.41}$$

when $\alpha^* = \hat{\alpha}v^{-2/3}$.

The three cases examined above show how the theory is sensitive to the ratio $\beta = \hat{\alpha}/\alpha^*$. With respect to q the above results summarize as

$$q \to \begin{cases} -\infty, & \text{if } \hat{\alpha}/\alpha^* \to 0, \\ = 0, & \text{if } \hat{\alpha}/\alpha^* = v^{2/3}, \\ +\infty, & \text{if } \hat{\alpha}/\alpha^* \to \infty, \end{cases} \tag{5.42}$$

in a manner that is independent of $\mathbf{B}$. For values of $\beta = \hat{\alpha}/\alpha^*$ that do not correspond to those given in (5.42) it would generally be the case that q is also dependent upon $\mathbf{B}$. Turning to the Cauchy stress, the result (5.42) for q in conjunction with (5.27) gives

$$\mathbf{T} \to \begin{cases} (\alpha v^{-1} + \hat{\alpha} v^{-5/3})\mathbf{B} - p\mathbf{I}, & \text{if } \alpha^* \to \infty \text{ at finite } \hat{\alpha}, \\ \alpha v^{-1}\mathbf{B} + \hat{\alpha} v^{-4/3}\sqrt{\mathbf{B}} - p\mathbf{I}, & \text{if } \hat{\alpha} = \alpha^* v^{2/3}, \\ (\alpha v^{-1} + \alpha^* v^{-1})\mathbf{B} - \bar{p}\mathbf{I}, & \text{if } \hat{\alpha} \to \infty \text{ at finite } \alpha^*. \end{cases} \tag{5.43}$$

For the case of $\hat{\alpha} \to \infty$ at finite α^* the scalar $\bar{p} = p - \hat{\alpha} v^{-1} + \alpha^* v^{-1} I_1/3$. Since however p is arbitrary the extra term in $\bar{p}$ can be absorbed into p.

It is to be emphasized that the internal balance theory considered here need not be tied to the swelling phenomena. In other words the isochoric material case (formally the specialization of all previous results to $v = 1$) is a viable material description in its own right. Indeed the previous works *Demirkoparan et al.* (2014); *Demirkoparan and Pence* (2015a) considered only this case. Thus it is worth remarking that the results (5.43) for the isochoric specialization become

$$\mathbf{T} \to \begin{cases} (\alpha + \hat{\alpha})\mathbf{B} - p\mathbf{I}, & \text{if } \alpha^* \to \infty \text{ at finite } \hat{\alpha}, \\ \alpha\mathbf{B} + \hat{\alpha}\sqrt{\mathbf{B}} - p\mathbf{I}, & \text{if } \hat{\alpha} = \alpha^*, \\ (\alpha + \alpha^*)\mathbf{B} - p\mathbf{I}, & \text{if } \hat{\alpha} \to \infty \text{ at finite } \alpha^*. \end{cases} \tag{5.44}$$

Comparing (5.43) with $(1.15)_2$ shows that both extreme cases of $\hat{\alpha}/\alpha^* \to 0$ and $\hat{\alpha}/\alpha^* \to \infty$ give neo-Hookean behavior in the limit. Specifically this correspondence with the neo-Hookean hyperelastic theory with swelling requires the identifications

$$\mu \leftrightarrow \begin{cases} \alpha + \dfrac{\hat{\alpha}}{v^{2/3}} & \text{if } \alpha^* \to \infty \text{ at finite } \hat{\alpha}, \\ \alpha + \alpha^* & \text{if } \hat{\alpha} \to \infty \text{ at finite } \alpha^*. \end{cases} \tag{5.45}$$

In contrast, as shown by the case $\hat{\alpha} = \alpha^*$, the general case gives behavior that does

not coincide with the hyperelastic neo-Hookean theory.

5.2 Homogeneous deformation for the internally balanced material model

Equation (4.3) provided an explicit relation for P_{lat} in terms of v for the hyperelastic swelling theory. We now inquire into the extent to which a similar relation can be obtained for the internally balanced material theory. To this end it is necessary to decompose $\mathbf{F}$ in (4.3) according to (1.3). By virtue of symmetry it is presumed that $\hat{\mathbf{F}}$ and $\mathbf{F}^*$ can be written in terms of positive parameters $\hat{\xi}$ and ξ^* in the forms

$$\mathbf{F}^* = \xi^*(\mathbf{e}_1\otimes\mathbf{e}_1+\mathbf{e}_2\otimes\mathbf{e}_2)+\frac{v}{\xi^{*2}}\mathbf{e}_3\otimes\mathbf{e}_3, \qquad \hat{\mathbf{F}} = \hat{\xi}(\mathbf{e}_1\otimes\mathbf{e}_1+\mathbf{e}_2\otimes\mathbf{e}_2)+\frac{1}{\hat{\xi}^2}\mathbf{e}_3\otimes\mathbf{e}_3. \quad (5.46)$$

These forms are consistent with the constraints (5.1). They are also consistent with the decomposition (1.3) provided that

$$\hat{\xi}\xi^* = \lambda_{lat}. \quad (5.47)$$

Also $\hat{\xi}$ and ξ^* may vary with v even though λ_{lat} is fixed. Using $(4.3)_1$ two nontrivial scalar equations then emerge from the diagonal entries of the stress tensor (5.27):

$$-P_{lat} = \frac{\alpha}{v}\lambda_{lat}^2 + \frac{\hat{\alpha}}{v}\hat{\xi}^2 - p, \qquad 0 = \frac{\alpha v}{\lambda_{lat}^4} + \frac{\hat{\alpha}}{v\hat{\xi}^4} - p. \quad (5.48)$$

Two nontrivial scalar equations also emerge from the diagonal entries of the internal balance (5.31):

$$\alpha^*\lambda_{lat}^2 - \hat{\alpha}\hat{\xi}^4 - qv\hat{\xi}^2 = 0, \qquad \frac{\alpha^* v^2}{\lambda_{lat}^4} - \frac{\hat{\alpha}}{\hat{\xi}^8} - \frac{qv}{\hat{\xi}^4} = 0. \quad (5.49)$$

For given λ_{lat} and $v > \lambda_{lat}^3$ equations (5.47)-(5.49) provide five scalar relations among the five unknown quantities: P_{lat}, $\hat{\xi}$, ξ^*, p and q. As shown below, this allows solutions for P_{lat}, $\hat{\xi}$, ξ^*, p and q in terms of v and λ_{lat}. In particular this then gives P_{lat} as a

function of v and λ_{lat} such that this P_{lat} represents the lateral confining pressure for the case $v > \lambda_{lat}^3$.

In order to verify the above claim, eliminate q between the two equations of (5.49) so as to obtain

$$\alpha^* v^2 \hat{\xi}^8 + \hat{\alpha}\lambda_{lat}^4 \hat{\xi}^6 - \alpha^* \lambda_{lat}^6 \hat{\xi}^2 - \hat{\alpha}\lambda_{lat}^4 = 0. \tag{5.50}$$

For a given pair (λ_{lat}, v) with $\lambda_{lat} > 0$ and $v > 0$ this polynomial equation in $\hat{\xi}$ has a unique positive root by virtue of Descarte's rule of signs. This defines a function $\hat{\Xi}(\lambda_{lat}, v)$ such that $\hat{\xi} = \hat{\Xi}(\lambda_{lat}, v)$ solves (5.50). This function also depends upon the ratio $\hat{\alpha}/\alpha^*$ (we do not show this in the argument list for $\hat{\Xi}$). Recall also that it is permissible to allow either $\hat{\alpha}$ or α^* to depend upon v provided that these moduli remain positive for all v. In such a case the dependence of $\hat{\Xi}$ upon v must also take this moduli dependence into account. Such a dependence has no effect upon the generality of the results given here.

Eliminating p between the two equations of (5.48) gives

$$P_{lat} = \alpha\Big(\frac{v}{\lambda_{lat}^4} - \frac{\lambda_{lat}^2}{v}\Big) + \frac{\hat{\alpha}}{v}\Big(\frac{1}{\hat{\xi}^4} - \hat{\xi}^2\Big). \tag{5.51}$$

Using (5.47) and (5.50) it follows that an alternative form for this result is

$$P_{lat} = \alpha\Big(\frac{v}{\lambda_{lat}^4} - \frac{\lambda_{lat}^2}{v}\Big) + \alpha^*\Big(\frac{1}{\xi^{*4}} - \xi^{*2}\Big). \tag{5.52}$$

This function (5.51) with $\hat{\xi} = \hat{\Xi}(\lambda_{lat}, v)$ defines a function

$$\Pi(\lambda_{lat}, v) = \alpha\Big(\frac{v}{\lambda_{lat}^4} - \frac{\lambda_{lat}^2}{v}\Big) + \frac{\hat{\alpha}}{v}\Big(\frac{1}{\hat{\Xi}^4(\lambda_{lat}, v)} - \hat{\Xi}^2(\lambda_{lat}, v)\Big) \tag{5.53}$$

such that $P_{lat} = \Pi(\lambda_{lat}, v)$ gives the lateral confining pressure. The result is general so as to accommodate any dependence of α, $\hat{\alpha}$ or α^* upon v provided that the

requirements $\alpha \geq 0$, $\hat{\alpha} \geq 0$ or $\alpha^* \geq 0$ always hold.

Because lateral confinement occurs for $v > \lambda_{lat}^3$, it follows that $v > \lambda_{lat}^3$ defines the physically meaningful range for the argument pair (λ_{lat}, v). The value $\lambda_{lat} = v^{1/3}$ corresponds to the free swelling threshold at which the plug has swollen by an amount that is just sufficient to allow all-around contact with the inner channel wall of the confining rigid pipe. This motivates the observation that if $\lambda_{lat} = v^{1/3}$ then the positive root $\hat{\xi}$ to (5.50) is $\hat{\xi} = 1$. Thus $\hat{\Xi}(v^{1/3}, v) = 1$. Use of this result in (5.53) gives $\Pi(v^{1/3}, v) = 0$. This is the expected result, namely $P_{lat} = 0$ at initial material contact with the wall, i.e., when $v = \lambda_{lat}^3$. The general dependence of confining pressure P_{lat} on swelling v when v exceeds the contact value λ_{lat}^3 then follows from $P_{lat} = \Pi(\lambda_{lat}, v)$ using (5.50) and (5.53). The detailed dependence of $\Pi(\lambda_{lat}, v)$ upon v is sensitive to how the moduli α, $\hat{\alpha}$ and α^* vary with v. Figure 5.1 then shows P_{lat} vs. v as determined from solution to (5.50) and (5.53) using chosen parameter values.

The initial slope of the curves in Figure 5.1 can be determined analytically. For this purpose let us suppose that the moduli α, $\hat{\alpha}$ and α^* are all independent of v. Now (5.53) can be differentiated with respect to v to get

$$\begin{aligned} \frac{\partial \Pi(\lambda_{lat}, v)}{\partial v} &= \alpha\Big(\frac{1}{\lambda_{lat}^4} - \frac{\lambda_{lat}^2}{v^2}\Big) - \frac{\hat{\alpha}}{v^2}\Big(\frac{1}{\hat{\Xi}^4(\lambda_{lat}, v)} - \hat{\Xi}^2(\lambda_{lat}, v)\Big) \\ &- \frac{2\hat{\alpha}}{v}\Big(\frac{2}{\hat{\Xi}^5(\lambda_{lat}, v)} + \hat{\Xi}(\lambda_{lat}, v)\Big)\frac{\partial \hat{\Xi}(\lambda_{lat}, v)}{\partial v}. \end{aligned} \tag{5.54}$$

As pointed out in the previous paragraph, $\hat{\Xi}(v^{1/3}, v) = 1$ when $\lambda_{lat} = v^{1/3}$. Therefore $\hat{\Xi}(\lambda_{lat}, \lambda_{lat}^3) = 1$. Moreover (5.50) can be differentiated with respect to v and then evaluated at $(\lambda_{lat}, \lambda_{lat}^3)$ to get

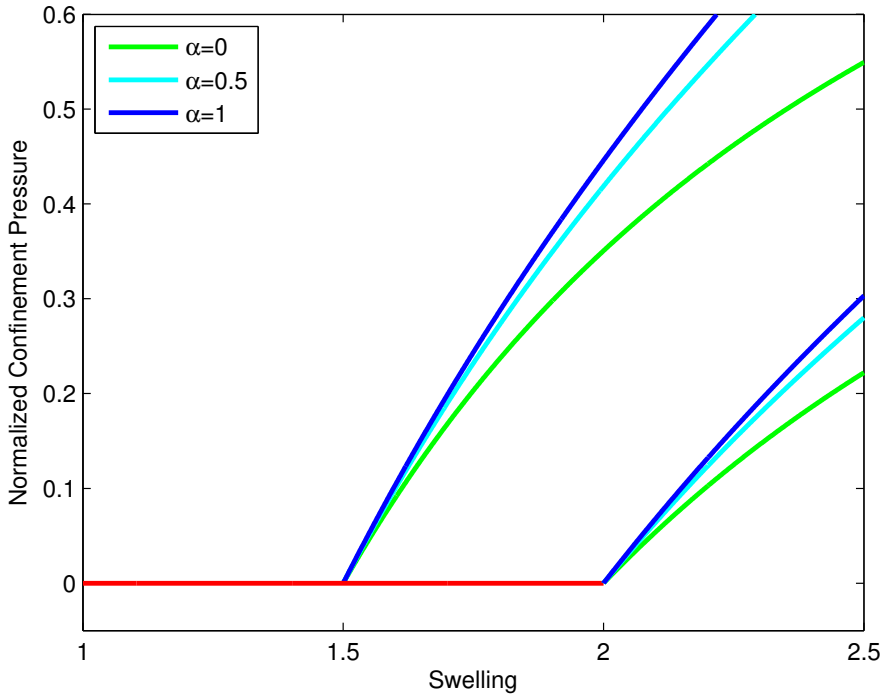

Figure 5.1 Confinement pressure $P_{lat} = \Pi(\lambda_{lat}, v)$ as a function of swelling v taking $\hat{\alpha} = 1$, $\alpha^* = 2$ and $R_o = 1$ (so that $\lambda_{lat} = R_c$). The three graphs on the left are for $R_c = 1.5^{1/3}$. The three graphs on the right are for $R_c = 2^{1/3}$. For each R_c the graph of P_{lat} is given for three different values of α. Here P_{lat} is normalized by $\alpha + (\hat{\alpha}\alpha^*)/(\hat{\alpha} + \alpha^*)$. Because of (5.56) this accounts for the common slope at the rightmost departure ($R_c = 2^{1/3}$) being less than the common slope at the leftmost departure ($R_c = 1.5^{1/3}$).

$$\frac{\partial\hat{\Xi}}{\partial v}\Big|_{(\lambda_{lat},\lambda_{lat}^3)} = \frac{-\alpha^*}{3(\alpha^*\lambda_{lat}^3 + \hat{\alpha}\lambda_{lat})}. \tag{5.55}$$

Consequently use of (5.55) in (5.54) and algebraic manipulations give

$$\frac{\partial\Pi}{\partial v}\Big|_{(\lambda_{lat},\lambda_{lat}^3)} = \frac{2}{\lambda_{lat}^4}\Big(\alpha + \frac{\hat{\alpha}\alpha^*}{\alpha^*\lambda_{lat}^2 + \hat{\alpha}}\Big). \tag{5.56}$$

This in turn describes the slope in Figure 5.1 when the pressure P_{lat} departs from zero due to first wall contact.

In order to recover the hyperelastic result, recall that (5.45) indicates how the hyperelastic neo-Hookean swelling theory follows from two special limits of the internally balanced material theory. Thus it must be the case that (4.3) will follow from (5.50) and (5.51) in these two special limits. We now verify that this is indeed the case.

Consider first the limit $\alpha^* \to \infty$ at finite $\hat{\alpha}$. It then follows that the dominant balance in (5.50) gives

$$\hat{\xi} \to \frac{\lambda_{lat}}{v^{1/3}} \qquad \text{as } \alpha^* \to \infty, \tag{5.57}$$

so that (5.47) gives $\xi^* \to v^{1/3}$. Thus (5.51) gives

$$P_{lat} \to (\alpha + \frac{\hat{\alpha}}{v^{2/3}})\Big(\frac{v}{\lambda_{lat}^4} - \frac{\lambda_{lat}^2}{v}\Big), \tag{5.58}$$

which matches (4.3) under the identification connection from (5.45).

Second consider the limit $\hat{\alpha} \to \infty$ at finite α^*. It then follows that the dominant balance in (5.50) gives

$$\hat{\xi} \to 1 \qquad \text{as } \hat{\alpha} \to \infty \tag{5.59}$$

so that (5.47) gives $\xi^* \to \lambda_{lat}$. Because (5.51) would generate the indeterminate form of infinity multiplied by zero we use the alternative form (5.52) to obtain

$$P_{lat} \to (\alpha + \alpha^*)\big(\frac{v}{\lambda_{lat}^4} - \frac{\lambda_{lat}^2}{v}\big) \tag{5.60}$$

which matches (4.3) under the correspondence from (5.45).

5.3 Cylindrical deformation in internally balanced material model

In this section we use the internally balanced material model for the same boundary value problem of the confined hollow tube that was considered in section 4.3. In this regard the cylindrical deformation (4.4) that is subject to the volume change (4.6) is again considered. Recall that the tube is still confined such that the (4.8), (4.9) and (4.10) still hold. The relation (4.9) again provides that $r_i = r_i(\lambda_z)$ and this makes the axial force requirement (4.13) be a single relation to obtain the ultimate unknown λ_z.

Here in this section in the internally balanced material model that is given by (5.26) for simplicity it is assumed that $\alpha = 0$. The left Cauchy-Green deformation tensor $\mathbf{B}$ is given by

$$\mathbf{B} = \mathbf{F}\mathbf{F}^T = \begin{bmatrix} r'^2 & 0 & 0 \\ 0 & (r/R)^2 & 0 \\ 0 & 0 & \lambda_z^2 \end{bmatrix} = r'^2(\mathbf{e}_r \otimes \mathbf{e}_r) + (r/R)^2(\mathbf{e}_\theta \otimes \mathbf{e}_\theta) + \lambda_z^2(\mathbf{e}_z \otimes \mathbf{e}_z). \quad (5.61)$$

Moreover, notice that it follows from (5.28) that an eigenvector of $\mathbf{B}$ is also an eigenvector of $\hat{\mathbf{B}}$ and this argument is shown in *Demirkoparan et al.* (2014). Hence it is reasonable to seek solutions in which $\hat{\mathbf{B}}$ is symmetric positive-definite in the form

$$\hat{\mathbf{B}} = \begin{bmatrix} \hat{B}_{rr} & 0 & 0 \\ 0 & \hat{B}_{\theta\theta} & 0 \\ 0 & 0 & \hat{B}_{zz} \end{bmatrix} = \hat{B}_{rr}(\mathbf{e}_r \otimes \mathbf{e}_r) + \hat{B}_{\theta\theta}(\mathbf{e}_\theta \otimes \mathbf{e}_\theta) + \hat{B}_{zz}(\mathbf{e}_z \otimes \mathbf{e}_z), \quad (5.62)$$

where its components satisfy the internal balance equations (5.31). It then follows

from (5.62) and (5.27) that the stress tensor $\mathbf{T}$ is of the form

$$\mathbf{T} = \begin{bmatrix} T_{rr} & 0 & 0 \\ 0 & T_{\theta\theta} & 0 \\ 0 & 0 & T_{zz} \end{bmatrix} = T_{rr}(\mathbf{e}_r \otimes \mathbf{e}_r) + T_{\theta\theta}(\mathbf{e}_\theta \otimes \mathbf{e}_\theta) + T_{zz}(\mathbf{e}_z \otimes \mathbf{e}_z) \tag{5.63}$$

where

$$\begin{aligned} T_{rr} &= \frac{\hat{\alpha}}{v}\hat{B}_{rr} - p, \\ T_{\theta\theta} &= \frac{\hat{\alpha}}{v}\hat{B}_{\theta\theta} - p, \\ T_{zz} &= \frac{\hat{\alpha}}{v}\hat{B}_{zz} - p. \end{aligned} \tag{5.64}$$

This will reduce the equilibrium equation into (4.11) that is associated with the boundary condition (4.12).

The boundary value problem for the deformation field (4.4) with given swelling amount v, the geometric configuration R_i, R_o and R_c and the stress field (5.64) is then formulated to seek the seven unknowns as follows: axial elongation λ_z, the outer confinement pressure P_{lat}, scalar functions p and q and a symmetric positive-definite tensor function $\hat{\mathbf{B}}$ (with the three unknown component functions of $\hat{B}_{rr}$, $\hat{B}_{\theta\theta}$ and $\hat{B}_{zz}$) such that the following equations are satisfied: the equilibrium equation (4.11), the zero resultant axial force , the requirement (5.1) and three scalar equations of Internal Balance that come from diagonal entries in (5.28). Once λ_z is determined then r_i is obtained directly from (4.9).

5.3.1 Internal balance requirement

We consider an approach in which q and $\hat{B}_{rr}$, $\hat{B}_{\theta\theta}$ and $\hat{B}_{zz}$ are regarded as the primary and λ_z, P_{lat} and the hydrostatic pressure function p are regarded as the secondary unknowns. Notice that instead of q, we seek for $\rho = qv/\hat{\alpha}$. Also because we assume finite and positive values for $\hat{\alpha}$ and α^* we choose to pick the notations in (5.33). The

primary unknowns are then formulated in terms of the secondary unknowns. Once the secondary unknowns are solved, the primary unknowns are consequently obtained. To formulate the four primary unknowns we use the three equations of Internal Balance (5.31) and the requirement of (5.1). Thus using the assumptions (5.61) and (5.62) in the internal balance (5.31), it gives three quadratic and decoupled equations relating $\hat{B}_{rr}$, $\hat{B}_{\theta\theta}$ and $\hat{B}_{zz}$ to ρ as follows

$$\begin{aligned}
&\hat{B}_{rr}^2 + \rho\hat{B}_{rr} - r^{'2}/\beta = 0,\\
&\hat{B}_{\theta\theta}^2 + \rho\hat{B}_{\theta\theta} - r^2/(\beta R^2) = 0,\\
&\hat{B}_{zz}^2 + \rho\hat{B}_{zz} - \lambda_z^2/\beta = 0.
\end{aligned} \tag{5.65}$$

These equations can be solved for positive $\hat{B}_{rr}$, $\hat{B}_{\theta\theta}$ and $\hat{B}_{zz}$. Making one additional replacement of $r^{'} = Rv/(r\lambda_z)$ from (4.6) and introducing $s = r/R$ these solutions are

$$\begin{aligned}
\hat{B}_{rr} &= \frac{1}{2}\Big(-\rho + \sqrt{\rho^2 + 4v^2/(\beta s^2\lambda_z^2)}\Big),\\
\hat{B}_{\theta\theta} &= \frac{1}{2}\Big(-\rho + \sqrt{\rho^2 + 4s^2/\beta}\Big),\\
\hat{B}_{zz} &= \frac{1}{2}\Big(-\rho + \sqrt{\rho^2 + 4\lambda_z^2/\beta}\Big).
\end{aligned} \tag{5.66}$$

Now we need one more equation in order to solve for the four primary unknowns. To this end, $\det\hat{\mathbf{B}} = 1$ requires that $\hat{B}_{rr}\hat{B}_{\theta\theta}\hat{B}_{zz} = 1$ which because of (5.66) becomes

$$\frac{1}{8}\Big(-\rho + \sqrt{\rho^2 + 4v^2/(\beta s^2\lambda_z^2)}\Big)\Big(-\rho + \sqrt{\rho^2 + 4s^2/\beta}\Big)\Big(-\rho + \sqrt{\rho^2 + 4\lambda_z^2/\beta}\Big) = 1. \tag{5.67}$$

This brings additional relation between ρ, s, v, λ_z and β and shows that ρ is independent of θ and z. The immediate question then arises if there is any unique ρ which satisfies (5.67). To investigate that let's define

$$h(\rho) = \frac{1}{8}h_1(\rho)h_2(\rho)h_3(\rho), \tag{5.68}$$

in which

$$
\begin{aligned}
h_1(\rho) &= -\rho + \sqrt{\rho^2 + 4R^2v^2/(\beta r^2\lambda_z^2)} > 0, \\
h_2(\rho) &= -\rho + \sqrt{\rho^2 + 4r^2/(\beta R^2)} > 0, \\
h_3(\rho) &= -\rho + \sqrt{\rho^2 + 4\lambda_z^2/\beta} > 0,
\end{aligned}
\tag{5.69}
$$

and seek the solution ρ to

$$
h(\rho) = 1 \tag{5.70}
$$

which is equivalent to (5.67). To this end observe that

$$
8\frac{dh}{d\rho} = h_1^{'}h_2h_3 + h_1h_2^{'}h_3 + h_1h_2h_3^{'} \tag{5.71}
$$

with

$$
\begin{aligned}
h_1^{'} &= (-1 + \frac{\rho}{\sqrt{\rho^2 + 4R^2v^2/(\beta r^2\lambda_z^2)}}) < 0, \\
h_2^{'} &= (-1 + \frac{\rho}{\sqrt{\rho^2 + 4r^2/(\beta R^2)}}) < 0, \\
h_3^{'} &= (-1 + \frac{\rho}{\sqrt{\rho^2 + 4\lambda_z^2/\beta}}) < 0.
\end{aligned}
\tag{5.72}
$$

This makes the channel argument $dh/d\rho < 0$ for all real ρ. Note also from (5.67) that

$$
\lim_{\rho\to-\infty} h(\rho) = \infty, \qquad \lim_{\rho\to\infty} h(\rho) = 0. \tag{5.73}
$$

It is concluded that the equation $h(\rho) = 1$ has a unique solution ρ which is a function of $s = r/R$ and also the parameters v, λ_z, β and R_i. We recall that all of these parameters are given with the exception of λ_z. It follows that we can write

$$
\rho = \rho(s; v, \beta, \lambda_z). \tag{5.74}
$$

To determine the sign of ρ notice that from (5.68) we have $h(\rho)|_{\rho=0} = v/\beta^{3/2}$. Hence, for the solution of $h(\rho) = 1$, it is seen that $v/\beta^{3/2} < 1$ gives $\rho < 0$ and $v/\beta^{3/2} > 1$

gives $\rho > 0$. In other words the sign of ρ which solves (5.67) depends on the value of $v/\beta^{3/2} = v(\alpha^*/\hat{\alpha})^{3/2}$. Hence, in any given problem ρ will either be restricted to vary through only positive values or through only negative values. If this ρ is taken such that $\rho = \rho(s; v, \beta, \lambda_z)$ solves (5.67), then from (5.66), the components of $\hat{\mathbf{B}}$ are found to be functions of s. With the help of the map $r = r(R)$ from (4.4), the function ρ and all the components of $\hat{\mathbf{B}}$ are obtained and found to be functions of s and the still unknown parameters λ_z and $r_i(\lambda_z)$. Depending on which aspect is to be emphasized we either write $\rho = \rho(s)$ or $\rho = \rho(s, \lambda_z)$.

The analytical solution to (5.67) is not available. Two numerical solutions of $\rho = \rho(s; v, \beta, \lambda_z)$ are graphed in the Figure 5.2. It is seen that for $\beta < v^{2/3}$ the solution $\rho(s)$ is positive and if $\beta > v^{2/3}$ the solution $\rho(s)$ is negative. Moreover, the solutions are finite over the channel range of s, it goes to zero when $s \to 0$ and asymptotes to zero when $s \to \infty$.

In order to identify the special value of the parameter $s = s_{ext}$ that makes the extremum of $\rho_{ext} = \rho(s_{ext})$ we can take the derivatives of the two sides of (5.67) with respect to s and use $d\rho/ds\big|_{s=s_{ext}} = 0$. This yields

$$\frac{1}{s_{ext}^4}\sqrt{\rho_{ext}^2 + 4s_{ext}^2/\beta}\left(-\rho + \sqrt{\rho_{ext}^2 + 4s_{ext}^2/\beta}\right) = \frac{\lambda_z^2}{v^2}\sqrt{\rho_{ext}^2 + 4v^2/(\beta s_{ext}^2\lambda_z^2)}\left(-\rho_{ext} + \sqrt{\rho_{ext}^2 + 4v^2/(\beta s_{ext}^2\lambda_z^2)}\right) \tag{5.75}$$

One obvious root of this equation for s_{ext} is $s_{ext} = \sqrt{v/\lambda_z}$ that is shown in Figure 5.2.

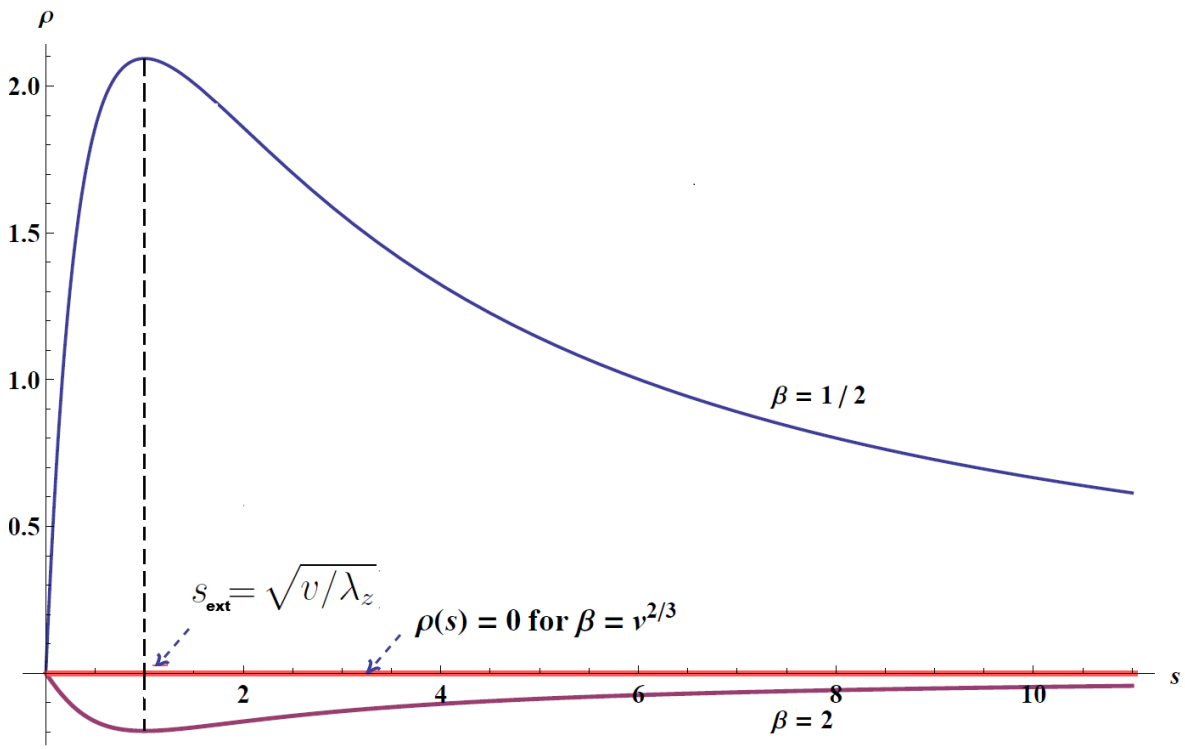

Figure 5.2 Three solutions of $\rho(s; v, \beta, \lambda_z)$ to the requirement (5.67) with one representative set of $v = 2$ and $\lambda_z = 2$. Two of the non-trivial solutions are obtained for different ration $\beta = 2$ and $\beta = 1/2$. If β is taken as $\beta = v^{2/3} = 2^{2/3}$ then the obvious solution is $\rho(s) \equiv 0$.

5.3.2 Stress and equilibrium

To find the secondary unknowns λ_z, P_{lat} and p, we first show that p is a function of R alone. We notice that since the components of $\hat{\mathbf{B}}$ are independent of θ and z, regarding (5.64) and equilibrium equations from (4.11) the components of $\mathbf{T}$ and consequently p, are also independent of θ and z. Hence it follows that $p = p(R)$ and by presuming that the map $r = r(R)$ is invertible we can write the function p as a function of $s = r/R$ and hence $p = p(s)$. The function $p(s)$ will then be solved from the first equilibrium equation (4.11) and satisfying the boundary condition (4.12) where $\mathbf{T}$ is given by (5.27). The parameter $r_i(\lambda_z)$ is obtained via (4.9) and recall that the unknown parameter λ_z is the solution to the requirement (4.13). Thus the procedure is as follows: after determining $\rho(s, \lambda_z)$ the stress components to be used

in (4.11) are from (5.27). If we rewrite the stress components from (5.64) it follows

$$T_{rr} = \frac{\hat{\alpha}}{v}\hat{B}_{rr} - p(s), \tag{5.76}$$

$$T_{\theta\theta} = \frac{\hat{\alpha}}{v}\hat{B}_{\theta\theta} - p(s), \tag{5.77}$$

$$T_{zz} = \frac{\hat{\alpha}}{v}\hat{B}_{zz} - p(s). \tag{5.78}$$

Thus the components of $\hat{\mathbf{B}}$ are used from (5.66) into (5.76) and it gives

$$T_{rr} = \frac{\hat{\alpha}}{2v}\big(-\rho(s,\lambda_z) + \sqrt{\rho(s,\lambda_z)^2 + 4v^2/(\beta s^2\lambda_z^2)}\big) - p(s), \tag{5.79}$$

$$T_{\theta\theta} = \frac{\hat{\alpha}}{2v}\big(-\rho(s,\lambda_z) + \sqrt{\rho(s,\lambda_z)^2 + 4s^2/\beta}\big) - p(s), \tag{5.80}$$

$$T_{zz} = \frac{\hat{\alpha}}{2v}\big(-\rho(s,\lambda_z) + \sqrt{\rho(s,\lambda_z)^2 + 4\lambda_z^2/\beta}\big) - p(s). \tag{5.81}$$

Hence (4.11) becomes the differential equation

$$\frac{\partial}{\partial r}T_{rr} + \frac{\hat{\alpha}}{2rv}\left(\sqrt{\rho(s,\lambda_z)^2 + 4v^2/(\beta s^2\lambda_z^2)} - \sqrt{\rho(s,\lambda_z)^2 + 4s^2/\beta}\right) = 0, \tag{5.82}$$

and notice that with the help of the connection

$$\frac{\partial}{\partial r}T_{rr} = \frac{1}{r'}\frac{d}{dR}T_{rr}, \tag{5.83}$$

into (5.82) it follows that

$$\int_{R_i}^{R} dT_{rr} = \int_{R_i}^{R} \frac{\hat{\alpha}}{2rv}\left(\sqrt{\rho(s,\lambda_z)^2 + 4s^2/\beta} - \sqrt{\rho(s,\lambda_z)^2 + 4v^2/(\beta s^2\lambda_z^2)}\right) r' dR. \tag{5.84}$$

The left hand side of the relation (5.85) is reduced with the help of the boundary condition (4.12) and in the right hand side we can use (4.6) to replace r' and perform

the integration to obtain

$$T_{rr}(s) = -\frac{\hat{\alpha}}{2}\int_{s_i}^{s} \phi\big(\rho(s,\lambda_z), v, \lambda_z, \beta\big)\, ds, \tag{5.85}$$

in which it is defined that $s_i = r_i/R_i$ and also

$$\phi\big(\rho(s,\lambda_z), v, \lambda_z, \beta\big) = \frac{1}{vs - \lambda_z s^3}\left(\sqrt{\rho(s,\lambda_z)^2 + 4v^2/(\beta s^2\lambda_z^2)} - \sqrt{\rho(s,\lambda_z)^2 + 4s^2/\beta}\right). \tag{5.86}$$

It can be confirmed that the parameter $s = r/R$ is either decreasing (with lower bound $\sqrt{v/\lambda_z}$) or increasing (with upper bound $\sqrt{v/\lambda_z}$) for $R_i \leq R \leq R_o$. Since the boundary value problem is defined such that $P_i = 0$ and $P_o = P_{lat} > 0$ then it is concluded that $s_i < s_o$. Consequently it follows that $s_i < s_o < \sqrt{v/\lambda_z}$. This guarantees a non-zero denominator in the function ϕ in (5.86) and it allows the integration (5.90) to be determined.

Once the radial component of the Cauchy stress tensor is obtained via (5.85), the hydrostatic pressure $p(s)$ follows from (5.79) and other stress components are also given by (5.80) and (5.81). We have

$$\begin{aligned} T_{\theta\theta}(s) = {} & \frac{\hat{\alpha}}{2v}\left(\sqrt{\rho(s,\lambda_z)^2 + 4s^2/\beta} - \sqrt{\rho(s,\lambda_z)^2 + 4v^2/(\beta s^2\lambda_z^2)}\right) \\ & - \frac{\hat{\alpha}}{2}\int_{s_i}^{s} \phi\big(\rho(s,\lambda_z), v, \lambda_z, \beta\big)\, ds, \end{aligned} \tag{5.87}$$

$$\begin{aligned} T_{zz}(s) = {} & \frac{\hat{\alpha}}{2v}\left(\sqrt{\rho(s,\lambda_z)^2 + 4\lambda_z^2/\beta} - \sqrt{\rho(s,\lambda_z)^2 + 4v^2/(\beta s^2\lambda_z^2)}\right) \\ & - \frac{\hat{\alpha}}{2}\int_{s_i}^{s} \phi\big(\rho(s,\lambda_z), v, \lambda_z, \beta\big)\, ds. \end{aligned} \tag{5.88}$$

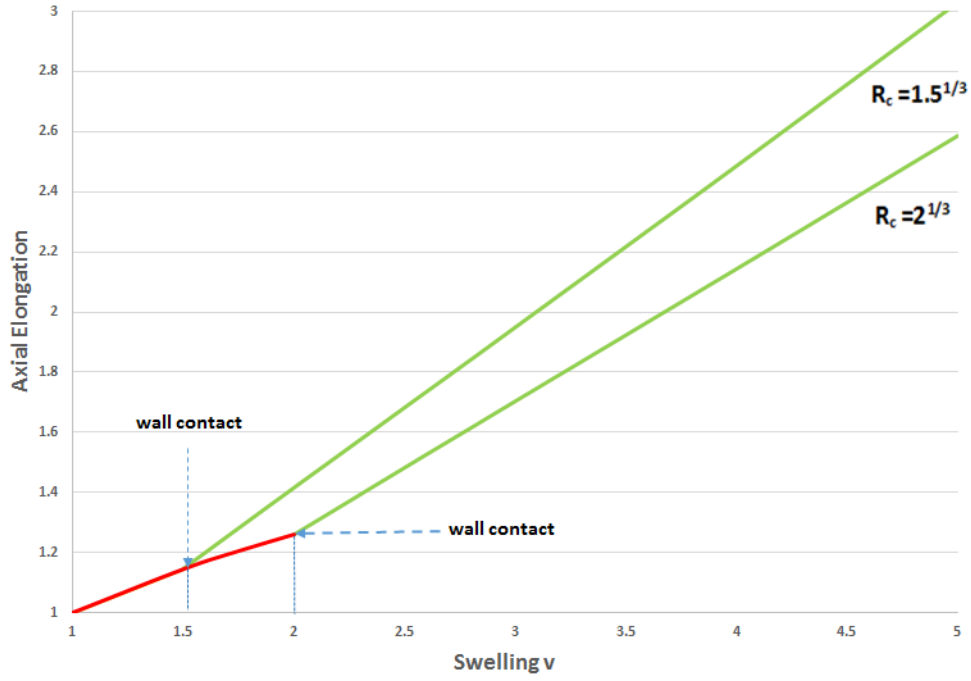

Figure 5.3 Axial elongation λ_z on a hollow tube as a function of swelling v taking $\alpha = 0$ $\hat{\alpha} = 1$, $\alpha^* = 2$ and $R_i = 1/2$, $R_o = 1$ (so that $\lambda_{lat} = R_c$). The graphs are the solution to (5.89) and are for two separate cases of outer pipe radius: $R_c = 1.5^{1/3}$ and $R_c = 2^{1/3}$, which are chosen so as to give contact v values of 1.5 and 2, respectively.

Moreover, λ_z is the only unknown in all above relations because the parameter r_o is prescribed as $r_o = R_c$ for $v > \lambda_{lat}^3$. To solve for λ_z recall that the requirements of volume conversation (4.9) and also the zero axial resultant load (4.13) with the axial component of Cauchy stress (5.85) are used. The latter is

$$2\pi \int_{r_i/R_i}^{\lambda_{lat}} T_{zz}(s)\Big|_{s=\frac{r}{R}} r dr \equiv 0, \tag{5.89}$$

in which the definition $s_o = r_o/R_o = R_c/R_o = \lambda_{lat}$ is again used and recall that $r_i(\lambda_z)$ is given by (4.9). Two different numerical solutions of (5.89) are graphed in Figure 5.3. As it is seen the solution is consistent with conventional M-R model that was obtained and shown in Figure 4.4. This leads to obtaining the inner radius from (4.9) that is shown in Figure 5.4. Once λ_z and $r_i(\lambda_z)$ are determined the lateral confinement pressure follows from $T_{rr}|_{\lambda_{lat}} = -P_{lat}$ which is equivalent to

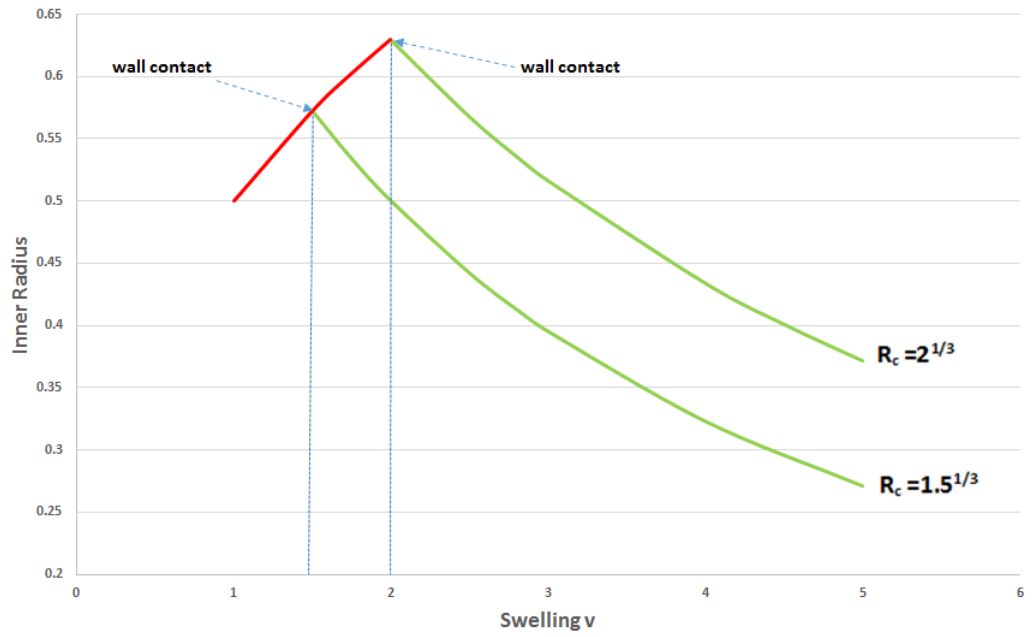

Figure 5.4 Inner radius r_i on a hollow tube as a function of swelling v taking $\alpha = 0$ $\hat{\alpha} = 1$, $\alpha^* = 2$ and $R_i = 1/2$, $R_o = 1$ (so that $\lambda_{lat} = R_c$). The graphs are the solution to (4.9) and are for two separate cases of outer pipe radius: $R_c = 1.5^{1/3}$ and $R_c = 2^{1/3}$, which are chosen so as to give contact v values of 1.5 and 2, respectively.

$$P_{lat} = \frac{\hat{\alpha}}{2} \int_{s_i}^{\lambda_{lat}} \phi(\rho(s, \lambda_z), v, \lambda_z, \beta)\, ds. \tag{5.90}$$

The values of lateral pressure are also plotted in Figure 5.5. This plot also shows the variation of lateral pressure with respect to changing the material parameter ratio $\beta = \hat{\alpha}/\alpha^*$. One special curve is for $\beta \to \infty$ that is obtained with very large values of $\hat{\alpha}$ at a finite α^*. Recall from (5.45) that in this limit the finite material parameter α^* retrieves the elastic modulus μ. This figure shows how the lateral pressure also recovers the hyperelastic behavior that was shown in Figure 4.7.

5.3.3 Explicit solution of the special case $v = \beta^{3/2}$

We recall the special case of the relation (5.66) when $v = \beta^{3/2}$ for which the solution $\rho(s)$ is identical to zero for all $s_i \leq s \leq s_o$ and this corresponds to the second special case introduced in (5.42). Note that in this case the axial stress component

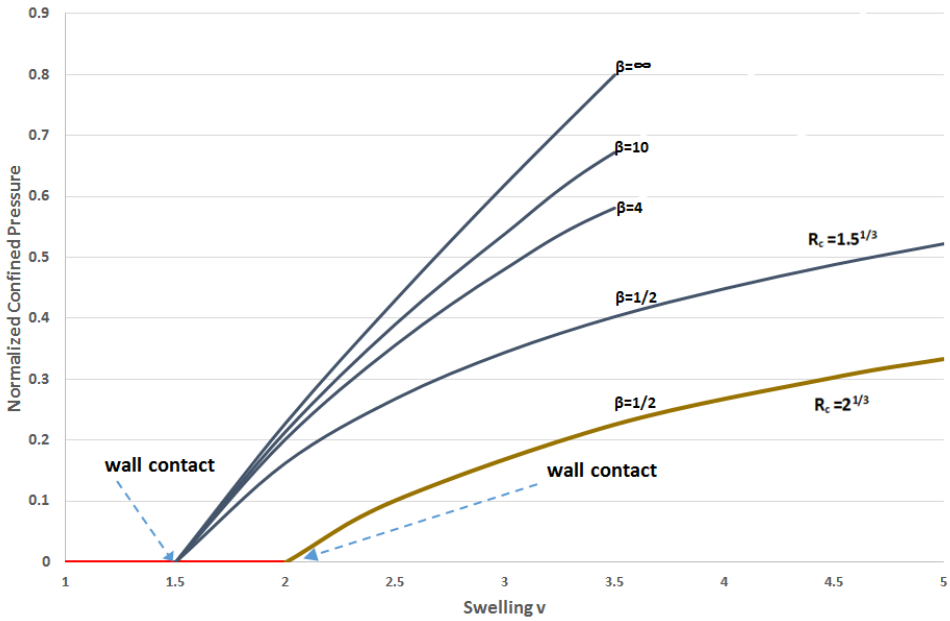

Figure 5.5 Confinement pressure P_{lat} on a hollow tube as a function of swelling v taking $\alpha = 0$ and $\beta = 1/2$ ($\hat{\alpha} = 1$, $\alpha^* = 2$) and $R_i = 1/2$, $R_o = 1$ (so that $\lambda_{lat} = R_c$) for longer graphs with $R_c = 1.5^{1/3}$ and $R_c = 2^{1/3}$. The graphs of $\beta = 4, 10$ and ∞ are also plotted for $R_c = 1.5^{1/3}$. Note that the graph of $\beta = \infty$ retrieves the hyperelastic behavior shown in Figure 4.6 based on (5.45). Here P_{lat} is normalized by $\hat{\alpha}\alpha^*/(\hat{\alpha}+\alpha^*)$.

given by (5.88) simplifies to

$$T_{zz}(s) = \frac{\hat{\alpha}}{\beta^{1/2}} \left(\frac{\lambda_z}{\beta^{3/2}} - \frac{1}{\lambda_z s_i} \right), \tag{5.91}$$

which is independent of the normalized radius s. The requirement of the zero axial load invokes that this radial stress is zero for all pointwise radial locations. Note that this result is unlike the M-R behavior that was described in Chapter IV and also in contrast with the internally balanced material model with swelling amounts $v \neq \beta^{3/2}$ where the pointwise zero axial stress could not be captured. This peculiar behavior shows that with the internally balanced material, the special value of swelling makes the axial stress field vanishes while the assumption $z = \lambda_z Z$ still holds.

The condition (5.91) provides the relation

$$\lambda_z = \frac{\beta^{3/4}}{s_i^{1/2}}, \tag{5.92}$$

that in conjunction with (4.9) obtains λ_z. It follows that λ_z is the solution to the single equation that is a forth order polynomial

$$\lambda_z^4 - \frac{\beta^{3/2}}{\lambda_{lat}^2}(1-\zeta^2)\lambda_z^3 - \frac{\beta^3\zeta^2}{\lambda_{lat}^2} = 0. \tag{5.93}$$

Since there is only one sign change to the coefficients of the polynomial it follows that there exists only one root to (5.93) which is the solution to λ_z. Note that once λ_z is obtained from (5.93) then the radial stress from (5.85) simplifies to

$$\begin{aligned} T_{rr}(s) &= -\frac{\hat{\alpha}}{2}\int_{s_i}^{s} \phi(\rho(s,\lambda_z), v, \lambda_z, \beta)\, ds \\ &= -\frac{\hat{\alpha}}{2}\int_{s_i}^{s} \phi(0, v, \lambda_z, \beta)\, ds \\ &= -\frac{\hat{\alpha}}{2}\int_{s_i}^{s} \frac{1}{vs - \lambda_z s^3}\left(\frac{2v}{s\lambda_z\beta^{1/2}} - \frac{2s}{\beta^{1/2}}\right) ds \\ &= \frac{\hat{\alpha}}{\beta^{1/2}}\int_{s_i}^{s} \frac{ds}{v - \lambda_z s^2} - \frac{\hat{\alpha}v}{\lambda_z\beta^{1/2}}\int_{s_i}^{s} \frac{ds}{vs^2 - \lambda_z s^4} \\ &= \frac{\hat{\alpha}}{\lambda_z\beta^{1/2}}\left(\frac{1}{s} - \frac{\lambda_z^2}{\beta^{3/2}}\right). \end{aligned} \tag{5.94}$$

It is clear that with (5.92) this radial stress vanishes at $s = s_i$ and it is decreasing (compression) toward the outer radius at which $s_o = \lambda_{lat}$ and the lateral pressure is given by

$$P_{lat} = \frac{\hat{\alpha}}{\lambda_z\beta^{1/2}}\left(\frac{\lambda_z^2}{\beta^{3/2}} - \frac{1}{\lambda_{lat}}\right). \tag{5.95}$$

If this pressure is normalized by $\hat{\alpha}\alpha^*/(\hat{\alpha}+\alpha^*)$ and is renamed to $\bar{P}_{lat}$ it follows that

$$\bar{P}_{lat} = \frac{\beta+1}{\lambda_z \beta^{1/2}} \left(\frac{\lambda_z^2}{\beta^{3/2}} - \frac{1}{\lambda_{lat}} \right). \tag{5.96}$$

In addition, the circumferential stress form (5.87) reduces to

$$T_{\theta\theta}(s) = \frac{\hat{\alpha}}{\beta^2} (s - \lambda_z). \tag{5.97}$$

Since $s_i \leq s \leq s_o \leq \lambda_{lat} \leq \lambda_z$ this hoop stress is also compressive. Moreover note that in a case where this special case coincides with the first wall contact we have $s = \lambda_{lat}$, $v = \lambda_{lat}^3$ and $\lambda_z = \lambda_{lat}$ for all $s_i \leq s \leq s_o$ and hence all three stress components vanish.

CHAPTER VI

Concluding Remarks, Speculations and Broader Connections

In this thesis we have shown how swelling can be treated in the framework of hyperelastic theory as a parametric volume change. We used the multiplicative decomposition of the deformation gradient to distinguish between swelling and other elastic accommodations within different processes. This allows for introducing the incorporation of swelling in the constitutive relations both in the conventional hyperelastic and in the internal balance theory. In the context of conventional hyperelastic constitutive model we considered spherical and cylindrical geometries and in the former case allowed the material parameters to depend on the swelling amount. In the context of the internally balance material theory we considered the cylindrical deformation and showed how swelling can lead to different response than that of the conventional hyperelastic theory.

The possibility of modeling a variety of swelling effects has immediate consequences in several areas of application, many of which are motivated by biomechanical modeling. Others have direct bearing on possible mechanical devices that achieve their control by soft material action. The combined effect of external loading and internal swelling can give rise to complicated states of deformation. Even in the simple setting of a spherical shell subject to combinations of simple pressure with uniform through-thickness (homogeneous) swelling, instabilities can arise that might

not otherwise be present if either pressurization or swelling was acting by itself. In this thesis we have explored the role that swelling can have on eliciting qualitative changes in the pressure-expansion inflation response of spherical deformation. Unlike in the context of conventional hyperelastic theory where the swelling is *imposed* as prescribed deformation, the internally balanced theory makes use of a deformation gradient decomposition to *obtain* the portion of deformation that is responsible for swelling. The additional requirement that obtains the swelling deformation is a natural consequence of energy minimization with respect to the new decomposition. We explored aspects of these two constitutive theories for cylindrical deformation of confined plug and tube.

In the first and second chapters considerations have been limited to the deformations of the spherical symmetry. Generalizing methods of analysis pioneered by Carroll in the context of incompressible hyperelasticity we have examined a rather straight forward constitutive model, one which is motivated by the well known Mooney-Rivlin model in the incompressible theory, so as to incorporate swelling dependent stiffness parameters. We have shown how certain dependencies preserve the overall qualitative nature of the inflation process independent of the amount of swelling, whereas other dependencies do not. In the latter case we have provided general rules, illustrated with examples, showing how certain constitutive forms cause a monotonic (benign) inflation response in the absence of swelling to become nonmonotonic (burst-inducing) as the swelling proceeds. Alternative constitutive forms have the opposite effect, burst-inducing inflation response in the absence of swelling can be mitigated into benign inflation response as the swelling proceeds. It is also important to note that the development of surface roughness due to swelling has been observed in solid hydrogel spheres. This may then give way to an aspherical and facetted surface morphology as the swelling proceeds *Bertrand et al.* (2016). These are typically confined

to distinct ranges of overall swelling and may be connected to nonuniform states of internal hydration ($v = v(R)$ in the notation of the third chapter), especially if the identified swelling ranges differ on the basis of whether the overall fluid content is increasing or decreasing.

It is interesting to speculate in the possible broader connections of this work to physical and biological phenomena. The overall considerations of the present study, as well as possible future studies that bring to bear the techniques in the above referenced works, give rise to the prospect that swelling, when viewed as a control variable, could be manipulated so as to tune the inflation response of spherical shells and membranes. This includes the possibility of both triggering and avoiding instances of inflation burst. On this basis, one may even speculate to what extent such processes of regulation might be present in biological systems. For example, colonies of soft celled creatures are capable of rapidly undergoing complex shape changes. This includes the green alga volvox in the shape of a spherical shell. At a crucial point in their embryonic development, volvox essentially turn themselves inside-out in a process that is conjectured to be triggered by cell shape change at a specific latitude on the shell *Höhn et al.* (2015); *Haas and Goldstein* (2015). An intriguing issue in this context is the extent to which the global conditions of the type examined here might possibly abet the resulting snap-through process.

In the final two chapters we have examined the finite strain swelling of cylindrical plugs (with original outer radius R_o) within a rigid cylindrical tube of radius $R_c > R_o$, all with circular cross-section. For a simple plug with no internal cavities or voids the wall contact deformation involves only a simple axial lengthening.

When the plug is not simply connected, in our case because of an internal channel of original radius R_i, the deformation after contact involves a combination of axial lengthening and channel closing. A boundary value problem must be solved in order

to determine the relative importance of these two ways to accommodate the swelling volume increase. For a conventional swelling model based on a generalized neo-Hookean response we show that this boundary value problem has a unique solution. Asymptotic analysis of the problem shows how the channel radius closing depends upon v as the swelling becomes large.

Figure 4.8 shows the various trends for the plug's internal channel radius as the swelling proceeds. Prior to wall contact the internal channel radius grows linearly with v causing r_i to reach its maximum size when the channel makes contact with the rigid tube wall. Additional swelling then constricts the internal channel in a manner that can be addressed analytically both for the immediate post-contact values of v and then again for sufficiently large v. While these trends are intuitive for the problem formulated here they can also provide useful insight for various hypothetical elastic systems involving tubes with multiple layers.

One reason for pointing out these connections is because certain biological tube organs have such a multi-layer structure, indeed, for the purpose of mechanics modeling, arteries are often regarded as three layered tubes *Holzapfel et al.* (2000). So is the windpipe (the trachea) *Gou and Pence* (2016). Moreover, it is typically the inner layer that is the most subject to distress and disease, thus exposing it to various possibilities for inflammation, edema or other phenomena that at least have some aspect of swelling. The analogy with our above hypothetical tube is however a highly imperfect one – it would typically be the swelling layer that is the least stiff and not the central layer. In any event, the type of formalism employed here might at least provide some insight into the behavior of such biological systems when subject to inflammatory swelling. Other soft tissue cylindrical structures in the body that are subject to swelling, although not in the sense of inflammation but rather in the sense of normal function, include the cervix, especially as it undergoes remodeling during pregnancy *Myers et al.* (2015). As indicated by the above references, all of these

systems are the subject of current biomechanics based modeling.

Finally brain swelling (hydrocephalus), while being confined to more of a spherical (not tubular) enclosure, is also the object of recent mechanics based modeling *Wilkie et al.* (2011). In this case the three layer system identification is again interesting, if we identify $R_i < R < R_o$ with the swelling brain, and $R > R_c$ with the surrounding skull. Detailed finite strain treatments relating to this issue are now being developed. The approach presented in this thesis could aid in the formulation of more precise mathematical models of this important human health concern.

BIBLIOGRAPHY

BIBLIOGRAPHY

Alexander, H. (1971), Tensile instability of initially spherical balloons, *International Journal of Engineering Science*, *9*(1), 151–160.

Ateshian, G. A. (2007), On the theory of reactive mixtures for modeling biological growth, *Biomechanics and Modeling in Mechanobiology*, *6*, 423–445.

Baek, S., and T. J. Pence (2011), Inhomogeneous deformation of elastomer gels in equilibrium under saturated and unsaturated conditions, *Journal of the Mechanics and Physics of Solids*, *59*(3), 561–582.

Baek, S., and A. R. Srinivasa (2004), Diffusion of a fluid through an elastic solid undergoing large deformation, *International Journal of Non-linear Mechanics*, *39*(2), 201–218.

Ben Amar, M., and P. Ciarletta (2010), Swelling instability of surface-attached gels as a model of soft tissue growth under geometric constraints, *Journal of the Mechanics and Physics of Solids*, *58*(7), 935–954.

Ben Amar, M., and A. Goriely (2005), Growth and instability in elastic tissues, *Journal of the Mechanics and Physics of Solids*, *53*(10), 2284–2319.

Bertrand, T., J. Peixinho, S. Mukhopadhyay, and C. W. MacMinn (2016), Dynamics of swelling and drying in a spherical gel, *Physical Review Applied*, *6*(6), 064,010.

Bowen, R. M. (1980), Incompressible porous medium models by the use of the theory of mixtures, *International Journal of Engineering Science*, *18*, 1129–1148.

Carroll, M. M. (1987), Pressure maximum behavior in inflation of incompressible elastic hollow spheres and cylinders, *Quarterly of applied mathematics*, *45*(1), 141–154.

Chen, Y.-C., and A. Hoger (2000), Constitutive functions of elastic materials in finite growth and deformation, *Journal of Elasticity*, *59*(1), 175–193.

Chester, S. A., and L. Anand (2010), A coupled theory of fluid permeation and large deformations for elastomeric materials, *Journal of the Mechanics and Physics of Solids*, *58*(11), 1879–1906.

Demirkoparan, H., and T. J. Pence (2007a), The effect of fiber recruitment on the swelling of a pressurized anisotropic non-linearly elastic tube, *International Journal of Non-Linear Mechanics*, *42*(2), 258–270.

Demirkoparan, H., and T. J. Pence (2007b), Swelling of an internally pressurized nonlinearly elastic tube with fiber reinforcing, *International journal of solids and structures*, *44*(11), 4009–4029.

Demirkoparan, H., and T. J. Pence (2008), Torsional swelling of a hyperelastic tube with helically wound reinforcement, *Journal of Elasticity*, *92*(1), 61–90.

Demirkoparan, H., and T. J. Pence (2015a), Finite stretching and shearing of an internally balanced elastic solid, *Journal of Elasticity*, *121*(1), 1–23.

Demirkoparan, H., and T. J. Pence (2015b), Magic angles for fiber reinforcement in rubber-elastic tubes subject to pressure and swelling, *International Journal of Non-Linear Mechanics*, *68*, 87–95.

Demirkoparan, H., and T. J. Pence (2017), Swelling–twist interaction in fiber-reinforced hyperelastic materials: the example of azimuthal shear, *Journal of Engineering Mathematics*, pp. 1–22.

Demirkoparan, H., T. J. Pence, and H. Tsai (2014), Hyperelastic internal balance by multiplicative decomposition of the deformation gradient., *Archive for Rational Mechanics & Analysis*, *214*(3).

Deng, H., and T. J. Pence (2010), Equilibrium states of mechanically loaded saturated and unsaturated polymer gels, *Journal of Elasticity*, *99*(1), 39–73.

Drozdov, A., et al. (2013), Constitutive equations in finite elasticity of swollen elastomers, *International Journal of Solids and Structures*, *50*(9), 1494–1504.

Drozdov, A. D. (2013), Finite elasticity of nanocomposite hydrogels, *Composite Interfaces*, *20*(9), 673–692.

Drozdov, A. D., and J. d. Christiansen (2013), Constitutive equations in finite elasticity of swollen elastomers, *International Journal of Solids and Structures*, *50*, 1494–1504.

Duda, F. P., A. C. Souza, and E. Fried (2010), A theory for species migration in a finitely strained solid with application to polymer network swelling, *Journal of the Mechanics and Physics of Solids*, *58*(4), 515–529.

Duda, F. P., A. C. Souza, and E. Fried (2011), Solvent uptake and cavitation, *Journal of the Mechanics and Physics of Solids*, *59*(11), 2341–2354.

Ericksen, J. L. (1975), Equilibrium of bars, *Journal of Elasticity*, *5*(3), 191–201.

Evans, E., V. Heinrich, F. Ludwig, and W. Rawicz (2003), Dynamic tension spectroscopy and strength of biomembranes, *Biophysical Journal*, *85*(4), 2342–2350.

Fang, Y., T. J. Pence, and X. Tan (2011), Fiber-directed conjugated-polymer torsional actuator: nonlinear elasticity modeling and experimental validation, *IEEE/ASME Transactions on Mechatronics*, *16*(4), 656–664.

Forest, S., K. Ammar, B. Appolaire, N. Cordero, and A. Gaubert (2014), Micromorphic approach to crystal plasticity and phase transformation, in *Plasticity and Beyond*, pp. 131–198, Springer.

Gibbons, M. M., and W. S. Klug (2008), Influence of nonuniform geometry on nanoindentation of viral capsids, *Biophysical Journal*, *95*(8), 3640–3649.

Goriely, A., D. E. Moulton, and R. Vandiver (2010), Elastic cavitation, tube hollowing, and differential growth in plants and biological tissues, *EPL (Europhysics Letters)*, *91*(1), 18,001.

Gou, K., and T. J. Pence (2016), Hyperelastic modeling of swelling in fibrous soft tissue with application to tracheal angioedema, *Journal of mathematical biology*, *72*(1-2), 499–526.

Graf, J., M. Rupnik, G. Zupancic, and R. Zorec (1995), Osmotic swelling of hepatocytes increases membrane conductance but not membrane capacitance., *Biophysical Journal*, *68*(4), 1359.

Green, A. E., and R. T. Shield (1950), Finite elastic deformation of incompressible isotropic bodies, in *Proceedings of the Royal Society of London A: Mathematical, Physical and Engineering Sciences*, vol. 202, pp. 407–419, The Royal Society.

Haas, P. A., and R. E. Goldstein (2015), Elasticity and glocality: initiation of embryonic inversion in volvox, *Journal of The Royal Society Interface*, *12*(112), 20150,671.

Hadoush, A., H. Demirkoparan, and T. J. Pence (2014), Updated lagrange formulation of internally balanced compressible hyperelastic materials, in *Qatar Foundation Annual Research Conference*, 1, p. HBPP0271.

Hadoush, A., H. Demirkoparan, and T. J. Pence (2015), A constitutive model for an internally balanced compressible elastic material, *Mathematics and Mechanics of Solids*, p. 1081286515594657.

Hadoush, A., H. Demirkoparan, and T. J. Pence (2017), Finite element analysis of internally balanced elastic materials, *Computer Methods in Applied Mechanics and Engineering*.

Havner, K. S. (1992), *Finite plastic deformation of crystalline solids*, Cambridge University Press.

Höhn, S., A. R. Honerkamp-Smith, P. A. Haas, P. K. Trong, and R. E. Goldstein (2015), Dynamics of a volvox embryo turning itself inside out, *Physical Review Letters*, *114*(17), 178,101.

Holzapfel, G. A., T. C. Gasser, and R. W. Ogden (2000), A new constitutive framework for arterial wall mechanics and a comparative study of material models, *Journal of Elasticity*, *61*, 1–48.

Hong, W., X. Zhao, J. Zhou, and Z. Suo (2008), A theory of coupled diffusion and large deformation in polymer gels, *Journal of the Mechanics and Physics of Solids*, *56*, 1779–1793.

Kröner, E. (1959), Allgemeine kontinuumstheorie der versetzungen und eigenspannungen, *Archive for Rational Mechanics and Analysis*, *4*(1), 273–334.

Kyriakides, S., and Y.-C. Chang (1990), On the inflation of a long elastic tube in the presence of axial load, *International Journal of Solids and Structures*, *26*(9-10), 975–991.

Lee, E. H. (1969), Elastic-plastic deformation at finite strains, ASME.

Li, F., C. U. Chan, and C. D. Ohl (2013), Yield strength of human erythrocyte membranes to impulsive stretching, *Biophysical Journal*, *105*(4), 872–879.

Markert, B., B. Monastyrskyy, and W. Ehlers (2008), Fluid penetration effects in porous media contact, *Continuum Mechanics and Thermodynamics*, *20*, 303=315.

McMahon, J., A. Goriely, and M. Tabor (2010), Spontaneous cavitation in growing elastic membranes, *Mathematics and Mechanics of Solids*, *15*(1), 57–77.

Müller, I., and P. Strehlow (2004), *Rubber and rubber balloons: paradigms of thermodynamics*, vol. 637, Springer Science & Business Media.

Myers, K. M., H. Feltovich, E. Mazza, J. Vink, M. Bajka, R. Wapner, T. Hall, and M. House (2015), The mechanical role of the cervix in pregnancy, *Journal of Biomechanics*, *48*, 1511–1523.

Nagel, T., S. Loerakker, and C. W. J. Oomens (2009), A theoretical model to study the effects of cellular stiffening on the damage evolution in deep tissue injury, *Computer Methods in Biomechanics and Biomedical Engineering*, *12*(5), 585–597.

Ogden, R. W. (1997), *Non-linear elastic deformations*, Courier Corporation.

Pence, T. J. (2012), On the formulation of boundary value problems with the incompressible consituents constraint in finite deformation poroelasticity, *Mathematical Methods in the Applied Sciences*, *35*, 1756–1783.

Pence, T. J., and H. Tsai (2005a), Swelling-induced microchannel formation in nonlinear elasticity, *IMA journal of applied mathematics*, *70*(1), 173–189.

Pence, T. J., and H. Tsai (2005b), On the cavitation of a swollen compressible sphere in finite elasticity, *International Journal of Non-Linear Mechanics*, *40*(2), 307–321.

Pence, T. J., and H. Tsai (2006), Swelling-induced cavitation of elastic spheres, *Mathematics and Mechanics of Solids*, *11*(5), 527–551.

Sadik, S., A. Angoshtari, A. Goriely, and A. Yavari (2016), A geometric theory of nonlinear morphoelastic shells, *Journal of Nonlinear Science*, *26*(4), 929–978.

Selvadurai, A. P. S., and A. P. Suvorov (2016), Coupled hydro-mechanical effects in a poro-hyperelastic material, *Journal of the Mechanics and Physics of Solids*, *91*, 311–333.

Stuart, M. A. C., et al. (2010), Emerging applications of stimuli-responsive polymer materials, *Nature Materials*, *9*(2), 101–113.

Treloar, L. R. G. (1975), *The physics of rubber elasticity*, Oxford University Press, USA.

Tsai, H., T. J. Pence, and E. Kirkinis (2004), Swelling induced finite strain flexure in a rectangular block of an isotropic elastic material, *Journal of Elasticity*, *75*(1), 69–89.

Van der Sman, R. G. M. (2015), Hyperelastic models for hydration of cellular tissue, *Soft Matter*, *11*(38), 7579–7591.

Vinod Kumar, K., and F. Demeke (2011), Analysis of mechanical behavior of red blood cell membrane with malaria infection, *World Journal of Mechanics*, *2011*.

Vujošević, L., and V. A. Lubarda (2002), Finite-strain thermoelasticity based on multiplicative decomposition of deformation gradient, *Theoretical and Applied Mechanics*, (28-29), 379–399.

Wilkie, K. P., C. S. Drapaca, and S. Sivaloganathan (2011), A nonlinear viscoelastic fractional derivative model of infant hydrocephalus, *Applied Mathematics and Computation*, *217*, 8693–8704.

Wineman, A. S., and K. R. Rajagopal (1992), Shear induced redistribution of fluid within a uniformly swollen nonlinear elastic cylinder, *International Journal of Engineering Science*, *30*, 1583–1595.

Yavari, A., and A. Goriely (2013), Nonlinear elastic inclusions in isotropic solids, in *Proc. R. Soc. A*, vol. 469, p. 20130415, The Royal Society.

Zamani, V., and T. Pence (2017), Swelling, inflation, and a swelling-burst instability in hyperelastic spherical shells, *International Journal of Solids and Structures*, *125*, 134–149.